LULEÅ UNIVERSITY OF TECHNOLOGY

MASTER THESIS

Optical Analysis of Plasma - Flame Emission in Cryogenic Rocket Engines

Author:
Carlo GIRARDELLO

Supervisor:
Dr. Robert STÜTZER
Examiner:
Prof. Victoria Barabash

A thesis submitted in fulfillment of the requirements
for the degree of MSc In Spacecraft Design

at

Luleå University of Technology

thanks to

Deutsches Zentrum für Luft- und Raumfahrt (DLR)

July 23, 2019

Declaration of Authorship

I, Carlo GIRARDELLO, declare that this thesis titled, "Optical Analysis of Plasma - Flame Emission in Cryogenic Rocket Engines" and the work presented in it are my own. I confirm that:

- This work was done wholly while in candidature for a master degree at LTU.
- Where any part of this thesis has previously been submitted for a degree or any other qualification at this University or any other institution, this has been clearly stated.
- Where I have consulted the published work of others, this is always clearly attributed.
- Where I have quoted from the work of others, the source is always given. With the exception of such quotations, this thesis is entirely my own work.
- I have acknowledged all main sources of help.

Signed: _____

Date: _____

LULEÅ UNIVERSITY OF TECHNOLOGY

Abstract

MSc In Spacecraft Design

Optical Analysis of Plasma - Flame Emission in Cryogenic Rocket Engines

by Carlo GIRARDELLO

This thesis contains the results of optical flame emission measurements of the Vulcain 2.1 engine and the plasma emission spectroscopy of the Lumen Project engine. The plume spectroscopy is analyzed, ordered and studied in detail to offer the best possible molecular composition. The main focus relied on the hydroxide radical, blue radiation and other molecules analysis of the intensities encountered during the tests. The plasma emission spectroscopy is focused on the determination of the plasma temperature value in LIBS measurements. The hydrogen plasma temperature determination of the local thermodynamic equilibrium, followed by the carbon and sequentially oxygen plasma is obtained. The quality of the LTE is to be determined to judge the truthworthness of the determined temperatures. Both the tests are analyzed thanks to the use of spectrographs, cameras and dedicated software for optical applications. The results related to the Vulcain 2.1 LOX/LH2 engine showed the evolution of the plume in different ROF or pressure variations. Furthermore, the results of the Lumen Project LOX/methane engine led to the determination of the plasma temperatures and a first estimation of the LTE quality.

Die vorliegende Arbeit präsentiert die Ergebnisse der Abgasstrahlspektroskopie des H2/LOX Vulcain 2.1 Triebwerks und der Zündplasma Spektroskopie des CH4/LOX Triebwerks des LUMEN Projektes. Die Abgasstrahlspektroskopie wurde analysiert und im Detail untersucht um die am besten passende molekulare Zusammensetzung herauszuarbeiten. Das Hauptaugenmerk liegt dabei auf dem Hydroxyl- Radikal, der Blauen Strahlung und molekularer Intensitätsanalyse. Bei der Zündplasmaanalyse liegt der Fokus auf der Bestimmung des LTE Zustands (Lokales thermodynamisches Gleichgewicht) in LIBS. Die Temperatur des Wasserstoff-, Kohlenstoff und Sauerstoffplasmas wird herangezogen, um die Qualität des LTE Zustands zu beurteilen. Für die Testdurchführung wurden Spektrographen, Kameras und bestimmte Auswertungstools für optische Anwendungen benutzt. Das Verhalten des Vulcain 2.1 Abgasstrahls abhängig von verschiedenen ROF und Druckstufen ist in den Ergebnissen beschrieben. Für das LUMEN Triebwerk konnten erste Zündplasmatemperaturen bestimmt werden und geben einen Rückschluss auf die Qualität des LTE.

Acknowledgements

I thank my supervisor, Dr. Robert Stützer, for the patience and guidance that he offered me.

I thank my examiner, Prof. Victoria Barabash, for having granted me support on this thesis.

I thank Deutsches Zentrum für Luft- und Raumfahrt (DLR) for giving me the opportunity to write this thesis and for increasing my knowledge.

I thank LTU, for having enormously enlarged my knowledge on Spacecraft Design and for having granted me the opportunity of doing this thesis abroad.

I thank my family for always having been at my side and for having supported me all along.

I thank my friends, old and new, for having taken the burden that is my friendship.

I thank Silvia, for everything.

Contents

List of Tables

List of Figures

List of Abbreviations

AC	**A**lternate **C**urrent
Ar	**Ar**gon
CCD	**C**harged **C**oupled **D**evice
Cu	**C**opper
DC	**D**irect **C**urrent
DLR	**D**eutsches Zentrum Für **L**uft- und **R**aumfart
FOFMS	**M**ultimode **F**iber **O**ptic **F**ilter **M**ounts
FTIS	**F**ourier **T**ransform **I**nfrared **S**pectrometer
H2	**H**ydrogen
Hg	**M**ercury
Hg(Ar) Lamp	**M**ercury **A**rgon Lamp
HiPoLas	**H**igh **P**ower **L**aser
ICCD	**I**ntensified **C**harged **C**oupled **D**evice
IFU	**I**ntegral **F**ield **U**nit
LAI	**L**aser **A**blation **I**gnition
LASER	**L**ight **A**mplification by **S**timulated **E**mission of **R**adiation
LH2	**L**iquid **H**ydrogen
LIBS	**L**aser **I**nduced **B**reakdown **S**pectroscopy
LIP	**L**aser **I**nduced **P**lasma
LOD	**L**imit **O**f **D**etection
LOX	**L**iquid **O**xygen
LNG	**L**iquefied **N**atural **G**as
LTE	**L**ocal **T**hermodynamic **E**quilibrium
NIR	**N**ear **I**nfra**R**ed
OES	**O**ptical **E**mission **S**pectroscopy
OH*	**H**ydr**O**xide Radical
QE	**Q**uantum **E**fficiency
ROF	**R**atio of **F**uel to **O**xidizer
TE	**T**hermodynamic **E**quilibrium
UV	**U**ltra**V**iolet

Physical Constants

Boltzmann Constant	$k = 8.617\,333\,262 \times 10^{-5}\,\mathrm{eV/K}$ (exact)
Boltzmann Constant	$k = 1.380\,649 \times 10^{-23}\,\mathrm{J\,K^{-1}}$ (exact)
Electron Rest Mass	$m_e = 9.109\,383\,701 \times 10^{-31}\,\mathrm{kg}$
Elementary Charge	$e = 1.602\,176\,634 \times 10^{-19}\,\mathrm{C}$
Pi	$\pi = 3.141\,592\,653\,5$
Planck Constant	$h = 6.626\,070\,04\,\mathrm{m^2\,kg\,s^{-1}}$ (exact)
Reduced Planck Constant	$\hbar = 1.054\,571\,726 \times 10^{-34}\,\mathrm{J\,s^{-1}}$
Rydberg Constant	$R = 1.097 \times 10^{7}\,\mathrm{m^{-1}}$
Speed of Light	$c_0 = 2.997\,924\,58 \times 10^{8}\,\mathrm{m\,s^{-1}}$ (exact)

List of Symbols

A_{nm}	Transition Probability Function	s^{-1}
d	Grating Constant	
E_{exc}	Energy of the excited state	eV
E_f	Energy necessary for an electron to perform a transition	eV
E_i	Starting Energy of an electron	eV
E_{inf}	Energy of the lower excited state	eV
E_n	Energy of the Degeneracy	erg or J
ϵ_{nm}	Emissivity	$W\,cm^{-3}$
g_n	Degeneracy of N_n	J
I_{nm}	Intensity Line	A.U.
l	Orbital Angular Momentum Quantum Number	
λ_n	Wavelength of a Transition n	m or nm
m	Order of Diffraction	
m_l	Magnetic Quantum Number	
m_s	Electron Spin Quantum Number	
n	Principal Quantum Number	
J	Total Angular Momentum Quantum Number n	
N_n	Population of a Quantum Level n	cm^{-3}
$U(T)$	Partition Function	A.U.
v, f	Frequency	s^{-1}

Chapter 1

Introduction

1.1 Structure of The Thesis

This thesis is the result of six months of work at DLR Lampoldhausen. It is divided in six chapters.

The first chapter gives the reader the information on how to read this thesis, it points out clearly what are the goals and the scope of the project work conducted at DLR and describes the hardware used during the experiments.

The second chapter explains in detail the theory necessary to understand fully the experiments. It is divided in two main subsections: the Lumen Project part and the Vulcain 2.1 part. The Lumen Project subsection is related to plasma. It explains to the reader the working principles of plasma, plasma spectroscopy and laser physics. It is necessary for the understanding and interpretation of the results. The Vulcain 2.1 subsection deals with flame emission. It is the summary of the basic knowledge necessary to understand the composition of the plume emitted by the nozzle of a rocket. It gives the reader the knowledge necessary to understand what will be observed during the experiments.

The third chapter analyzes the state of the art of the two engines studied. It introduces the reader to the facilities and the equipment used in both the experimental setups together with a step by step procedure of how the data have been acquired, processed and analyzed.

The fourth chapter describes everything that is needed to know concerning the experiments. It is a summary with tables indicating the main milestones for the Vulcain 2.1 and a summary with the expected results for the Lumen Project.

The fifth chapter analyzes in detail the results. Every relevant spectra is plotted, introduced, explained and then sequentially analyzed with scientific methodology. When in doubt, the reasons and some possible solutions are introduced.

The sixth chapter contains the conclusion of this thesis work. It gives some final statements on the tests and highlights the main results together with the upcoming campaigns.

1.2 Goal & Scope

This thesis has multiple goals. One is related to plasma spectroscopy, the other is linked to flame emission. The goal of this thesis concerning plasma spectroscopy is the expansion of the knowledge of the processes occurring with laser ignition in space propulsion. This is interesting from a physical and engineering point of view. The performance of the rocket is the most important aspect from the engineering perspective, requiring an in depth study of the best position for the laser focus.
The physicist wants to investigate the reasons behind the ignition generated by a laser beam. To understand what the plasma generated before ignition is composed of, it is necessary to know what are the physical laws ruling this field of space propulsion, which is the generation of plasma in combustion chambers with the aid of lasers.
A recently developed injection method is tested at the European Research and Technology Test Bench P8 at the DLR Institute of Space Propulsion in Lampoldshausen, Germany.
In order to ignite the rocket propellants, which are commonly gaseous hydrogen or gaseous methane, together with liquid oxygen, laser ignition will be applied besides other techniques. A lens focusses the high-energetic laser beam onto the shear layer between fuel and oxygen. The electron-ion recombination after the induced plasma (breakdown) leads to the emission of bright light, ranging from ultraviolet (UV) to near infrared (NIR) wavelengths. This light will be used for analyzing crucial parameters such as local ROF, plasma temperature and electron density. Furthermore, the ignition behavior will be monitored using a high-speed camera that records the development and propagation of the ignition spark and subsequent combustion.

The second goal of this thesis is related to the flame emissions of the Vulcan 2.1. The study of the plume is really important because it can give a lot of information on the engine's health to engineers and technicians. Based on the chemical composition recorded, it is possible to estimate the quality of the combustion processes. From an academic point of view it is educational to study, analyze and process the data obtained by a real applications rocket engine in order to increase the personal knowledge on propulsion systems.

1.3 Hardware and Fundamentals

- **Shamrock SR-163**
  The Shamrock SR-163 is the spectrograph used for the tests carried out at P5 for the Flame Emissions Measurements. Shamrock SR-163 is a spectroscope developed by Andor Technology based on a Czerny-Turner optical design. This tool is a spectrometer which is capable of measuring a single wavelength over a wide spectral range. SR-163 consists of fixed entrance and exit slits, two concave mirrors and a grating.
  Light enters through the entrance slit, which is in the same plane of the first concave mirror which, consequently, directs parallel rays of light towards the grating. The grating acts like a prism, separating all the different wavelengths and pointing them to the second concave mirror. The light from the second mirror is directed through the slit which is in the focal point of the ellipsis and it is then observed by the high speed camera.
  A sketch of this working principle is presented in Figure 1.1, note that instead

of the exit slit, a chip to catch the light is actually used.
The wavelength range of a monochromator varies with the choice of grating, but commonly they can scan from 160 nm to 500 nm or ever wider ranges. The spectral resolution depends on the widths of the slits, the choice of grating and focal length, but commonly can be less than 10 pm for high resolution OES (Optical Emissions Spectroscopy).
A key to the performance of monochromators is the design of the grating movement: the grating is placed on a large drive wheel with motor control, allowing fine and precise positioning of the grating [29]

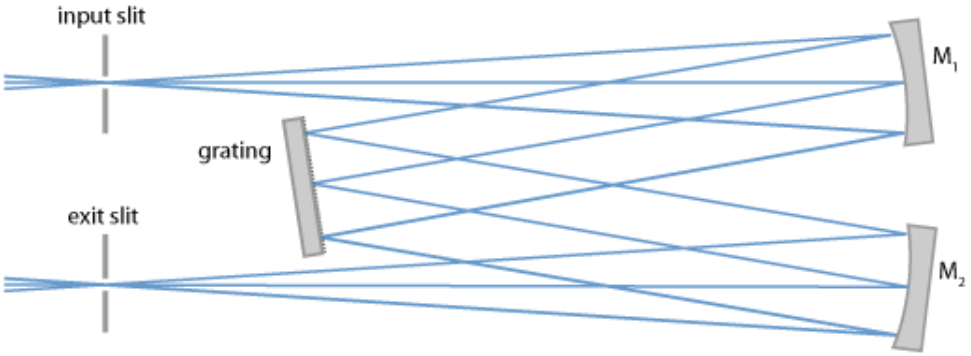

FIGURE 1.1: Czerny-Turner Spectrograph Working Principle, courtesy of [19]

The SR-163 can be used either as an imaging spectrograph in the so-called "Imaging Mode" with a shutter or as a non-imaging spectrograph in the so-called "Spectral Mode". The latter is commonly applied in LIBS studies [4]. A CAD model, internally developed at DLR, of the spectroscope used, together with a picture of the device, can be found in Figure 1.2 while in Spectral mode.

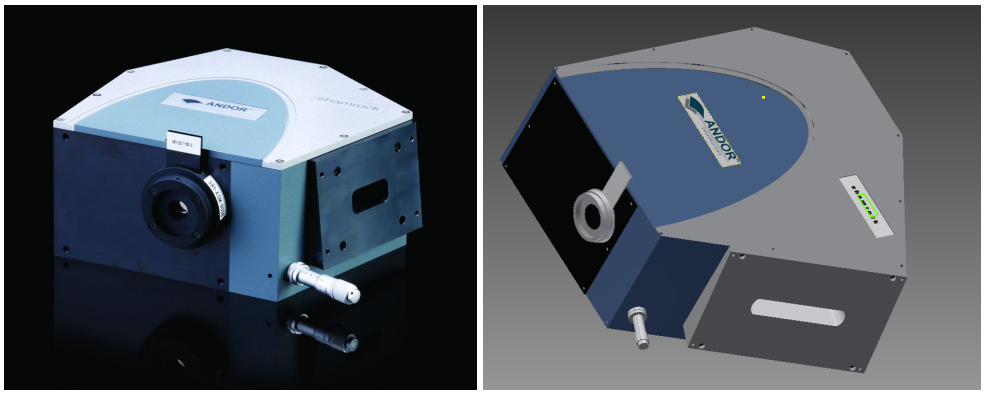

FIGURE 1.2: Shamrock SR-163 (left), courtesy of [4] and CAD model (right)

- **ICCD DH720 Gen II**
  The IStar 720 intensified CCD camera is one of the best ICCD available with its digital delay generator and the image quality offered during measurements. It is developed by Andor Technology and is currently in use at the laboratory at DLR Lampoldhausen. It is the camera used for the recordings of the Flame Emission measurements of the P5 tests. It has been designed to fulfill the needs of low-light spectroscopy requiring fast gating and the ability to detect LIBS (Laser Induced Breakdown Spectroscopy) events. The 1024x256 array has a 4:1

aspect ratio coupling very good with the Shamrock. A picture of this tool is presented in Figure 1.3. Some of its main features are the possibility to be re-

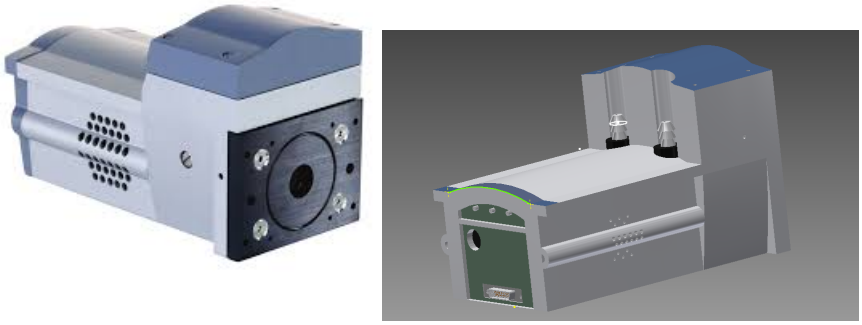

FIGURE 1.3: ICCD DH720 Gen II (left), courtesy of [5] and CAD model (right)

motely controlled, the single photon sensitivity and the software gain control. [5]

- **iStar sCMOS 18 F 03**
  The iStar sCMOS 18 F 03 is a camera which is ideal for flame and plasma imaging. Like the ICCD DH720 Gen II, it has been developed by Andor Technology for High Quality measurements and it is the one used at DLR Lampoldhausen Test Bench P8 for its reliability and durability. The digits 18 F 03 stands for the different design settings chosen by scientists and engineers at DLR based on their needs. 18 stands for the diameter of the intensifier, in millimeters. F stands for the minimum grating speed, and for this camera is a Fast Grating. The 03 is for the image intensifier option and, for this camera, is a W-AGT photocathode. It is the camera head for the Mechelle spectrograph used during the Lumen Project recordings. In Figure 1.4 are presented a real life model and a CAD model of this camera.

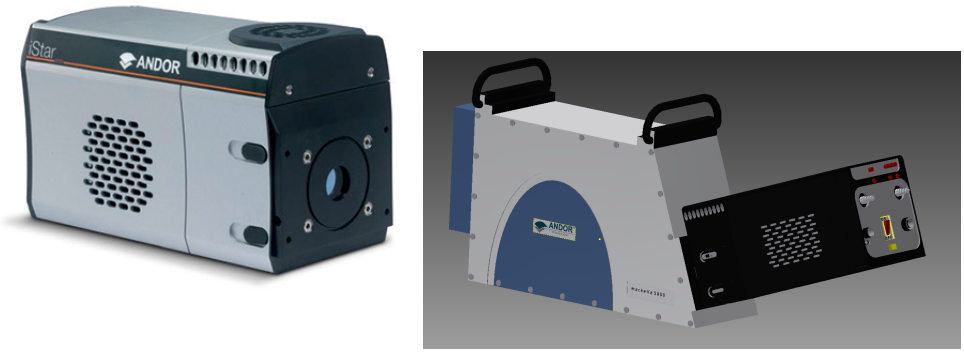

FIGURE 1.4: iStar sCMOS 18 F 03(left), courtesy of [3] and CAD model (right)

- **Mechelle 5000**
  The Mechelle 5000 is another spectrograph used during the experiments carried out in the Test Campaign performed at Test Bench P8 for the Lumen Project. It has been developed by Andor Technology and it provides recording

of a wide range of wavelengths, from 200 nm up to 975 nm in one acquisition. One of the main features is that it does not have any movable components and is available in a pre-aligned detector/spectrometer format. [2]
The working principle is based upon the echelle grating. An echelle grating is a type of diffraction grating which consists of many slits with a width very similar to the wavelength of the diffracted light. While in normal gratings the light is diffracted at different orders at specific angles, with reflective gratings, the reflected part can be blazed to direct most of the light through the preferred direction. In the echelle grating the blaze is optimized for multiple overlapping higher orders of diffraction.

- **Laser**
  The Laser used is presented in Figure 1.5 It has been designed entirely by the

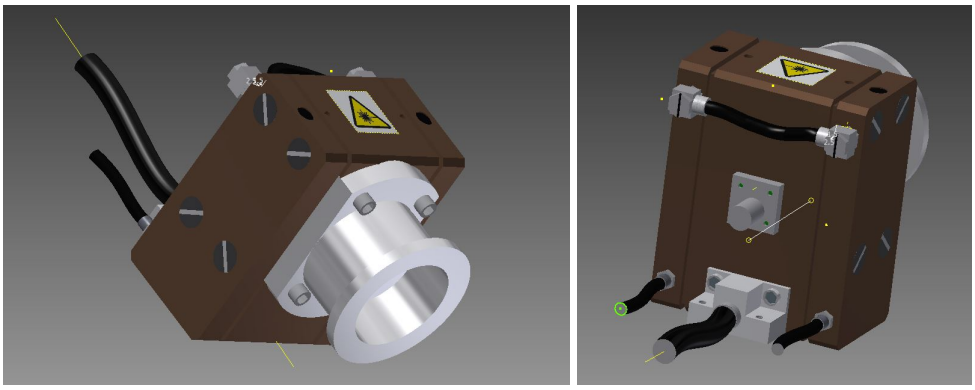

FIGURE 1.5: HiPoLas Laser

Carinthian Tech Research (CTR), Austria. It is an HiPoLas (High Power Laser) ignition system for aerospace applications. CTR has a 16 year old history in developing lasers. It started developing a high power, side pumped and passively Q-switched Nd-YAG (neodymium-doped yttrium aluminum garnet) laser system named HiPoLaser. The result of further researches, multiple iterations and improvement of this laser is the one that is being used at DLR for conducting the tests on the Lumen Project. It has been specifically designed and optimized for the use in upper stage cryogenic rocket combustor. The combination of a monolithic laser rod with a ring of pump allows this laser to have a very good mechanical stability. [46]

- **Optic Filter**
  The optical filter used for the experiments is a FOFMS - In-Line Multimode Fiber Optic Filter Mount developed by Thorlabs. It is used to ensure the correct triggering of the spectrograph during the Lumen Project tests. The filter ensures that only photons emitted by the laser are triggering the system. It is a free-space, fiber to fiber coupling system that uses off-axis parabolic (OAP) mirrors. FOFMS is ideal for fiber based applications. It acts like a filter for the light. The item described is presented in Figure 1.6.

FIGURE 1.6: FOFMS (left), courtesy of [31] and CAD model (right)

The last picture in Fig. 1.6 represent one of the two CFH2-F filter holders. The operating principle of this device is simple. It uses two OAP mirrors to transport light from the input fiber to the output fiber: This means that as light is entering the FOFMS system, it is aligned with the first OAP. Afterwards, it crosses the two slots where the optical filters represented Figure 1.6. Once the light has passed through the optical filter, it is then coupled to the output fiber using the second OAP and is finally measured using a Fourier Transform Infrared Spectrometer (FTIR). [31]

- **Laptop**

- **Calibration Lamp**
  The calibration lamp used is a ORIEL Mercury(Argon) lamp. It supports both AC and DC power supplies. The most important thing concerning the calibration lamp is the safety of the user. Since these kind of lamps have a strong UV output, the direct eye contact with it must be avoided. For this reason, a pair of protective glasses have been used for the whole duration of the calibration procedure. The Hg(Ar) lamp contains a small amount of Mercury that dominates the output spectrum and uses Argon as starter gas. This lamp is temperature sensitive, which means that in order to have the spectra presented in Figure 1.7, a reasonable amount of time must be waited.

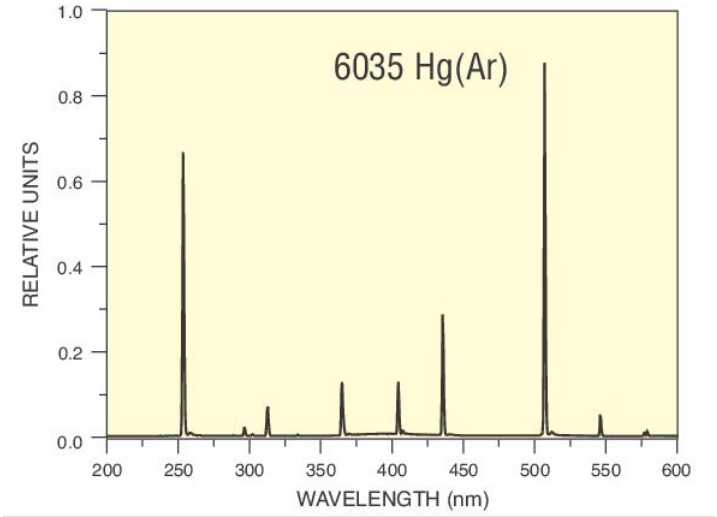

FIGURE 1.7: ORIEL Mercury(Argon) Calibration Lamp, courtesy of [32]

After the following spectra is seen on the spectrometer, the calibration can be considered over and successful.

Chapter 2

Theory

This chapter explains the theory behind the two different spectroscopic analysis methods performed. The first part is related to the Lumen Project and will mainly deal with plasma, LIBS and Hydrogen theories. The second part is related to the Vulcain 2.1 and it contains the basic information necessary for the complete understanding of the experimental data obtained in Chapter 5.

2.1 Spectroscopy

[10] The purposes of spectroscopy are:

- To determine accurate wavelengths of emission and absorption lines
- To measure the relative strength and/or equivalent widths of emission or absorption lines e.g. ionization states, temperatures...
- To identify shapes of emission or absorption lines
- To measure the spectral energy distribution of the continuum radiation

2.1.1 Spectrographs

The spectrograph is the tool that allows the study of all the above cited phenomena. There are many types of spectrographs but they can be summarized in two main families: by type of dispersing element or by geometry. The former is generally divided into multiple sub levels which are grating (transmission or reflection), prism (rare, except as a cross), grism (grating on a prism), narrow band imaging and interferometry. The latter has sub divisions too, like long-slit, aperture of multi fiber, Integral Field Units (IFU) or Tunable imagers. The diffraction grating is the principal device which is used to generate wavelength dependent interference patterns at various wavelengths like UV, NIR and visible regime. It consists of a series of equally spaced slits in an otherwise opaque screen where each slit can be considered as radiating secondary waves. [10] The most common diffraction grating used is the reflective diffraction grating. The working principle can de deduced from Equation 2.1:

$$m\lambda = d[sin(\alpha) + sin(\beta)] \tag{2.1}$$

Where m represents the order of diffraction, λ is the diffracted wavelength and d is the grating constant, which is the difference between the grooves, while α and β are respectively the angle of incidence measured from the normal and the angle of diffraction measured from the normal. The extremely high blaze angle of the Echelle grating concentrates the energy in the higher orders. In the simplest case where

light is incident on the grating at an angle of 0° the grating equation simplifies to $m\lambda = d[sin(\beta)]$ and if solved for $sin(\beta)$ it becomes:

$$sin(\beta) = \frac{m\lambda}{d} \tag{2.2}$$

It can be deduced from Equation 2.2 that in higher orders the angular separation between two wavelengths increases. [49]
The blaze grating, which is the one used in the Mechelle 5000 and in the Shamrock SR-163, is designed to concentrate light away from $m = 0$ to higher orders of m. The reflecting surfaces are inclined at a fixed angle with reference to the surface of the grating in order to reflect light in a preferred direction. The blaze has the goal of increasing the grating efficiency so it can achieve higher orders. With the particular inclined design of the blazed grating, the whole surface can be reflecting, since the step where the two faces join provides a phase difference that allows diffraction. A sketch of a blazed grating can be seen in Figure 2.1 In this Figure, it is possible to see

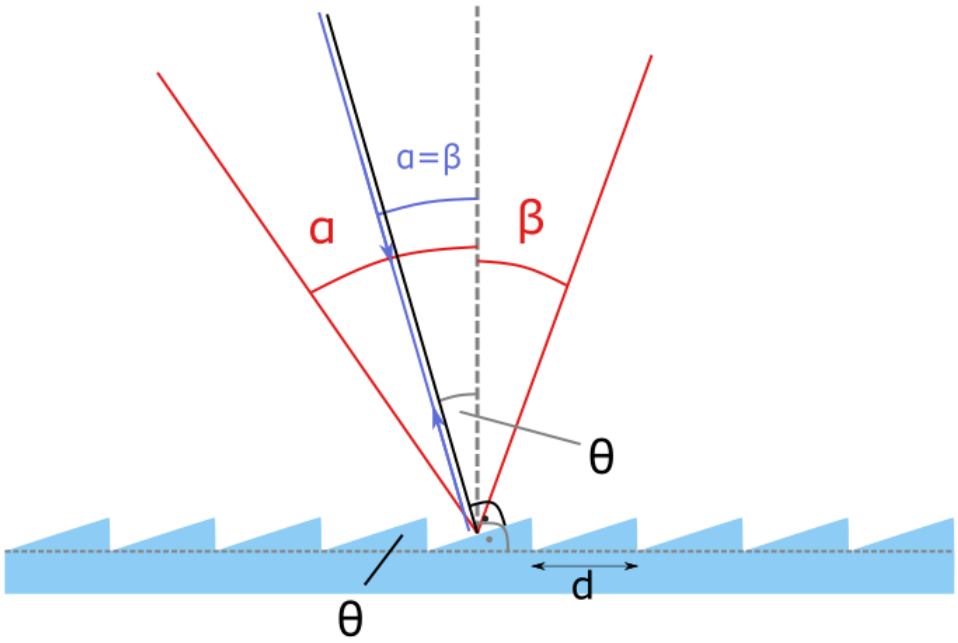

FIGURE 2.1: Blazed Grating Scheme

a ray of light hitting the grating with an α angle. Given the particular inclination of the grating θ, the reflected light will have an angle β, corresponding to a particular order of diffraction. The working principle follows Eq. 2.2 and in the case the angle of incidence is equal to the angle of the grating the light is reflected at the same angle θ.

2.2 Lumen Project Theory

2.2.1 Plasma Theory

Plasma is the fourth state of matter, after liquid, solid and gaseous. It is a cloud of positively charged ions and electrons, giving to the whole plasma the ability of acting as a whole and not as a group of atoms. Clarifying, a plasma is a quasineutral gas

of charged and neutral particles which exhibits collective behavior [14]. Quasineutral means that plasma is neutral enough to have approximately the same density of ions and free electrons, but not neutral enough to have all the electromagnetic forces equal to zero. Furthermore, the collective behavior describes perfectly the fact that in plasma the motions depend not only on local conditions but on the state of the plasma in far regions too. For an in depth analysis of the previously mentioned phenomena refer to [14].

In order to understand completely the phenomena that has been encountered during the experiments, some introduction on LIP (Laser Induced Plasma) is necessary. LIBS is the technique used to study the LIP phenomena when the energy of the laser focused on the sample exceeds its threshold value and plasma appears. LIP is the result of a very powerful laser beam concentrated onto one point in a sample, the heat generated is so strong that it reaches an high temperature which, as a result, will change the state of the sample in that point to plasma. The processes taking place in a laser induced plasma are many, and it is important to state that they happen simultaneously, not with a defined order. These processes are collision ionization, photo-ionization, radiative and three-body recombination, radiative decay, collisional excitation and de-excitation process. LIBS is very effective when it comes to spectroscopy of plasma over other measurements techniques for many reasons. It requires a simple procedure for samples and only a small quantity of them to run an analysis. Also can be used for conducting and non-conducting materials. On the other hand, LIBS has some disadvantages too. It has detection limits and the results are hard to reproduce. The processes cited above and the interaction of the laser with the sample and the plume expansion are the reason for these disadvantages. For a more detailed discussion on LIBS, refer to Section 2.2.4. The main parameter that is used to determine the quality of the plasma is the emitted light. The light is captured through the spectroscope in order to obtain all the information necessary to perform a spectroscopic analysis. One of the most important data that can be obtained from LIBS is the plasma temperature, which enables the understanding of the entire LIP process. [7]

2.2.2 Plasma Temperature

In the previous section it has been stated that an important parameter concerning plasma is its temperature. The word temperature might be confusing : Electron temperature? Plasma gas temperature? Molecular vibration temperature?
The term temperature which is interesting for the spectroscopic analysis performed at Test Bench P8 for the Lumen Project refers to the particular situation where the above cited temperatures, and many others, are all the same. When this happens, the plasma is in Local Thermodynamic Equilibrium (LTE).
In case Thermodynamic Equilibrium (TE) is achieved in a plasma, three equations are valid: Maxwell Distribution, Boltzmann Distribution, Saha's Distribution. [38]
This means that each process present in the plasma is in equilibrium with its corresponding reverse process. It is easy to understand that this particular situation of LTE is not achievable in measurements because of deviations and of all the processes that are running simultaneously. However, if it is possible to measure an LTE in a particular region of the plasma, the above mentioned equations can be used. The methods used to measure LTE are many, but the ones that interest the experiments carried out at DLR are the Boltzmann Method and the Boltzmann-Saha Method.

Boltzmann Method

In order to understand completely the Boltzmann Method for calculating LIP temperature a short introduction on the emissivity of a particular transition of the species in a particular area of the plasma is presented:

$$\epsilon_{nm} = \frac{hc}{\lambda_{nm}} A_{nm} N_n \tag{2.3}$$

In Equation 2.3, n and m are the upper and lower excited levels of the species observed while ϵ_{nm} , which is measured in $\mathrm{W\,cm^{-3}}$, is the emissivity. λ_{nm} is the wavelength of the transition measured in m, h is the Planck constant and A_{nm} is the transition chance of happening. N_n stands for the population of a quantum level n, it is measured in $\mathrm{cm^{-3}}$ and it is obtained solving the Boltzmann Distribution Law presented in Equation 2.4:

$$N_n = N \frac{g_n exp(-E_n/kT)}{U(T)} \tag{2.4}$$

Where g_n is the degeneracy of the population at an n quantum level, E_n is the energy of the same, measured in J, k is the Boltzmann Constant measured in $\mathrm{J\,K^{-1}}$ while $U(T)$ is the partition function. Solving Eq. 2.3 with N_n obtained from Eq. 2.4 it id be possible to write an easier form of the emissivity equation, as presented in Eq. 2.5.

$$\epsilon_{nm} = \frac{hc}{\lambda_{nm}} A_{nm} g_n N \frac{exp(-E_n/kT)}{U(T)} \tag{2.5}$$

The partition function though, it is not an easy function from which one can derive the temperature, which is the actual purpose of this method. For this reason, when it comes to experiments, the emissivity value is replaced with the intensity line I_{nm}, which is calculated by the integer of the signal on the line of sight. By selecting two separate spectra lines and correlating them Eq.2.6 is obtained:

$$\frac{I^i_{nm}}{I_{nm}} = \frac{g^i_{nm} A^i_{nm} \lambda_{nm}}{g_{nm} A_{nm} \lambda^i_{nm}} \left(- \frac{\mid E^i_n - E_n \mid}{kT} \right) \tag{2.6}$$

Where the new values I^i_{nm}, g^i_{nm}, A^i_{nm} and E^i_n are the line intensity, degeneracy, transition function and upper energy level of a different spectral line. Since the wavelength and intensity can be measured while the remaining quantum variables are calculated through different methods, it is possible to solve Eq. 2.6 for the temperature.
A more generic method that takes into account more spectral lines is called "Boltzmann Plot", which is better in terms of precision and temperature determination in the case of various spectra. The equation describing this new method is reformulated from the previous Eq. 2.5 considering only neutrals and ions as shown in Eq.2.7:

$$ln\left(\frac{I_{nm}\lambda_{nm}}{A_{nm}g_n}\right) = -\frac{E_n}{kT} + ln\left(\frac{hcN}{U(T)}\right) \tag{2.7}$$

If one plots the left part of the equation versus the upper level energy E_n the slope of the straight line found will be $-\frac{1}{kT}$. In this fashion, it will be possible to calculate automatically T without knowing the value of the partition function $U(T)$. [7]

Saha-Boltzmann Method

The Saha-Boltzmann Methods works in a slightly different way. It can describe the population distribution of two separate ionization stages of the same species. It works with the Saha-Eggart principle, which is expressed through Eq. 2.8

$$\frac{n_e N^{z+1}}{N^z} = 2\frac{U_{z+1}(T)}{U_z(T)}\left(\frac{m_e kT}{2\pi\hbar^2}\right)^{3/2} exp\left(-\frac{E_\infty - \Delta E}{kT}\right) \tag{2.8}$$

Which describes the number densities of the same species at different ionization stages, as it can be deduced by the various $z+1$ present in the equation. In the Eq. 2.8 n_e, N_z and N_{z+1}, which are all expressed in cm^3, are respectively, the electron number density, the number density of a certain ionization stage z and of the next stage $z+1$. The mass of the electron, expressed in g, is symbolized by m_e, while E_∞ represents the first ionization energy for an isolated system and ΔE is the correction of E_∞, both expressed in J, for the plasma interactions and it is obtained as follows:

$$\Delta E = 3z\frac{e^2}{4\pi\epsilon_0}\left[\frac{4\pi N_e}{3}\right]^{1/3} \tag{2.9}$$

The remaining term is $\hbar$, which is the Planck Constant ratio with 2π. Knowing all these terms, it is clear that the only terms that are isolated are the partition functions and the temperature. Combining the Saha-Eqqart Eq. 2.8 with Boltzman Eq. 2.3 and considering only the neutral atoms and the first ionization stage the Saha-Boltzmann Equation is obtained as below in Eq. 2.10:

$$\frac{I_{ion}}{I_{atom}} = 2\frac{(2\pi m_e kT)^{3/2}}{N_e h^3}\left(\frac{gA}{\lambda}\right)_{ion}\left(\frac{\lambda}{gA}\right)_{atom} exp\left[\frac{-(V^+ + E_{ion} + E_{atom})}{kT_{ion}}\right] \tag{2.10}$$

Where V^+ is the ionization potential of an atom, E_{ion} and E_{atom} are, respectively, the excitation energy of the ionic line and of the atomic line. T_{ion} is the ionization temperature which can be derived by solving Eq.2.10. A similar procedure to the Boltzmann Method for multiples spectra can be used also for this method. The equation is obtained by combining Eq. 2.8 with the Boltzmann Equation 2.7 for multiple spectral lines. The final equation is presented in Eq. 2.11

$$ln\left(\frac{I^z_{nm}\lambda_{nm}}{A^z_{nm}g^z_n}\right)^* = -\frac{1}{kT}E^{z*}_n + ln\left[\frac{hcN^0}{U^0(T)}\right] \tag{2.11}$$

Where the apex 0 is representative of the neutral atoms. The terms with the "*" superscript instead, can be easier understood if represented as:

$$ln\left(\frac{I^z_{nm}\lambda_{nm}}{A^z_{nm}g^z_n}\right)^* = ln\left(\frac{I^z_{nm}\lambda_{nm}}{A^z_{nm}g^z_n}\right) - z\,ln\left[2\left(\left(\frac{m_e k}{2\pi h^2}\right)^{3/2}\right)\frac{T^{3/2}}{N_e}\right] \tag{2.12}$$

and

$$E^{z*} = E^z_n + \sum_{k=0}^{z-1}\left(E^k_\infty - \Delta E^k_\infty\right) \tag{2.13}$$

Eq. 2.13 might seem confusing but, since the excitation energy is added to the ionization energy, the term E^z_n will have a range that is bigger than the one of the Boltzmann Plot resulting thus in a higher accuracy in determining the temperature. Since

the term $z\ ln\left[2\left(\left(\frac{m_e k}{2\pi h^2}\right)^{3/2}\right)\frac{T^{3/2}}{N_e}\right]$ present in Eq. 2.12 is dependent on temperature, the process will be iterative. The data are plotted irrespective of the newly added term initially and a start temperature value is obtained. This starting value is obtained and it is then put into the equations and a new value is calculated. The process ends when convergence is achieved. [7]

2.2.3 Plasma Transitions

Plasma, when generated, is immediately subject to ion-electron recombination. Here, the most interesting for the scope of this thesis are described in detail.

Plasma is mainly subject to:

- **Free-Free Transitions (also known as Bremsstrahlung)**
  Bremstrahlung derives from the German words *bremsen*, which means to brake, and *Strahlung*, radiation. Bremsstrahlung radiation is emitted when a charged particle is deflected by another charge. It is a phenomena that happens commonly in plasma, since it produces radiation in this fashion. The generated radiation can escape the environment without further interaction. An electron, encountering a ion on hits path, may absorb or emit a photon. Depending on this, the process will be called free-free emission (Bremsstrahlung) or free-free absorption (Inverse Bremsstrahlung). If the electron emits energy and its acceleration decreases, it is direct Bremsstrahlung, if it absorbs a photon and it accelerates, it is inverse Bremsstrahlung. Since the electron is not bound to the atom and it is free after and before the process, this phenomena is called Free-Free Transition. In the actual spectra though, it is not possible to differentiate one from the other since the spectrograph only detect a photon, it does not concern if it has been emitted or absorbed, so only Bremstrahlung will be used in the terminology for pointing out a free-free transition. [40]

- **Free-Bound Transition**
  This kind of transition happens when an electron that is bound to an atom absorbs a photon coming from another source (ionization) or when a free electron emits a photon and it is influenced by a nucleus once again (recombination). With the new energy the electron has acquired it can free itself from the influence of the nucleus leaving the atom positively charged. Recombination happens when the freed electrons emits a photons and falls back under the nucleus influence. Since the electron moves from being bound to being free or viceversa, this particular transition is called "Free-Bound Transition". [40]

- **Bound-Bound Transition**
  Bound-bound Transitions happens when an electron moves between two ions or atoms in a bound state or between different energy states. An electron orbiting around a nucleus can move from its original ground state to an higher state through excitation, or absorption of a photon, or it can fall back from an higher state to its ground state through de-excitation, or emission of a photon.[40]

The relevant transitions for this study are given by the Bound-Bound transition, represented by peaks in plots, while the Free-Free and Bound-Free transition will constitute the base. As an example of what has been just written, the following Figure 2.2 is presented. In this graph, plasma has been induced on air with the use of the Laser described in Section 1.3.

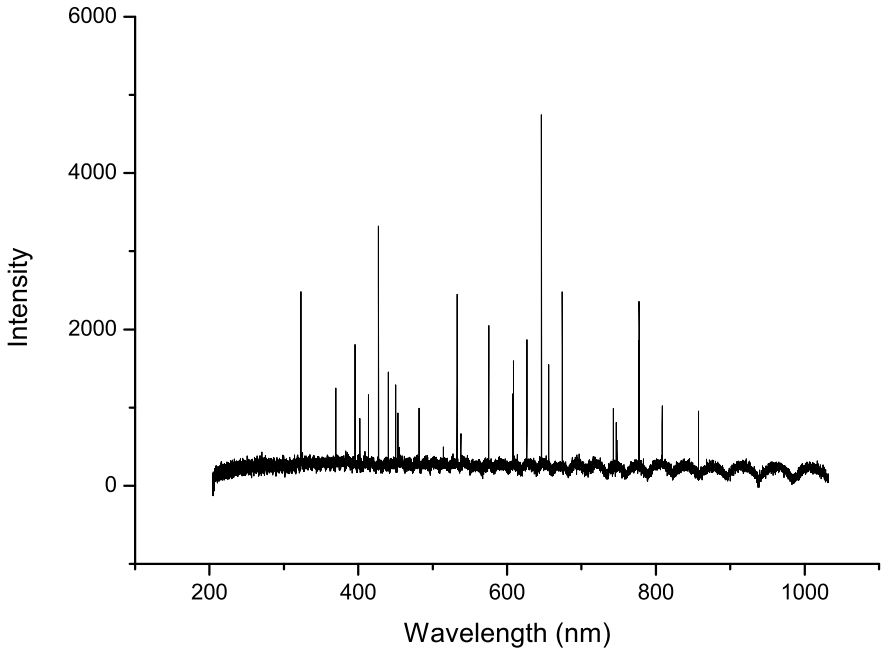

FIGURE 2.2: Plasma Induced On Air

As it is possible to see, the Bound-Bound Transitions are shown in the peaks representing the characteristic transitions of a specific element (e.g. Nitrogen, Hydrogen, Oxygen), while the Free-Free and Bound-Free Transitions compose the background. The wavy form is given by the spectrograph. [23]

2.2.4 LIBS

LIBS stands for **L**aser **I**nduced **B**reakdown **S**pectroscopy, or it can be found also under the acronym LIPS, **L**aser **I**nduced **P**lasma **S**pectroscopy. LIBS is a technique that allows to perform both a quantitative and qualitative analysis of the plasma induced in a gas, solid or liquid sample material thanks to the high energy of a high frequency laser. The absence of a preceding preparation of the samples and the simple experimental setup have allowed the use of this technique as an elementary analysis tool. The tests carried out at P8 on the Lumen Project Engine are non ablative, so there is no damage to the samples or the surroundings.

Basic setup includes a laser, target sample, optical fiber and a spectrometer. It has been already introduced in previous sections but a short detailed list that summarizes the advantages and disadvantages of LIBS are:

Advantages

- Higher Resolution over other measurements techniques
- Better Limit Of Detection (LOD)
- Neglible Sample Preparation
- Easy Setup

- Reliability
- Remote Analysis
- Stand-Off

Disadvantages

- Poor accuracy
- Results are hard to reproduce
- Uncontrolled atmosphere
- Variation in Experimental Parameters

One of the disadvantages of LIBS is, actually, an advantage. The fact that one can not control the atmosphere in which the experiment is run means that it can be potentially applied everywhere. Be it a furnace, a nuclear reactor or the combustion chamber of a cryogenic rocket, LIBS can still be used without any scientific issue. [30]
LIBS works on the principle of Optical Emission Spectroscopy (OES). OES is a well trusted analytical technique used to determine the elemental composition of a wide range of materials. OES works in the UV regime and Visible regime. A list of common elements necessary for such a device are : an Electrical Source used to excite atoms in a metallic sample in order to make it emit, an Optical system used to detect the plasma and measure the intensity of it and a Computer System. When the energy of an electrical discharge interacts with an atom, some of the electrons in the outer shell are rejected since their bound to the nucleus is weaker and they require less energy to be ejected. The ejected electrons create a vacancy, turning the atom in an unstable state. In order to restore stability, electrons from higher orbitals further away from the nucleus fall down to the lower orbital in order to fill the empty spaces. The energy excess that is released during this process is emitted as light. Every element has its particular spectral line of emission corresponding to the different electron transition between different energy orbitals. [45]
In this sense OES and LIBS have a similar working principle but the latter is not confined only to metals and it can be used in every state of the matter. Laser Induced Breakdown Spectroscopy uses, as the words suggest, a plasma as source for atomic and ionic emissions. The laser, in ablative tests, is the cause of the breakdown on the material surface and it ablates the material, resulting in a plasma. In non ablative laser experiments, the beam is focused into a point that is transformed into plasma due to the high heat. Excited species in plasma decay and emit a particular spectra through radiation processes. Since multiple species can be present in the plasma, all decaying and radiating at the same time, they overlap each other and, for distinguishing them, a monochromator or a spectroscope is used in order to separate the emitted wavelengths in individual lines that are accumulatively recorded as a spectra. This spectra is essential to understand the fundamental parameters of the plasma like electron density, plasma temperature, LTE and the composition of the ionized gas. The latter is done based on the emission wavelengths registered while the intensity provides data regarding the plasma temperature. [30]
The equations used for the determination of these parameters are the Saha-Boltzmann and Boltzmann Equation described intensively in Section 2.2.2.
LIBS then is divided into Single Pulse LIBS and Multiple-Pulse LIBS. Single Pulse LIBS (SP LIBS) uses only one powerful pulse of the laser for the formation of plasma.

It is the easiest technique between the two cited and the one used during the experiments at Test Bench P8. The instrumentation for SP LIBS does not require the alignment of optical components and, for this reason, it is very simple. Using a single pulse means that only one single plasma plume is produced and studied per each pulse. One of the greatest disadvantages of SP LIBS is the impossibility to reproduce every shot because multiple factors can alter the measurements. The most influencing disturbing factor is the coupling of the laser pulse and the sample surface which results in variations for the plasma temperature. Since SP LIBS lacks in terms of detection and precision, it is not used for quantitative analysis, but there are no limitations concerning qualitative analysis. [13]
The Laser used during the experiments at DLR is presented in Figure 1.5

2.2.5 Laser Physics

The laser used for the experiments carried out at DLR Test Bench P8 is a HiPoLas designed by CTR. This section will describe:

- The working principle of a LASER
- The stimulated and spontaneous emission relation
- The amplification, generated by stimulated emission, of microwaves
- The principal types of LASER in use

The energy levels in an atom are discrete and the lowest of them is called the ground state while the others are simply referred as excited states. As the energy of each level increases, the gap between them decreases until it becomes so small that it is not possible to distinguish an energy gap from the other, this is called continuum.

The most common form of interaction that can be found with an energy level is given by incident radiation.

The ways in which this incident radiation can interact with the energy levels are:

- **Absorption**
  Supposing to have an electron in a lower energy level orbital with a starting energy of E_i, a transition to an higher energy level will be possible if the electron is able to reach the minimum, energy threshold for the "jump" E_f. This energy can be acquired by absorbing an incident photon. A necessary condition for absorption to occur is presented in Eq. 2.14

$$v = \frac{E_f - E_i}{h} \tag{2.14}$$

  Where h is the Planck Constant and v is the frequency of the absorbed photon. If the previous equation is not satisfied, the matter becomes transparent to incident radiation and no photon absorption takes place. [52]

- **Spontaneous Emission**
  An atom will not stay in an excited state for long, if not stimulated. It will not be in thermal equilibrium with the surroundings and eventually it will return to its initial state by emission of a photon. Following a reasoning similar to the one presented in Eq. 2.14, if E_{exc} is the energy of the excited state and E_{inf} of the lower state, the frequency v of the emitted photon will be expressed by Eq. 2.15: [52]

$$v = \frac{E_{exc} - E_{inf}}{h} \tag{2.15}$$

- **Stimulated Emission**
  Stimulated emission is a phenomena that occurs when an electron in an excited energy state E_{exc} and a photon, with an energy equal to the difference between E_{exc} and a lower state E, meets. The incident photon forces the electron in the higher state to perform a transition to a lower energy state emitting a photon. This emitted photon travels in the same direction of the incident photon that caused the transition to happen. This emitted photon is traveling perfectly in phase with the incident photon in the same direction. [52]

LASER stands for Light Amplification by Stimulated Emission of Radiation.
The idea of LASERs came in 1958 to Charles H. Townes and to Arthur L. Schawlow when they realized that the effect of a single stimulated emission could be amplified to multiple atoms in order to obtain a source of light coherent (in phase and travelling in the same direction) and able to travel for long distances without losing beam width. [21]
The working principle of modern lasers is the one described in the **Stimulated Emission** point but repeated multiple times. Clarifying, one starts with one photon which hits an atom that releases consequently a photon. Now there are two photons traveling in phase in the same direction when before there was only one. These two photons may impact two different atoms generating a cascade. This simple idea can give some hints on how it works but, in reality, it is not applicable and some further analysis is needed. The reason why the example just proposed is not enough lays on the fact that the time in which an electron remains in an excited state is of approximately $10^{-}8$ s. For this reason, it is difficult to keep electrons in the excited states for a long period in order to be stimulated by a photon. The atom is more inclined to spontaneously emit a photon, which is problematic since the emission will have a random direction.
A laser can be considered as the result of the mixture of an high frequency oscillator and a resonator. The resonator, or laser cavity, is where the laser radiation can circulate.The optical resonator has a gain medium or a light amplifier within it. This gain medium amplifies the light that would have slowly faded away if the gain was not present. The laser can not operate if the gain is lower than the resonator losses. If this situation happens, the laser is said to be below the so called laser threshold and it only emits some luminescence. In the opposite case the gain is higher than the losses and the light power will quickly increase. At a fixed high value the gain will be saturated and the laser power will be constant and equals to the resonator losses. This situation is called Gain Clamping.

Some of the light inside the resonator is transmitted by the use of a partially transparent window called output coupler mirror. This ray of light represents the useful output of the laser. The parameter that indicates the effectiveness of the transfer of light through the quasi-transparent mirror is called Slope Efficiency.

Some lasers can be operated continuously, while other are operated in a pulse fashion. The latter is the type used for the experiments here at DLR.

There are many types of lasers, the most commonly used are :

- Semiconductor Lasers
- Solid State Laser
- Fiber Laser
- Gas Laser

The one that has been chosen for the Lumen Project tests is a solid state laser. Working with lasers can raise significant safety issues regarding the eyes of the operator due to the high intensity of emission and accidental eye contact. For this reason, a pair of plastic glasses are to be always on while the operations are running. [42]

2.2.6 Quantum Numbers: An Overview

The reason why quantum numbers are introduced into this thesis is due to the nature of the topic analyzed. Plasma physics, as described in the previous sections, is a complex phenomena that involves a high number of processes that can not be explained in a classical way. Some basic quantum mechanics principles, like quantum numbers, must be introduced before moving on.

Quantum numbers describe completely the behavior and the position of an electron in an atom, i.e. they describe each unique solution of the Schrödinger Equation. They are important because they can be used to determine the configuration of the electron and the possible position of the electron in the atom's shell, the ionization energy and the atomic radius. They represent the specific shell, the subshell, the orbital and spins of the electrons around a nucleus. The amount of quantum numbers used for describing those parameters is four:

- Principal Quantum Number n
  n describes the electron level of the electron. This means that it is actually symbolizing the most likely distance that particular electron has from the nucleus so the larger the number, the further the electron is. The first electron level, $n = 1$, represents the ground state and this explains why there can not be negative or zero values of the principal quantum number. The "jump" to an higher shell happens when the electron is excited by the absorption of a photon. For the same reason, if an electron is not excited it will normally come back to the ground state. The values the Principal Quantum Number can acquire range from 1 up to the last level of the atom which has an electron. [18]
  n= 1, 2, 3, 4...

- Orbital Angular Momentum Quantum Number l
  This particular number, defined analytically by the l letter, indicates the shape of the orbital and so the angular distribution. In fact, l represents the number of the angular nodes and each value represent a different orbital, which are s for $l = 1$, p for $l = 2$, d for $l = 3$ and f for $l = 4$ and so on. This number is dependent by the principal quantum number because this number can also be 0. [18] The relationship is below presented:
  l = 0, 1, 2, 3, 4, and so **l = (n - 1)**

- The Magnetic Quantum Number m_l
  The Magnetic Quantum Number m_l represents the actual number of orbitals present and their orientation. For this reason, its value depends on the Orbital Angular Momentum Quantum Number l. [18] For any l, m_l will range between $-l$ and $+l$ following:
  m_l **= -l, (-l + 1), (-l + 2),..., 0,..., (l - 1), (l - 2), l**

- Electron Spin Quantum Number m_s
  The Electron Spin Quantum Number m_s does not depend on any of the numbers described above. It indicates the spin direction of the electron, meaning that it can be $\pm\frac{1}{2}$. When $m_s = +\frac{1}{2}$ means that the spin is upward, while when it is negative it spins downward. The spin of an electron gives information

regarding the possibility for the atom to have a magnetic field or not.[18]

- Total Electronic Angular-Momentum Quantum Number J
  The total electronic angular momentum quantum number is a particular term which is introduced for the identification of a particular ion using the NIST website. It parameterises the total angular momentum of a given particle by combining its orbital angular momentum and its intrinsic angular momentum. [26] It is described as follows:
  $$J = m_s + l$$

Unique Identification of Ionization States

Since there are many ionization states for every element, it is necessary to introduce a way to distinguish one from the other.

The NIST website uses four different terms for this. The lower energy levels and the upper energy levels are described with the electron configurations deriving from the Bohr atomic model, the Term, that is simply a way of grouping the energy levels, and the J which is the Total Electronic Angular-Momentum Quantum Number. As an example, Figure 2.3 is presented. It represents the second ionization state of Carbon in a very tiny wavelength range at 426.7 nm. Marked in red is the area where the identification takes place. The first column represents the electron configuration, the one in the middle represents the term and the last one represents the J. The same applies for the upper energy level. [35]

Observed Wavelength Air (nm)	Ritz Wavelength Air (nm)	Rel. Int. (?)	A_{ki} (s^{-1})	Acc.	E_i (cm^{-1})	E_k (cm^{-1})	Lower Level Conf., Term, J	Upper Level Conf., Term, J	Type	TP Ref.	Line Ref.
426.700	426.7001	800	2.23e+08	C+	145 549.27 -	168 978.34	$2s^23d$ ^2D $^3/_2$	$2s^24f$ $^2F^o$ $^5/_2$		T3999LS	L1113
426.726	426.7261	1000*	2.38e+08	C+	145 550.70 -	168 978.34	$2s^23d$ ^2D $^5/_2$	$2s^24f$ $^2F^o$ $^7/_2$		T3999LS	L1113
426.726	426.7261	1000*	1.59e+07	C+	145 550.70 -	168 978.34	$2s^23d$ ^2D $^5/_2$	$2s^24f$ $^2F^o$ $^5/_2$		T3999LS	L1113

FIGURE 2.3: Example of Ion identification, courtesy of [35]

Following this Figure, it will be possible to note in the upcoming analysis of the peaks there will not be any mistake possibilities concerning the identification of the ionization states. They will always be listed accordingly to the previously described picture so, as an example, CII (LOWER: $2s^23d$, ^2D, 3/2 UPPER: $2s^24f$, $^2F^o$, 5/2).

2.2.7 Quantum Efficiency Curve

Quantum Efficiency is a feature of ICCDs. It is one of the most important factors when one has to determine if an ICCD is the most efficient one for the experiment or not. It is described as a curve, as shown in Figure 2.5, with Quantum Efficiency, measured in % on the y axis and wavelength (λ) (nm) on the x axis. The quantum efficiency of an ICCD will depend in the photocathode as opposed to the CCD chip that is used. A photocathode is a negatively charged electrode that when gets hit by a photon emits an electron due to the photoelctric effect. This electron is then attracted by an electric field generated by the Micro Channel Plate and it will then proceed to the optic fiber in order to produce the final output image. A scheme of an ICCD internal structure is presented in Figure 2.4.

Summarizing, it indicates how sensible the ICCD is on a given wavelength. Supposing that the QE is of 10%, it means that there is a 10% chance of detecting the

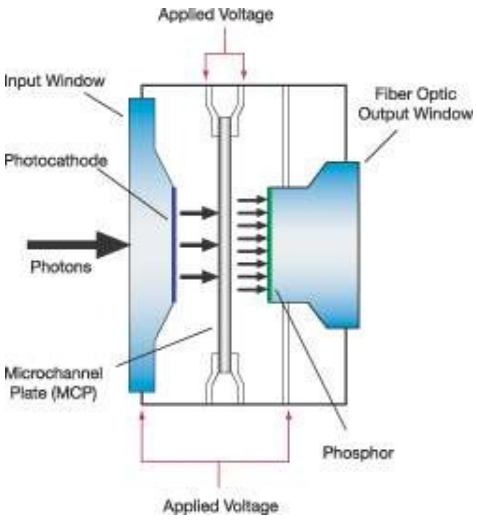

FIGURE 2.4: ICCD internal Scheme, courtesy of [1]

photon at that particular wavelength. In experiments which involve NIR or UV observations, it could be crucial to choose the right camera. The one used for all the experiments is the W-AGT photocathode presented in Figure 2.5. This means that when a spectra is captured, it must be taken into account that the quantum efficiency curve is altering the relative intensity. [6]

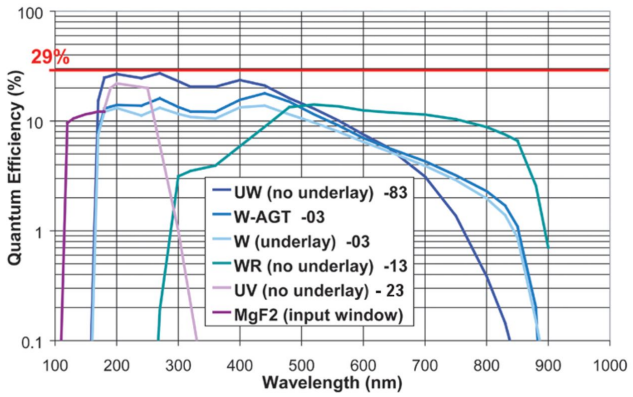

FIGURE 2.5: Quantum Efficiency W-AGT, courtesy of [6]

2.2.8 Hydrogen

Since an high presence of Hydrogen is expected, some basic notions on this chemical element are presented. This section will include the Balmer series and a short introduction on this element.

Hydrogen: An Overview

Hydrogen is a chemical element that is described in the Meneleev Table with the atomic number 1. It has a standard atomic weight of 1.008 and this gives it the title of "lightest element in the periodic table". It is the most common element that can be found in the entire Universe and it has one proton and one electron. It appears naturally as a colorless gas. Liquid hydrogen (LH2) is commonly used as a liquid

rocket fuel usually mixed together with Liquid Oxygen (LOX) and burned with vapor with traces of ozone and hydrogen peroxide as an exhaust product. LNG could be used as a oxidizer in LNG/LOX rockets, which is the case of the Lumen project. LNG is a natural gas, which is mainly formed of Methane (CH_4) with some mixture of ethane (C_2H_6), that has been cooled down to liquid form. Hydrogen is one of the most studied elements, and the vast literature that could be find about it is the proof of this ([44], [33]). Since LNG has a high presence of Hydrogen in it, it is most likely that when the tests will start, it will be possible to find high emission of it.

Balmer Series

Balmer series is the name given to six named series that describe the spectral line emissions of Hydrogen. The origin of this series is empirical and it was discovered by Johann Balmer in 1885.
Hydrogen atoms in a discharge lamp emit a series of lines in the visible part of the spectrum, which is the best definition of what a Balmer series is. The formula that describes the wavelengths measured in this way is shown in Eq. 2.16

$$\frac{1}{\lambda} = R\left[\frac{1}{2^2} - \frac{1}{n^2}\right] \tag{2.16}$$

Where n are the integers up to infinity and R is the Rydberg Constant and λ is the wavelength. Balmer Series is valid only for describing the spectral lines of Hydrogen. In 1889 Robert Rydberg discovered another empirical formula able to describe the spectra of other elements, which is presented in Eq. 2.17

$$\frac{1}{\lambda} = R\left[\frac{1}{n_f^2} - \frac{1}{n_i^2}\right] \quad n_i > n_f \tag{2.17}$$

Where n_i and n_f are integers up to infinity. The $n_i = 2$ indicates Hydrogen. Figure 2.6 represents the hydrogen spectrum lines for four main wavelengths positioned at 410 nm, 434 nm, 486 nm and 656 nm. It is significant because they represent the emissions of photons performed by electrons that transits between excited states, which is described by the principal quantum number $n = 2$.

FIGURE 2.6: Balmer Series: Hydrogen Emission Lines, courtesy of [28]

The blue lines on the far left represent the Balmer Lines for the UV regime with wavelengths between 410 nm and 434 nm. [41]

The electron transitioning from $n \geq 3$ to $n = 2$ is what characterizes the Balmer Series. The transitions are named sequentially as shown in Table 2.1:

Hydrogen-α

Hydrogen-α is a specific deep red line in the Balmer series of Hydrogen spectra. It has a wavelength of 656.281 nm and it express the transition from the $n = 3$ state to the $n = 2$ state. [50]

Transition	Name	Color	Wavelength (nm)
n=3 to n=2	H-α	Red	656.453
n=4 to n=2	H-β	Aqua	486.13
n=5 to n=2	H-γ	Blue	434.04
...	...	...	...

TABLE 2.1: Balmer Series: Main Hydrogen Transitions

Hydrogen-β

Hydrogen-β is a specific deep aqua line in the Balmer series of Hydrogen spectra. It has a wavelength of 486.1 nm and it express the transition from the $n = 4$ state to the $n = 2$ state. [50]

Hydrogen-γ

Hydrogen-β is a specific deep blue line in the Balmer series of Hydrogen spectra. It has a wavelength of 434 nm and it express the transition from the $n = 5$ state to the $n = 2$ state. [50]

2.2.9 Typical Plasma Emission Spectral Lines

In this section the typical plasma emission lines for the main elements that are found during the experiments will be presented. Those lines are quite important because referring to them, it will be possible to compare the results obtained during the experiments with these empirical data in order to have a first idea of the possible element detected. Since all elements emit at a particular frequency, comparing a spectra with the below presented plots will help identifying the nature of the plasma. The main characters in these experiments are: Hydrogen, Carbon and Oxygen. Hydrogen lines, presented in Figure 2.7, follow Balmer series lines, and it is possible to correlate the above mentioned Figure to Table 2.1. It has to be noted that the intensity axis is represented by arbitrary units (Counts).

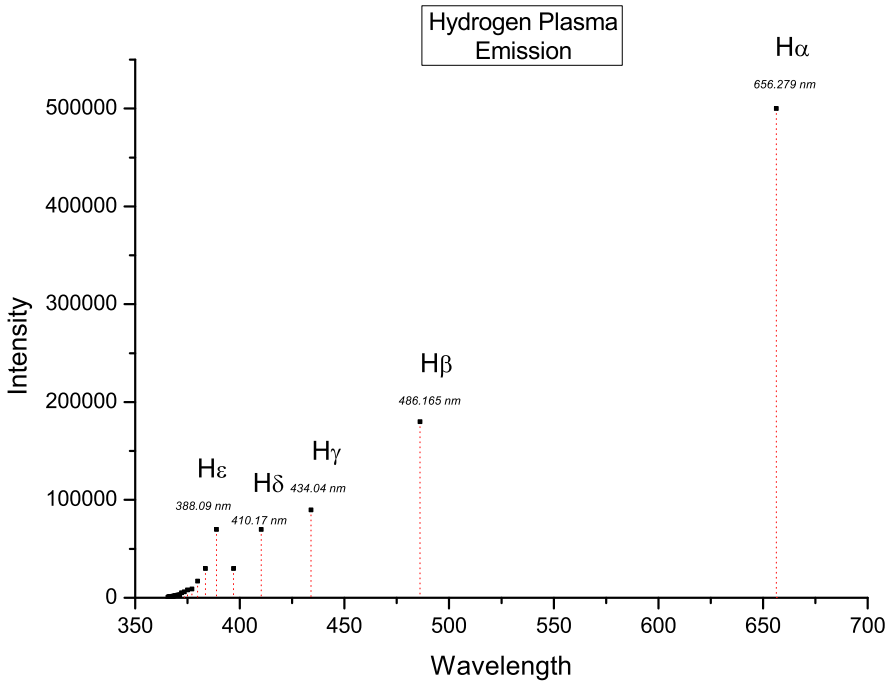

FIGURE 2.7: Hydrogen Plasma Lines

In Figure 2.8 are represented all the emission lines for the various ionization levels of Carbon. The first one, the second, the third and the fourth are displayed since they are the most likely to be encountered during the experiments.

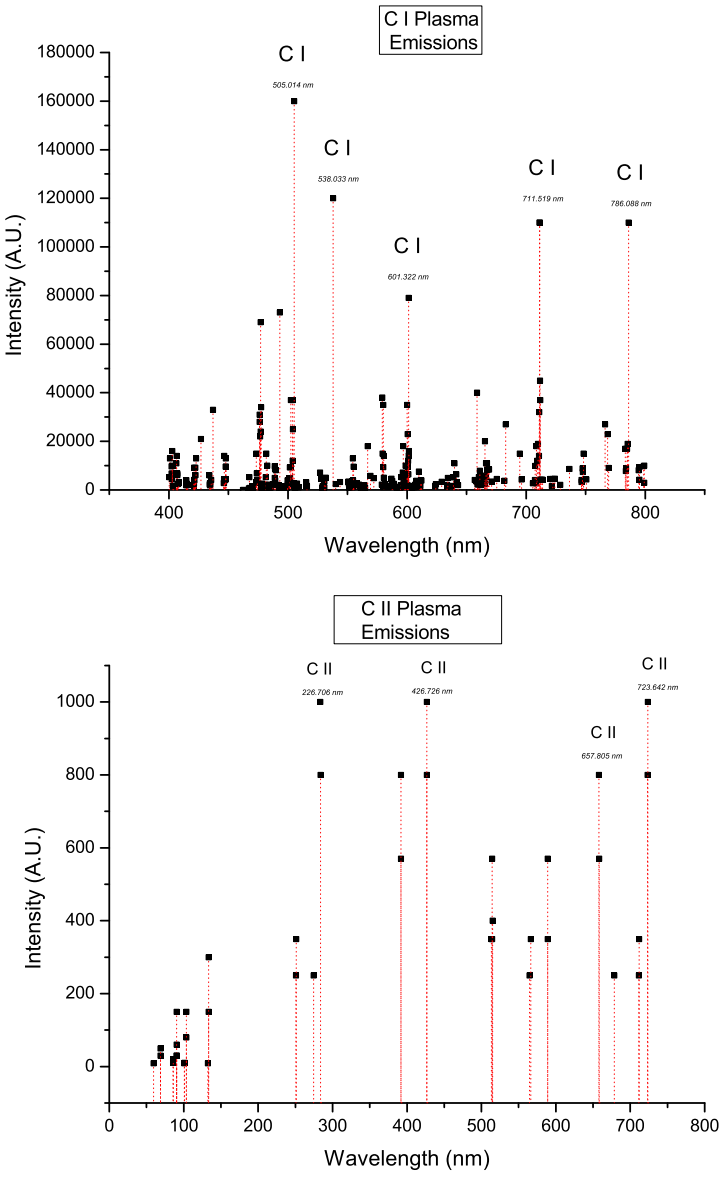

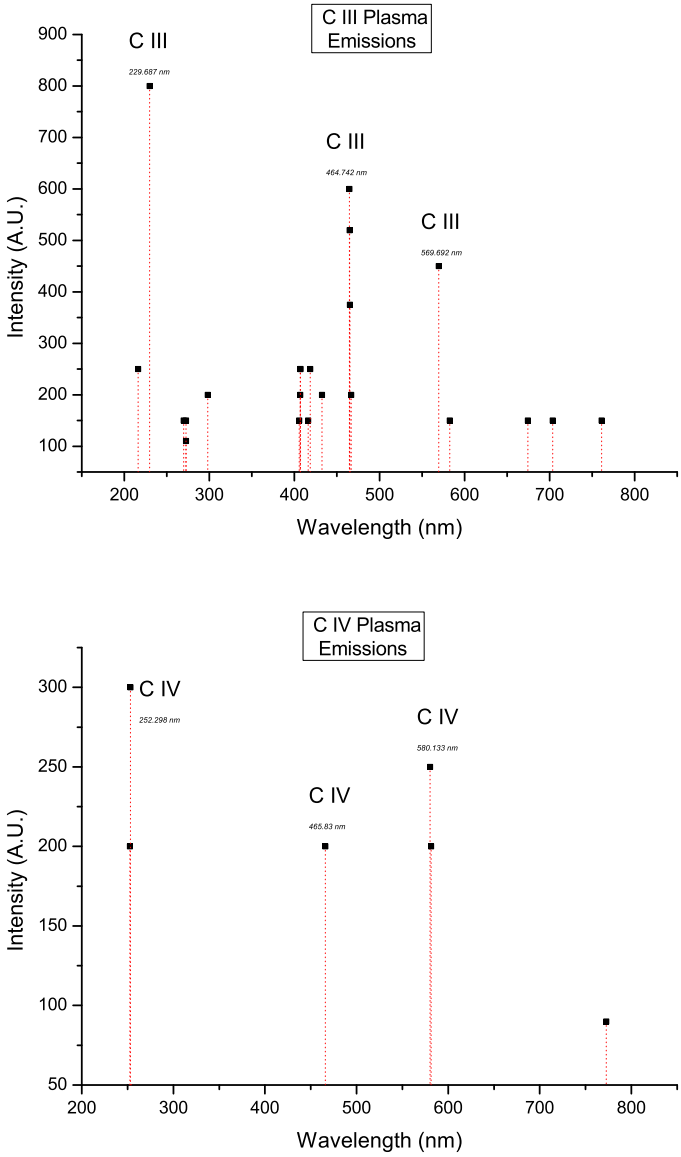

FIGURE 2.8: Carbon Plasma Emission Lines

Concerning Oxygen, Figure 2.9 shows the spectral lines of oxygen for each ionization state.

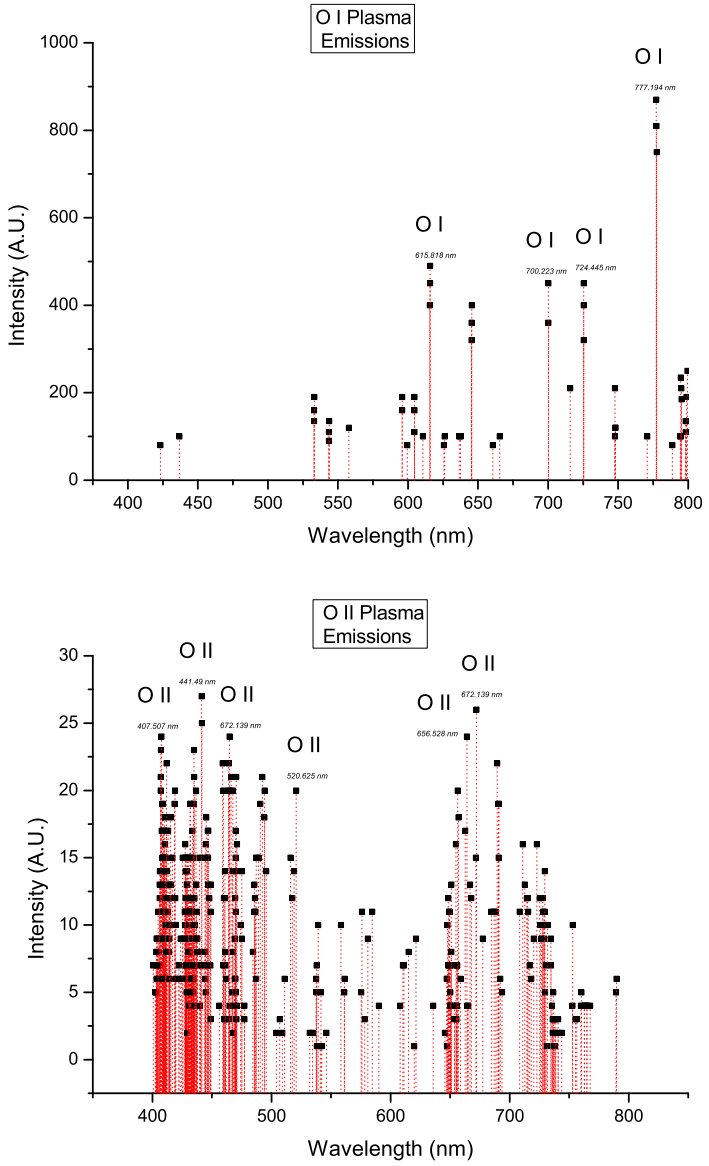

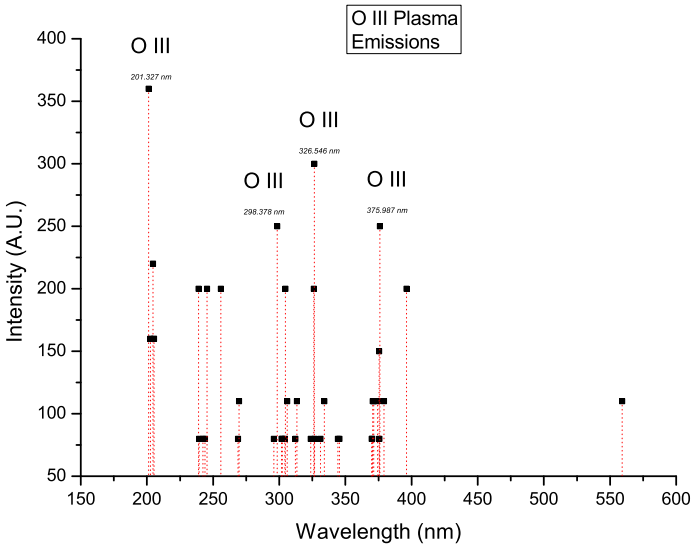
O III Plasma Emissions
O III
201.327 nm
O III
326.546 nm
O III
298.378 nm
O III
375.987 nm
Intensity (A.U.)
Wavelength (nm)

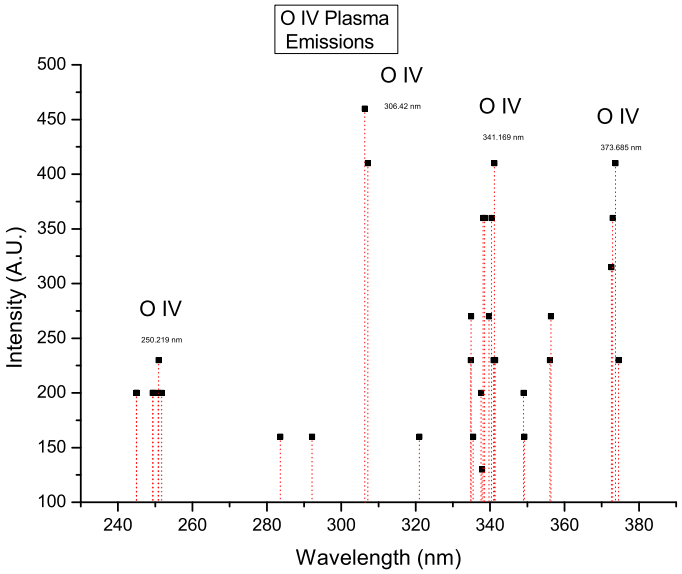
O IV Plasma Emissions
O IV
306.42 nm
O IV
341.169 nm
O IV
373.685 nm
O IV
250.219 nm
Intensity (A.U.)
Wavelength (nm)

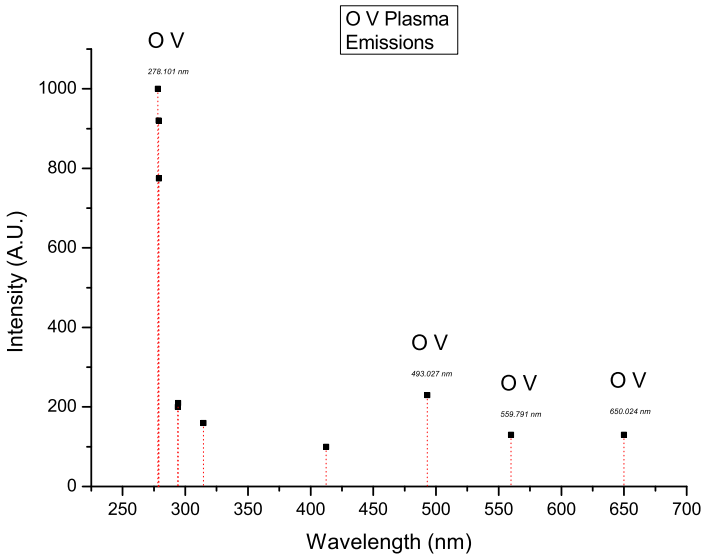

FIGURE 2.9: Oxygen Plasma Lines, NIST Data Website

From The Spectra to the LTE Measurement

The procedure that will be used during the Lumen Project tests is introduced. Further details are given in Section 3.5. Once the LNG and LOX are introduced into the combustion chamber, the laser will start the ignition. The high energy carried by the laser will ionize the gas turning it into a plasma. This plasma will be detected by the fiber glass present inside the combustion chamber, which will carry the signal to the spectrograph placed far from the rocket engine, which will consequently be triggered. The spectrograph prism will then diffract the light in multiple lines that will be recorded by the camera. The data will be stored on a laptop in an *.ascii* format. This kinetic series recorded will then be studied by the user in order to acquire information about the processes in the chamber. The data from this will then be analyzed taking into account the Transition Probability (A_{nm}), the Degeneracy (g_n), the Energy Levels of the excited states (E_{exc} and E_{inf}) and the Relative Intensity (I_{nm}). They are needed to find at least three excited state of the same element in a single spectra. Once this has been done, it will be possible to proceed using the Boltzmann equation to see if any LTE-like phenomena has been recorded. The quality of the spectra is something that the user needs to take into account. Once the perfect spectra is detected, some filtering to refine the result is performed and then the intensity value is used to calculate the Boltzmann-plot with Eq. 2.7. The results will be the temperature values and, if the values measured for the observed elements (e.g. Hydrogen Balmer Series) are linear, the LTE condition has been recorded and the experiment can be considered satisfactory. Since high emissions are expected from Hydrogen, it is useful to have an idea of how the ideal slope should look like in Figure 2.10.The hydrogen wavelengths taken into account are exactly the Balmer Series ones.

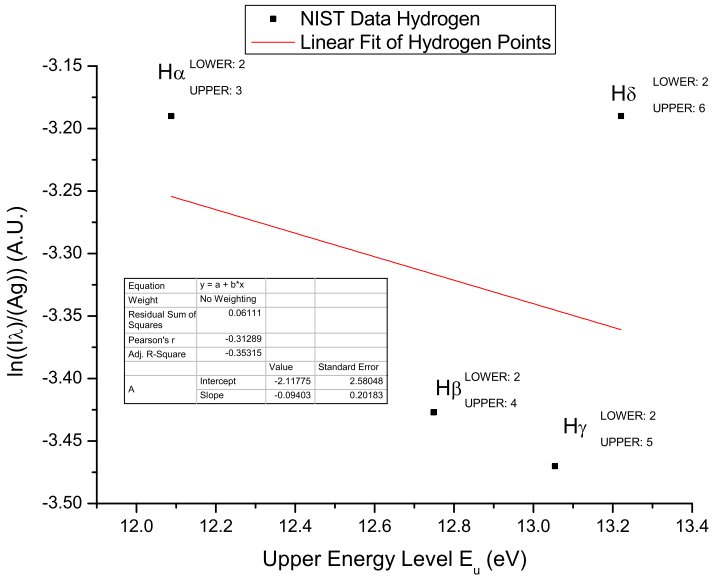

FIGURE 2.10: Boltzmann Plot: Ideal Hydrogen Fit (NIST Data Website)

Taking the data regarding the degeneracy and the transition probability from the NIST database, it is possible to calculate a Boltzmann Plot using Eq. 2.7. In Figure 2.10 the results are presented. It is remarkable to not how the slope value m is used

to calculate the plasma temperature via the following:

$$m = \frac{1}{kT} \tag{2.18}$$

Equation 2.18 uses the Boltzmann Constant expressed in eV/K to calculate the temperature of the plasma thanks to the slope inclination.

According to the closeness of the points to linear fit, it is possible to estimate the precision of the temperature obtained. The plot presented is not in good LTE conditions since the data points are set far from the slope. The reason why is because the dataset of the NIST website is not compiled for LTE measurements but for general spectroscopy.

It may be useful to have an idea of the ideal fit for both Carbon and Oxygen since they are the remaining elements present in the combustion chamber. In Figure 2.11 the Carbon fit is shown while Figure 2.12 shows the Oxygen fit. The wavelengths taken into account are 505.21 nm for C I, 426.7 nm for C II and 580.133 nm for C IV.

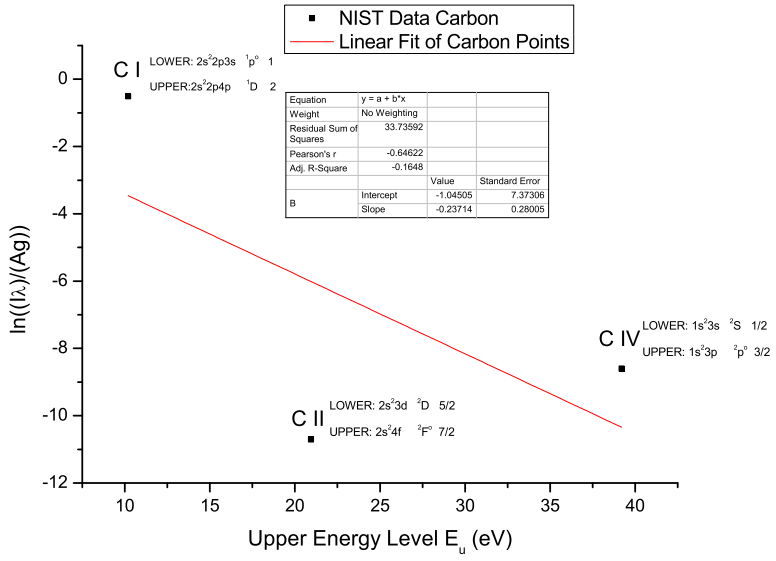

FIGURE 2.11: Boltzmann Plot: Ideal Carbon Fit (NIST Data Website)

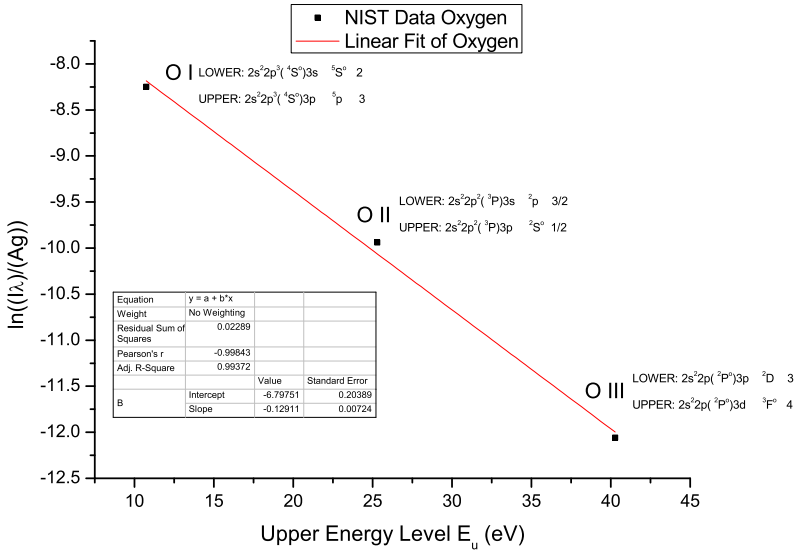

FIGURE 2.12: Boltzmann Plot: Ideal Oxygen Fit (NIST Data Website)

2.2.10 Organic Flames

Even if the flames of the Lumen Project are not studied in this thesis, some basic notions on the combustion products and propellants are introduced.
Organic flames are generally the result of the combustion of LOX and Methane. The literature with this mixture of propellant is vast and the working principle is well known and understood like [48] explains in detail. LNG/LOX literature however is not so big, probably because it is an innovative technique. Its applications in space propulsion vary from service module thrusters, descent vehicle thruster to upper stages. This technology is currently the center of a deep international study for its future uses on a possible Mars colony [15]. It is low cost, high thrust and able to perform re ignition.

LNG

LNG stands for **L**iquefied **N**atural **G**as. It is a natural gas in liquid form. Being a liquid natural gas means that it is composed of Methane (CH_4), Ethane (C_2H_6) and other gases in smaller quantity, that have been cooled down to 110 K. LNG it is not explosive and it will stay in liquid form at ambient pressure if stored at the above mentioned temperature. [27]

LOX

LOX is the liquid form of Oxygen. It is a cryogenic oxidizer propellant that can be used together with LNG, Liquid Hydrogen and Kerosene [9].

2.2.11 Error Estimation

The estimation of the error that occurs in the determination of the temperature is widely discussed in literature. The scientific community agrees on pointing out that the temperature determination error is primarily caused by the uncertainties of the

transition probabilities and the statistical errors coming from the line intensity measurements.[7] [8] [39]

2.3 Vulcain 2.1 Theory

2.3.1 Flame Emission Spectroscopy

Flames are the most visible result relative to a combustion process. Each flame has its own specific spectra dependent on multiple factors not only related on the propellants used [25]. Since multiple factors comes into play when it is time to define the emission of a flame, it is difficult to give an exact definition of how to perform a spectroscopic study of the flame. This is because radiation is dependent on temperature, wavelength, gas mixture, gas/oxygen mixture ratio, gas purity, burner type and many more. There are many types of combustion flame, they can be classified based on the emission spectra. The main emission spectra are : Line Spectra, Band Spectra and Continuous Spectra. [51]

Line Spectra

The lines found in this spectrum are emitted or absorbed by free atoms. In this way, each line represents a transition of an electron to another energetic state.

Band Spectra

Band spectra difference with the previous one is given by the fact that the electronic change of state is accompanied by simultaneous changes in the internal vibrational and rotational energy of the molecules, giving rise to a number of bands.

Continuous Spectra

Continuous spectra are due to transitions in which one of the states involved in the combustion process is unquatized, having thus free kinetic energy. In this way, referring to a continuous spectra, one will use the terms ionization, dissociation and association instead of absorption and emission.

In this thesis, when a spectra will be shown it will always be a Line Spectra (Lumen Project) or a Band Spectra (Vulcain 2.1). The Lumen Project is an organic flame, given the presence of methane or LNG and it is not studied, while the Vulcain 2.1 flame is an Hydrogen flame and it is deeply analyzed. The study of the flame spectra for the above cited typos is related to the emittance or absorbance radiation. These radiations are expressed through the wavelength of the photons emitted/absorbed.

2.3.2 Hydrogen Flames

The main characters present in hydrogen flames are OH^* at 310 nm and blue radiation, which is a continuum of radiated wavelengths with peaks at around 450 nm [51]. OH^* derives from the chemiluminescent reaction given by Eq. 2.19:

$$O + H \rightarrow OH^* \tag{2.19}$$

other possible reactions are presented in Eq. 2.20, 2.21:

$$O_2 + H \rightarrow OH^* + O \tag{2.20}$$

$$OH + (O)H + H \rightarrow OH^* + H_2O \tag{2.21}$$

Eq. 2.21 is of importance because it points out that OH^* can be obtained even when, from the ground state, it is involved in recombination processes as a third agent, which is a situation that can easily occur inside a combustion chamber [51]. The combustion of hydrogen and oxygen is so mainly used because of its high efficiency for liquid propellants rockets. Ideally, in these flames, only molecules from hydrogen and oxygen will be recorded by a spectrometer. It is remarkable to state, even comparing the different Figures presented in Section 5.2 that OH^* is not as sensible as blue radiation to pressure changes. Further information on the dependence on pressure of blue radiation can be found at [47].

OH*

OH^* is the hydroxil radical and it is the neutral form of the hydroxide ion. This radiation comes from the spontaneous transitions of the first electronically excited state of the hydroxyl to the ground state [47]. As mentioned before, the wavelength at which it can be visualized on a spectra is approximately at 310 nm. It is the clearest radiation of flames in the UV regime and the constant product of a combustion containing hydrogen [22]. OH^* is in thermodynamic equilibrium at approximately 2700 K [24] while the radiation from colder flames is caused by chemiluminescence, which, as stated above, is the emission of light as the result of a given chemical reaction.

Blue Radiation

Blue radiation is a particular term which refers to a continuum part of the spectra of hydrogen flames with broad peaks at approximately 450 nm. It is clearly in the visible regime and, as stated in [47], it it dependent on the pressure of the combustion chamber. This last notion is the reason why in the Figures presented in 5.2 the continuum spectra of the visible regime is changing. In contrast to OH^* radiation, little information is available on the blue radiation of hydrogen flames [47]. It is thought to be a chemiluminescence reaction, but it is only a possibility. Further information can be found at [22].

Chapter 3

Experiments

3.1 State Of The Art: Lumen Project

Laser Ignition in combustion chambers is an innovative and efficient technology. DLR applies laser ignition for the Lumen project. The use of lasers in combustion chambers is 20 years old and in the past decade it has gain importance in Space Propulsion [37]. It is attractive because of the precise timing and simplicity of execution if compared with other ignition system (e.g. sparky plug ot pyrotechnical devices [47]). A core development was the production of miniaturized Q-switched solid state lasers. This was necessary in order to produce low weight and robust laser system capable of being applied in Space Systems. In recent years, at the test bench M3.1 of the DLR Institute for Space Propulsion, laser ignition of a single and a five coaxial injector configuration of a research thruster has been successfully tested with hundreds of ignitions performed for high altitude injection conditions for two propellant combinations, liquid oxygen and gaseous hydrogen (LOX/H_2) and liquid oxygen and gaseous methane (LOX/CH_4) [37].Once these experiments gave satisfactory results, more research was necessary to develop this technology in order to be used for large cryogenic engines. To achieve this goal, a test campaign at Test Bench P8 has been carried out to investigate on the perks of laser ignition on rockets as well as to demonstrate the feasibility of this idea. The basic setup for the experiment is composed of a conventional 15 coaxial injector head, a segmented cylindrical combustion chamber with an inner diameter of 50 mm, a nozzle with a diameter of 33 mm. The propellant used back then was a LOX/H_2 while the combustion chamber was composed of 5 watercooled segment. Those segments were an igniter, which included two inputs for for a different mounting position of the laser, 3 ports for optical analysis via spectrometer, 2 dynamic pressure sensors, a spectrometer and the nozzle.[12]

The laser used is the same used for the LUMEN Project, so it was a HiPoLas developed by CTR AG which was mounted directly on the combustion chamber. It used 50 mm focal lens for focusing the laser beam on the shear layer of LOX and LNG. The focal point was placed in proximity of one of the coaxial injectors. The trigger system and the optical probe were connected via glass fiber with the spectrograph. A picture of the overall setup for this experiment is presented in Figure 3.1.[11]

In the course of this previous test, more than 400 ignitions have been registered. This is the final proof for the feasibility and simplicity of laser ignition for cryogenic rocket engines. It is remarkable to underline that the same engine has been re-ignited more than 60 times, proving also that this ignition methodology is also capable of reignition of upper stage rockets. [12]

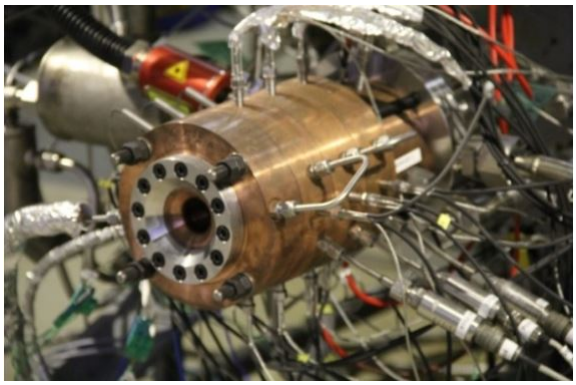

FIGURE 3.1: State of the Art: Previous Test Campaign at Test Bench P8. Courtesy of [12]

3.2 State Of The Art: Vulcain 2.1

The new Vulcain 2.1 represents the pinnacle of rocket engine technology of Arianegroup for carrying Ariane 6 to space in 2020. It is intended to outcome its previous ancestors in terms of reliability and costs. The Vulcain 2.1 must show its capability of surviving temperatures of approximately 3000 K in the combustion chamber, high rotational speed of turbopumps and to withstand the pressure given by the propellant lines together with the delivery of the necessary thrust. Its predecessor, Vulcain 2, was used on Ariane 5 as the main stage rocket engine and was able to carry out more than 70 flights. The state of the art of the Vulcain 2.1 derives directly from the Vulcain 2. It is basically the same engine but re-designed in order to prove itself to be cheaper, more reliable and able to be produced in series. The main differences with the predecessors are a gas generator, a simpler nozzle, a combustion chamber that can be ignited by the ground support system and an oxygen heater for tank pressurization. The reason why Arianegroup decided to re-design an existing rocket engine was taken after an ESA Meeting in December 2014. It was done in order to adapt to the growing competition of other agencies/companies. Tests will try the engine at its own limits, higher temperatures, higher pressures and different ROF [36].

3.3 Facilities

The facilities in which the tests have been run is the Test Bench P8 for what concerns the plasma analysis and the Test Bench P5 for what concerns the flames emission spectroscopy performed on the Vulcain 2.1 engine.

3.3.1 Test Bench P5

Test facility P5 was built between April 1988 and July 1990. In the period from 1990 to 1996, the development tests for the Vulcain engine of the cryogen main stage for the European carrier launcher Ariane 5 were carried out here. Acceptance campaigns for aircraft engines were run on P5 between 1996 and 1998. From 1999 to 2004 development tests for the enhanced Vulcain 2 engine were done here. Currently and in the future, P5 serves and will serve for flight-accompanying campaigns for the Vulcain 2 engine tests. At the moment, test facility P5 is converted to the new main stage engine Vulcain 2.1. The upcoming Ariane 6 will use this engine. [43]

3.3.2 Test Bench P8

The Lumen Test Camapign at DLR Test Bench P8 uses a mixture of Liquefied Natural Gas (LNG) and LOX as propellant. LNG is a natural gas that is mainly formed of Methane (CH_4) with some mixture of ethane (C_2H_6) that has been cooled down to liquid form. Refer to Section 2.2.10 for further information. Test Bench P8 was built in 1993 by DLR with the financial support of the German Government together with CNES, DASA and SEP [34]. This test bench is able to supply a combustion chamber with propellants delivered at high pressure up to 360 bar. The supplier is able to withstand a delivery of a maximum of $5\,\mathrm{kg\,s^{-1}}$ of LNG and $8\,\mathrm{kg\,s^{-1}}$ of LOX. It is able to supply gaseous hydrogen, if needed, at both a warm state or cold state. with the ability of substituting LNG with LH2 or Methane. There are two many more building in the P8 Test Bench named P8.1 and P8.2 actually operational and a new one, P8.3 is currently being built. All these three structures can be operational up to 100 days each year, assuring an high availability for testing activities. In the control room of the P8 the tests can be observed from a safe distance and operators are able to modify parameters while the experiment is running. [17]

3.4 Equipment

Equipment For The Lumen Project

The equipment needed for the Lumen Project are:

- Mechelle 5000
- HiPoLas Laser 1064 nm
- iStar sCMOS 18 F 03
- Glass Fiber
- FOFMS Filter
- BNC Cable
- Laptop

Equipment For The Vulcain 2.1

The equipment needed for the Vulcain 2.1 are:

- Shamrock SR-163
- ICCD DH720 Gen II
- Glass Fiber
- FOFMS Filter
- BNC Cable
- Laptop

3.5 Procedure

3.5.1 Procedure For The Lumen Project

The procedure used for all the experiments relative to the Lumen Project are presented here. In Figure 3.2 are shown the guidelines and milestones to be surpassed at every measurement.

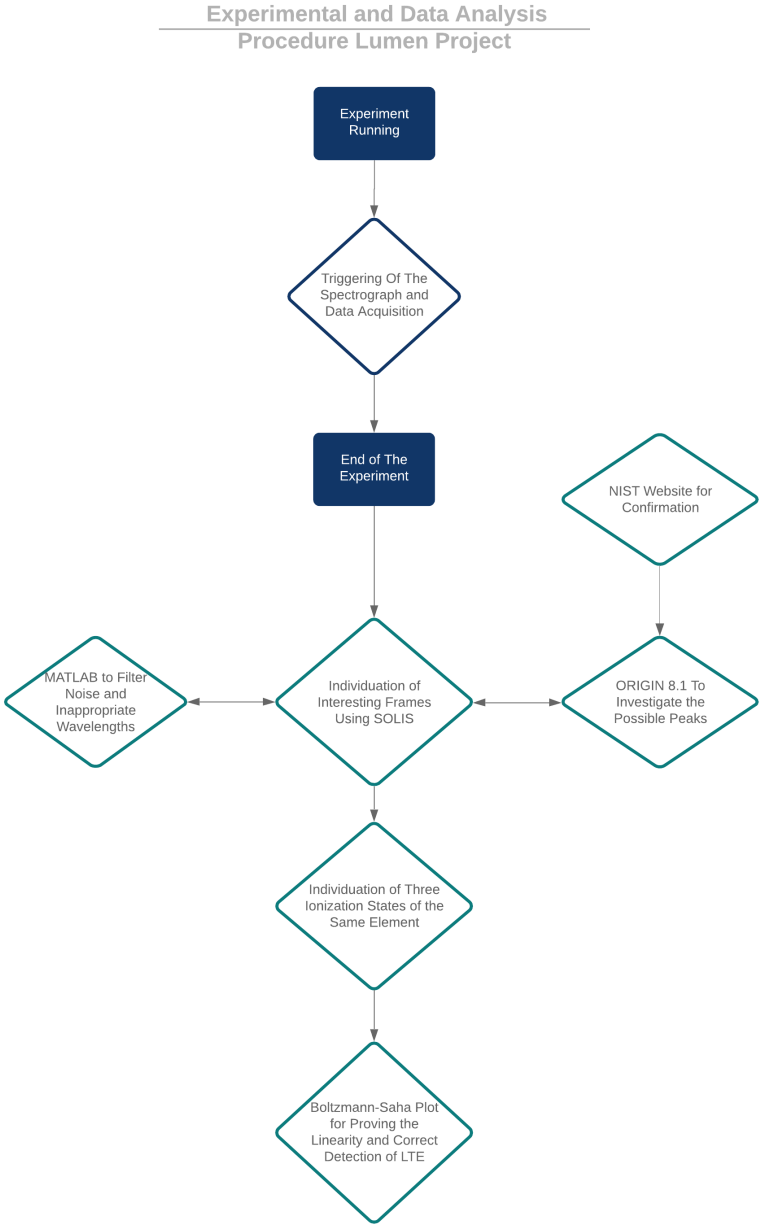

FIGURE 3.2: Procedure Flowchart For the Lumen Project

The most important step to be done happens even before the experiment starts. It is the calibration of the spectrograph. If the spectrograph is slightly off calibration, the user will not be able to perform a correct analysis of the results because, since every elements emit on a fixed wavelength, if the spectrograph has been set up with an error of 1 nm what is thought to be , as an example, H_α could be CuI in reality. The calibration is performed correctly thanks to a Hg(Ar) with a known spectra. Once the experiment has started, the spectrograph will be automatically triggered at the first plasma detection and the data acquisition will start, all *.sif* files are saved automatically in the designated folder of the user. The pulses generated by the laser were emitted once every 20 ms, the spectrograph is then triggered by the detection of the 1064 nm wavelength and the recording of the plasma starts. The Mechelle 5000 is triggered following the sketch presented in Figure 3.3. As it is possible to see, the laser is directed towards the combustion chamber. When the laser excites the propellants in the combustion chamber, it will emits photons. These photons will then be detected by the glass fiber placed right close to the laser head. These photons will be carried to the FOFMS optic filter, this is done because the spectrograph must be triggered only by the laser and, given an exposure time, it will start the recording after this condition has been satisfied. Once the photons have been filtered, a converter will read that the laser has been activated and it will turn the photons into rectangular 5 V waves that will be carried to the spectrograph via BNC and the recording will start. During the experiment, it will be possible to see the spectra live. When the

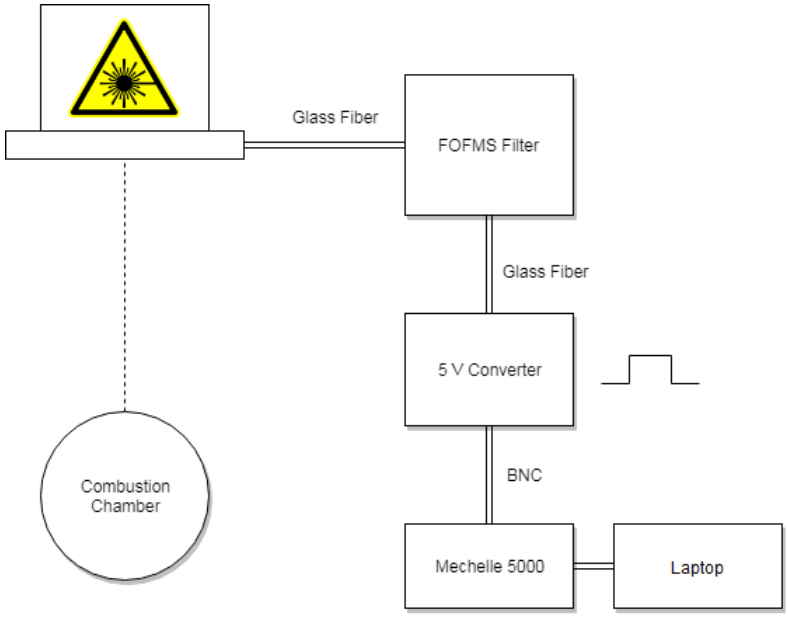

FIGURE 3.3: Hardware Setup For the Lumen Project

experiment is concluded, the analysis of the data can begin. Using *SOLIS*, which is a designated software for Spectroscopy developed by Andor Technology based on their equipment, it will be possible to isolate and study single frames. Once a list of the most likely LTE frames have been detected, MATLAB comes into play in order to filter the frames concerning the noise derived from the spectrograph and from the Bound-Free and Free-Free Transitions. Once this has happened, only the peaks of the Bound-Bound Transitions will be shown together with the baseline. Depending

on the spectra, the user could prefer to have just a reduced wavelength (E.G. only H_α is wanted) and to do so, it will be possible to use the code *reducedwavelength.m* file attached in the Appendix A.1.3. When the peaks have been found, the file containing the baseline together with the peaks can be moved to ORIGIN 8.1 where they will be plotted. With the features of this program it will be possible to detect the peak's wavelength and, together with the NIST website, it will be possible to determine the element and its ionization state. *NIST* stands for *N*ational *I*nstitute of *S*tandards and *T*echnology. In the moment three ionization states of the same element have been found, there is a very high chance of having detected an LTE. In order to prove this, the use of a previously written code at DLR to automatically solve and plot the Boltzmann plot will be necessary. This particular code is an automation of calculus for solving the Equations presented in Section 2.2.1. In order to do so, the code will require from the user to input all the data useful for the solving e.g. Transition Probability, Degeneracy etc.

If the Boltzmann Plot is solved, the Figure obtained will ideally be a three dots graphs with a line intersecting them, demonstrating the linearity of it and the correct detection of an LTE measure. The next useful step will be the evaluation of the temperature.

3.5.2 Procedure For The Vulcain 2.1 Hotrun

In this section the procedure for the equipment of the Vulcain 2.1 hotruns is presented.

The tests are observed by a bunker at a safety distance from the engine's high noise close to test bench P5 or in remote, through internet connection on a laptop that is linked to the spectrograph. The procedure applicable for every test run presented in this thesis is shown in Figure 3.4.

As it is possible to see, there are only small differences from the Lumen Project procedure presented in Figure 3.2. This experiments do not investigate LIBS or other plasma phenomena but they investigate on flame emissions from a main stage rocket engine. Once the experiment is running, the spectrograph, which is placed in a shielded box outside the nozzle, will be triggered by the high emissions of photons generated by the plume and it will start recording. The user then will be connected to the spectrograph and will be able to have a live feed of it. All the spectra captured are automatically saved on the designated folder and a copy is instantaneously created in order to avoid accidental loss of data. Once the experiment has ended, the analysis part takes place. With the aid of SOLIS, it is possible to study frame per frame the entire run. Changes in the ROF of the test can for example be detected by observation of sudden variations in the relative intensity of the main elements.

Once this has been done, a time table of the multiple time steps encountered is created in order to place the various events at the correct point in time.

Furthermore, MATLAB is used to isolate a single (or more) wavelength during the entire run to have a detailed analysis of the emission of an element during the different phases of the hotrun. When the dataset is ready, ORIGIN 8.1 is used to plot the results. Sequentially, a power point presentation is prepared to present the complete spectroscopic analysis of the plume to ArianeGroup staff members.

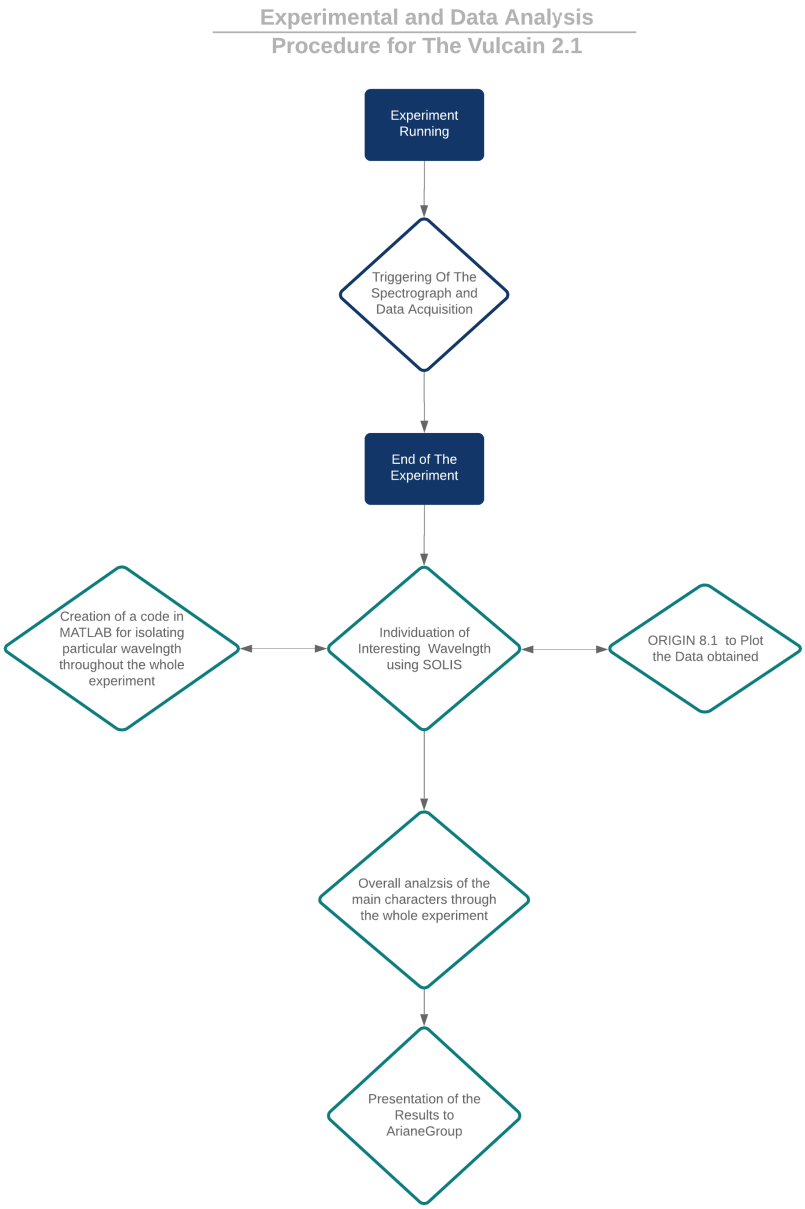

FIGURE 3.4: Procedure Flowchart For the Vulcain 2.1

3.6 Setup

Setup For The Lumen Project Recordings

The Lumen Project hardware flowchart has been introduced in Subsection 3.5.1. In this section the setup will be analyzed with the aid of real laboratory figures. All the tests performed concerning the Lumen Project took place in Test Bench P8, which is presented in Figure 3.5.

FIGURE 3.5: Test Bench P8, courtesy of DLR Lampoldhausen

In the designated test room, the Lumen Project Combustor is assembled as Figure 3.6 shows. In this picture, it is possible to see the combustor during a pressure test. This can be deduced by the fact that the nozzle is sealed. In Figure 3.7 the current

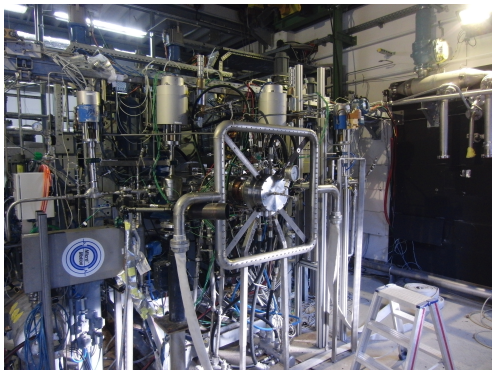

FIGURE 3.6: Lumen Project Combustor, courtesy of DLR Lampoldhausen

design of the whole combustion chamber and nozzle part is shown. The red cable represents the glass fiber and, following its path, it is possible to note how it ends just below the laser in order to catch the 1064 nm photons emitted by the CTR HiPoLas. The CTR Laser is fixed to the combustion chamber external plate and it has a direct link to the injector plate in order to stimulate the combustion.

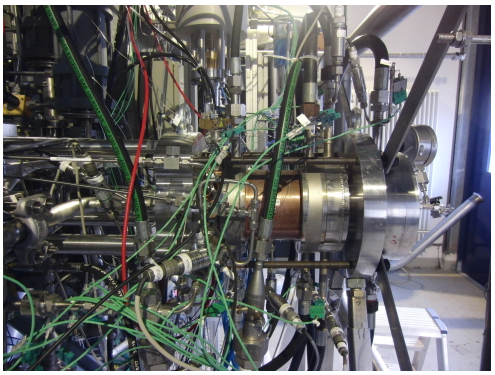

FIGURE 3.7: Lumen Project Combustor Closer View, courtesy of DLR Lampoldhausen

In Figure 3.8 the application of Figure 1.4 is presented. The black cable on the top left is the output pin port. The brown/orange cable is connected to the triggering system and black cable with the two metallic pins is connected to the computer. The alluminium cable is connected to the Mechelle 5000 for syncronization.

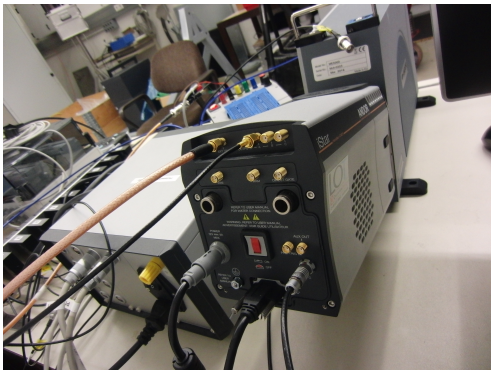

FIGURE 3.8: Lumen Project sCMOS, courtesy of DLR Lampoldhausen

Setup For The Vulcain 2.1 Recordings

The setup for the Vulcain 2.1 recordings involved the Shamrock SR-163 as a spectrograph and the ICCD DH720 Gen II as a camera.
The spectrograph was triggered before the ignition remotely and started recording the emissions of the plume. It is calibrated for recording without stopping for the whole duration of the experiment, automatically saving the data in the user's folder.

Chapter 4

Results

This Chapter describes in detail the experiments performed on the Vulcain 2.1 and the Lumen Project engines with a brief description of the results. A more detailed discussion will be carried out in Chapter 5. The Vulcain 2.1 tests were carried out at the Test Bench P5 while the Lumen Project tests were implemented at the Test Bench P8.

4.1 Vulcain 2.1

The experimental results obtained by the spectroscopic observation of the combustion flame of the above mentioned engine are linked to plume spectroscopy. This means that the spectrograph will be able to detect molecules and not only single elements. The results are important for all the information that they bring to Arianegroup concerning the operational status of the Vulcain 2.1. First the Vulcain 2.1 results are presented, the Lumen Project ones follow.

Before the analysis, a short summary of the wavelength regimes interested is presented in Table 4.1. The acquisition frequency is 10 Hz

TABLE 4.1: Wavelength Regimes

Name	**Range (**nm**)**
UV	120-400
Visible	380-740
NIR	780-2500

4.1.1 First Hotrun Test on Vulcain 2.1

The test consisted in a spectroscopic analysis of the flames of the Vulcain 2.1. The expected results consist in emission lines of the OH^* spectra.
$OH^*$is present at approximately 330 nm in the UV regime while Copper (Cu), has been recorded for the whole duration of the combustion at 543 nm.

Only the major events have been listed in Table 4.2.

TABLE 4.2: Major Events of the first Vulcain 2.1 Hotrun

Time	**Event**	**Notes**
t_0	Start of the Ignition	Immediate emission of OH^* at $\sim$ 330 nm and Copper at $\sim$ 543 nm
$t_0 + 8s$	Increase of Intensity in the Visible Regime, Most likely caused by an higher pressure flame	
$t_0 + 13s = t_1$	Visible regime is stronger than UV and NIR in Intensity	$\sim$450 nm peaks in the visible wavelength
$t_1 + 3s$	Combustion seems to proceed stably	OH^* and Copper are the main characters in the spectra
$t_1 + 4s$	OH^* almost disappeared	Possible Change in ROF
$t_1 + 4s - 120s$	High Emissions in the Visible regime.	OH^* still present in high quantities
$t_1 + 120s = t_2$	Combustion seems to be exhausted.	Really low countings, if compared to previous frames.
$t_2 + 10s = t_3$	Low rise in the Visible Regime	OH^* and Copper intensity unchanged throughout the whole process
$t_3 + 100s = t_4$	Visible regime counts are really high (1.0×10^4)	OH^* unchanged, Copper spectral lines low.
$t_4 + 90s = t_5$	Peaks on Copper	Possible Change in ROF
$t_5 + 40s$	Increase of OH^* in counts and in Copper	Visible regime is really low in intensity
$t_5 + 54s = t_6$	Increase in OH^*	Decrease in Visible light regime, Cu slightly increases
$t_6 + 70s$	Highest peak in OH^* (1.6×10^4)	
$t_6 + 101s = t_7$	Visible regime and NIR regime almost null	OH^* is still very intense in counts
$t_7 + 1s$	NIR starts rising sligthly	
$t_7 + 155s = t_8$	Combustion proceeds normally	
$t_8 + 76s$	Still peaks of OH^* and Copper	Visible regime at zero, combustion has ended.

The point of the spectroscopic analysis is that Arianegroup is interested in the spectra measured by the Shamrock in order to understand the overall efficiency of the engine. OH^* is a residual of the combustion process that is ejected by the nozzle. It is the result of chemical reactions or thermal collisions [47]. Depending on his intensity value, it is possible to deduce any changes in the ROF and the overall performance of the rocket engine.

The curious thing that has been measured during this test is the peak measured around 543 nm of Copper. In Table 4.2 one can see, using as an additional proof Fig 4.1, that at frame ∼700/8000 the presence of it is still really high and it has been measured throughout the whole spectroscopic analysis. It has been noticed later that the Copper recorded was coming from the cooling film. For the discussion on the combustion, refer to Table 4.2 and Chapter 5.

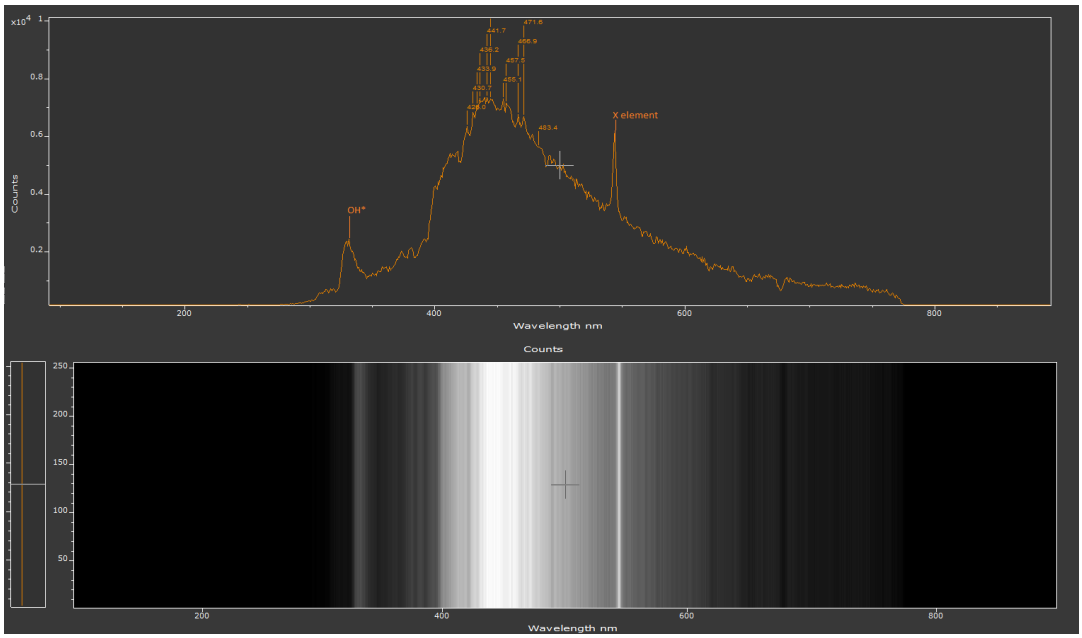

FIGURE 4.1: Spectral Emission of the Vulcain 2.1 Hotrun at 700/8000 Frame

4.1.2 Second Hotrun for Vulcain 2.1

The equipment, the place and the purpose of the test is the same of the first hotrun. A list of the principal events recorded during the test is presented in Table 4.3.

The interesting aspect of this new hotrun is based on the new wavelength presence at 670 nm. According to the emission spectra, it is in the visible light regime and the color is red. The nature of this particular element is found with the aid of the NIST website (`https://physics.nist.gov/PhysRefData/ASD/lines_form.html`). Inserting the wavelength acceptable range between 650 nm and 680 nm it is possible to detect the most likely molecule or element that has been seen by the spectrometer. According to this procedure, the element recorded could be Cu III or Cu II which is the element composing the cooling film.

TABLE 4.3: Major Events of the second Vulcain 2.1 Hotrun

Time	Events	Notes
t_0	Start of the Ignition	Peaks at 543 nm (Cu)
$t_0 + 1s$	Combustion starts	Emission in the OH^* wavelength range High emission in the Visible Regime Peaks at 543 nm (Cu)
$t_0 + 2.5s = t_1$	Stable Combustion	OH^* Emissions are stable High preaks at Cu Stable Peaks at 670 nm
$t_1 + 32s$	Decrease in Cu intensity Decrease in 670 nm Intensity	OH^* unchanged
$t_1 + 53s$	Increase in Cu Intensity	
$t_1 + 65.5s$	Increase in OH^* Intensity	
$t_1 + 135s$	Increase in Cu Intensity	OH^* unchanged
$t_1 + 243s = t_2$	Decrease in Intensity for all elements	
$t_2 + 1s = t_3$	Intensity Increases again for all elements up to t_1 regime	
$t_3 + 74s = t_4$	Decrease In Intensity for all elements	Possible change in ROF Instantaneous Frames where OH^* and Cu are both present Overall Intensity very low
$t_4 + 18s = t_5$	Increase in Intensity for OH^* and Cu (2000 counts) like if there is still combustion	
$t_5 + 6s = t_6$	All elements are low (OH^* and Cu included)	
$t_6 + 7s = t_7$	OH^* and Cu are measured again for a short period. Higher presence of OH^*.	
$t_7 + 12s = t_8$	Unstable Combustion. High peaks with OH^* and Cu followed by sudden decreases in intensity.	
$t_8 + 10s = t_9$	Unstable Combustion	
$t_9 + 30s = t_{10}$	Stable combustion that decreases in intensity over time similar to t_1	
$t_{10} + 15s = t_{11}$	Unstable Combustion	High emissions at 770 nm wavelength
$t_{11} + 30s = t_{12}$	Sudden increase in intensity for all elements Peaks in Cu wavelength	Possible change in ROF
$t_{12} + 4.5s = t_{13}$	Unstable Combustion.	
$t_{13} + 90s = t_{14}$	Stable Combustion	Peaks on the whole spectra, in particular Cu
$t_{14} + 10s$	End of Combustion processes	

4.2 Hotruns Lumen Project

The engine behaved as planned and the whole design was confirmed to be fail-proof. The first two hotruns did not lead to the correct detection of enough plasma lines to determine LTE conditions. The probe dedicated to the detection of the plasma, was not in the same line of sight with the laser. The detected peaks presented in Figure 4.2 are the result of scattered light and, even if they testify that plasma was present, the LTE condition could not be proven fully. Anyway, looking at the spectra obtained, it is possible to see how some frames contained plasma values as Figure 4.2 shows as it is presented on screen using SOLIS.

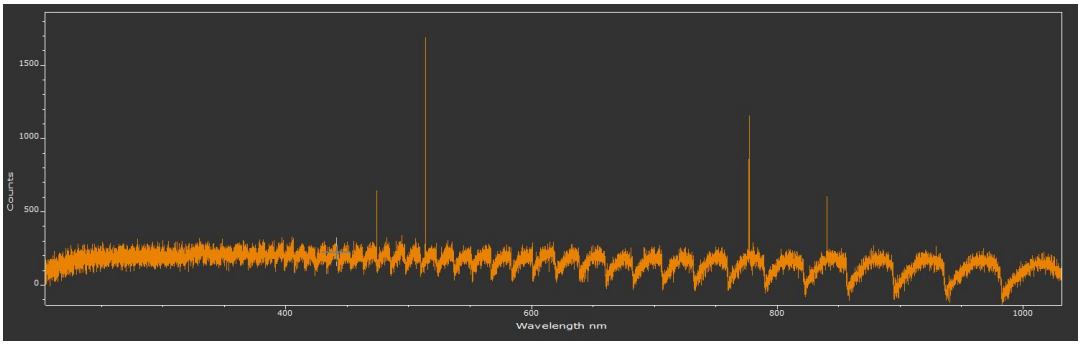

FIGURE 4.2: Lumen Project First Hotrun: Plasma Detection

The peaks captured in the previous mentioned figure represent the plasma. Each spike is a different element, and the counts indicate the intensity. For a deeper analysis, refer to section 5.3. The ideal spectra will have three or more spectral Balmer series lines of the Hydrogen or of some other element (Carbon, Oxygen). If this result is seen, the next step would be of plotting them in the Boltzmann Plot verifying the linearity and determining the temperature. In order to do so though, every single frame of the test must be examined and for this reason, only the relevant ones are presented in this thesis. The wavy signal on the bottom of the picture is given by the Bound-Free and Free-Free transitions of the plasma and by the Echelle principle, since lots of spectral orders have to be added together by the internal software. In order to have satisfactory results this so called "baseline" must be erased and only the peaks shall remain.

It is remarkable to state that the Delay Time and the Exposure Time could not be modified during these hotruns for the particular setup of the engine during this test campaign.

Chapter 5

Discussion Of The Results

5.1 Discussion Of The First Hotrun Vulcain 2.1

This section will read into the spectroscopic analysis performed at DLR on the Vulcain 2.1 engine. All the intensity values are measured in Counts (Arbitrary Units). The main events recorded will be presented with a short description. All the following material has been given to Arianegroup for general evaluation of the combustion test.

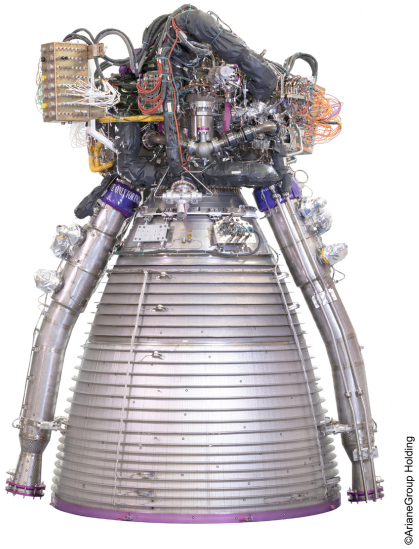

FIGURE 5.1: Vulcain 2.1, courtesy of [20]

5.1.1 Test Analysis

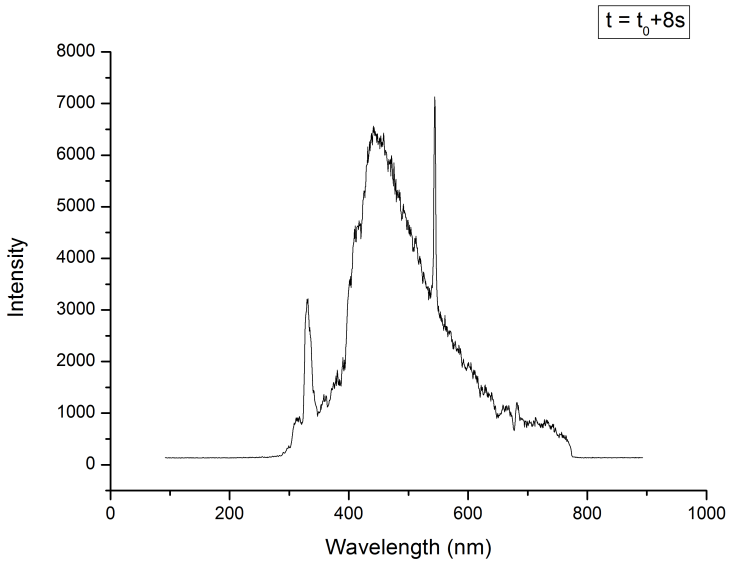

FIGURE 5.2: Vulcain 2.1: Combustion Starts $t_0 + 8s$

The start of the combustion is visible in Figure 5.2. It is the first frame where OH^* at 330 nm and Copper are found. It is remarkable that Cu has the strongest intensity of the entire frame at 543 nm. The high intensity of the visible light regime is caused by the high pressure, as suggested by [47].

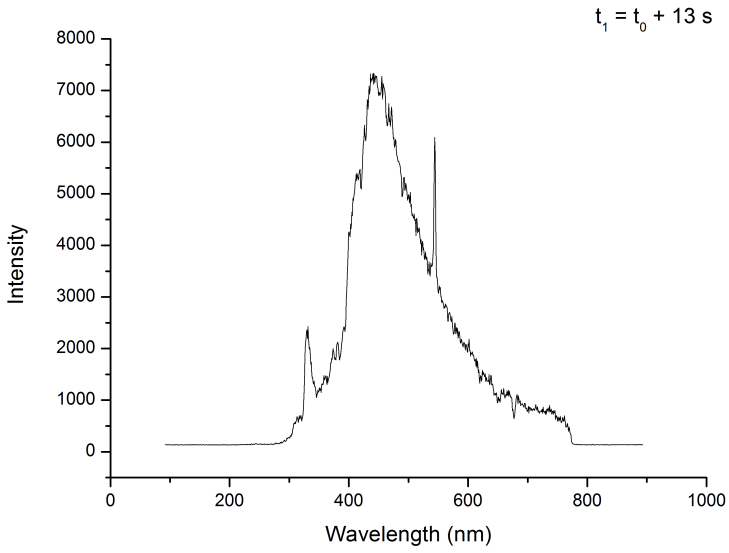

FIGURE 5.3: Vulcain 2.1: Stable Combustion t_1

In Figure 5.3 it is possible to see how, at t_1, the combustion plot seems to act stably soon after the first ignition. The emissions in OH^* are still present, together with the emissions of the Copper. The counts measured are relatively high.

In Figure 5.4 is clear that something has changed inside the combustion chamber since the intensity measured on the visible light has become really high, with peaks

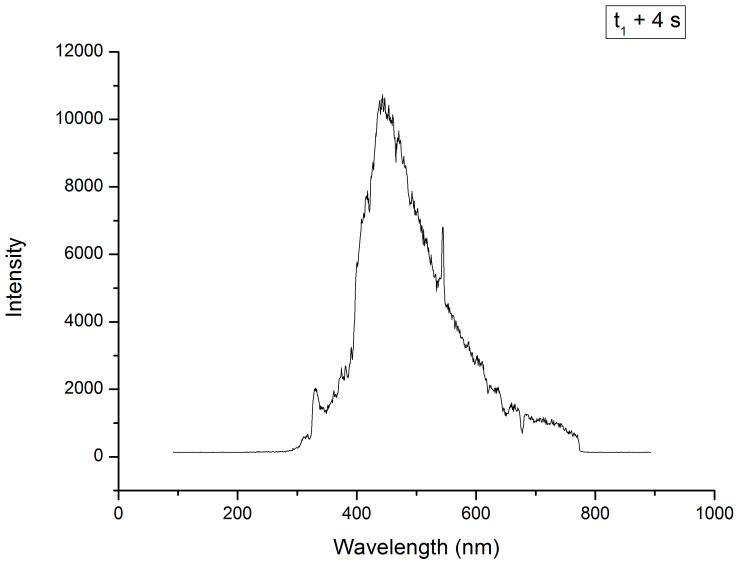

FIGURE 5.4: Vulcain 2.1: OH^* almost disappeared $t_1 + 4s$

at 11000. The emission of OH^* and Cu is unchanged.

High emissions in the visible range have been measured up to $t_1 + 120s$ with similar presence of OH^* as in Figure 5.4. The variation in intensity of the visible range has been deduced to be caused by pressure changes in the combustion chamber.

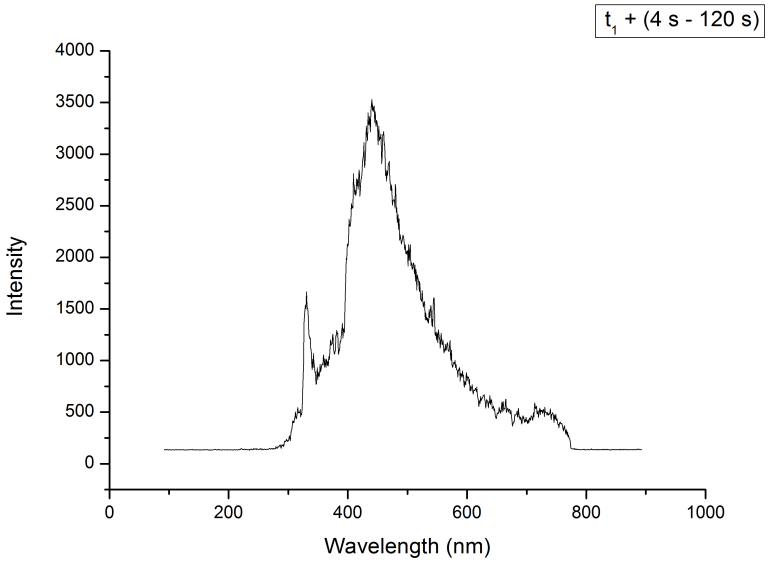

FIGURE 5.5: Vulcain 2.1: Low intensity t_3

The flame measured in Figure 5.5, relative to the t_3 frame, shows that the intensity of the visible light range has decreased drastically, this is an hint that suggests that the combustion is proceeding at a lower pressure or that a change in the ROF is happening. The OH^* is recorded and it clearly visible, unchanged in intensity if compared with previous figures. The Cu is lower in intensity.

This situation went on for quite a long time in the recordings. The OH^* and the Copper remained unchanged for the whole duration of t_3 in terms of intensity until t_4 is reached as Figure 5.6 shows. It might suggest that some low combustion mode was being tested.

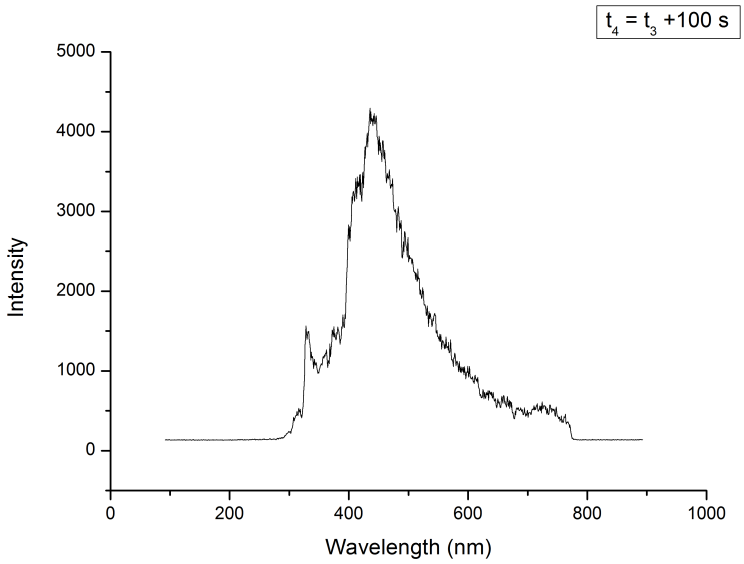

FIGURE 5.6: Vulcain 2.1: Visible light's peaks t_4

Suddenly, at t_4 a strong increase in the visible light regime has been measured. It did not last long but the intensity was higher, symbolizing an increase in the chamber pressure. The most likely hypothesis is of a new ROF. It is remarkable to note how the peak is concentrated betweed the UV and Visible light regime, while towards the NIR the counts are really low and with a decreasing behavior.

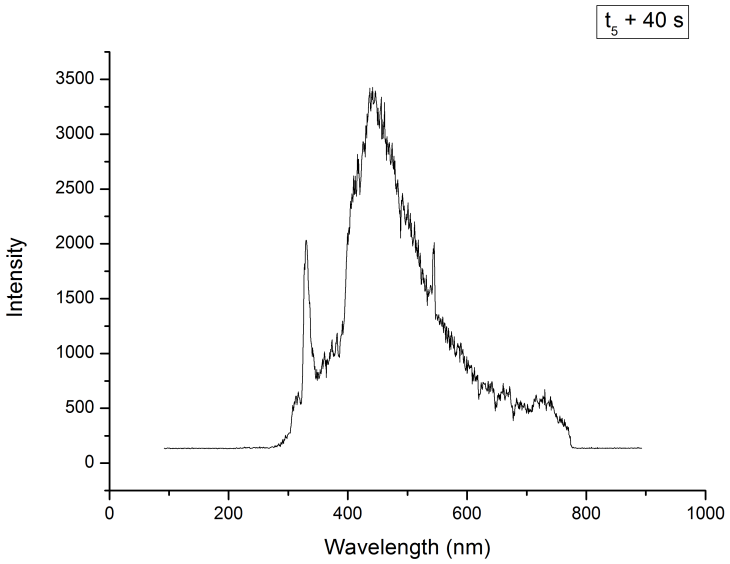

FIGURE 5.7: Vulcain 2.1: Stable combustion for the interval t_4 up to $t_4 + 90s$

The combustion remained stable for the interval t_4 up to $t_4 + 90s$ maintaining, with a certain accuracy, the same shape that could be found in Figure 5.7. As it is possible to see from the picture above, the OH^* emission remained constant throughout this whole period of time while the Copper spectral line is quite variable, but always present at the same intensity level. The intensity of all the elements is low, this hints thatthe pressure with which the flame is expelled is low. This could imply another change in ROF.

In Figure 5.8 is presented a curious phenomena that has been recored $t_5 + 40s$. As the picture suggests, the count of OH^* are really high, while the visible light regime and NIR remains the same. This could have been the effect of a suddenly change in ROF, resulting in a higher presence of Hydroxyl in the spectra. It is remarkable to present some other events that have happened during the period of time interested by this increase in intensity of the OH^*. As Figure 5.9 shows, the counts for OH^* are incredibly high in this figure, 1.5×10^4.

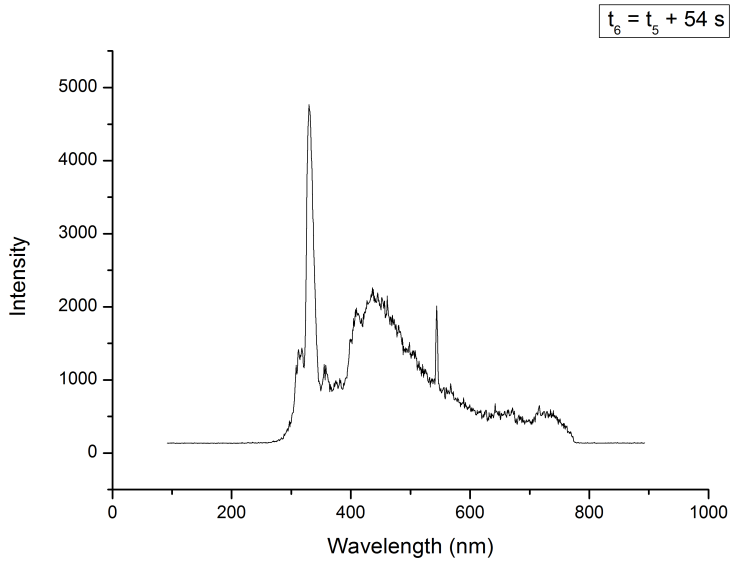

FIGURE 5.8: Vulcain 2.1: Increase in OH^* at $t_5 + 40s$

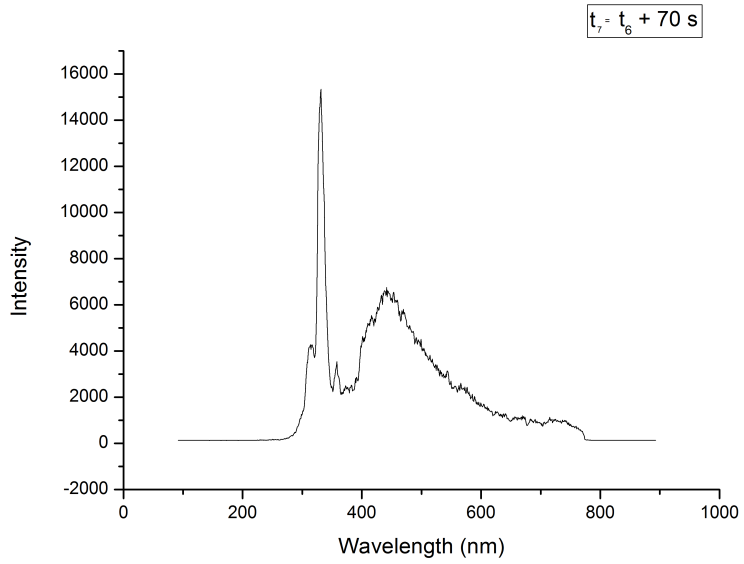

FIGURE 5.9: Vulcain 2.1: Highest peak of OH^* recorded at t_6

Afterwards, the spectra looked very much like Figure 5.7 until t_8, meaning that the actual ROF has not been modified together with other settings, so the combustion was stable.

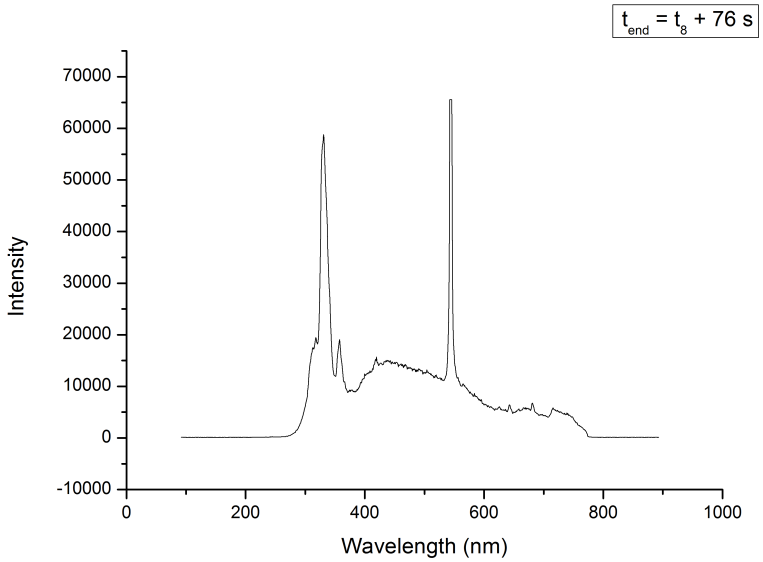

FIGURE 5.10: Vulcain 2.1: Last peaks of OH^* and lower UV and NIR $t_8 + 76s$

In Figure 5.10 is presented the frame recorded at $t_8 + 76s$. It shows the final stages of the combustion, where the visible regime is almost disappeared and the only molecules recorded are the OH^* and the Copper, plus some elements in the NIR regime. Some peaks at really low intensity have been recorded in the low UV at 141 nm and 156 nm too, together with a rise of the NIR measurements, probably due to end of combustion processes or thermal noises.

After this frame, the recording went on until reaching $t_0 + 743s = t_{end}$. The main features of the combustion though have already been analyzed and the remaining frames show only the end of the combustion.
Following the spectroscopic analysis the data obtained were studied with MATLAB in order to have a better idea of how the combustion process worked.
The concentration of the intensities of the major elements present in the hotrun was requested to be plotted over time since it was a really useful data for the understanding of the combustion efficiency.
The concentration of OH^* over time is presented in Figure 5.11. As it is possible to see, except for the starting and ending events, the intensity measured suggests that two major phenomena happened during the hotrun which resulted in an increase of the intensity of the OH^*. The first happened shortly before 100 s, the second happened after 400 s. The interval considered for the OH^* was from 300 nm up to 340 nm.

The same plot, but referred to Cu, can be seen in Figure 5.12.

This plot suggests that the Copper presence was measured as soon as the spectrograph started recording. It is always present throughout the whole hotrun, but the most intense range of time can be measured from 60 s to 200 s, with small peaks

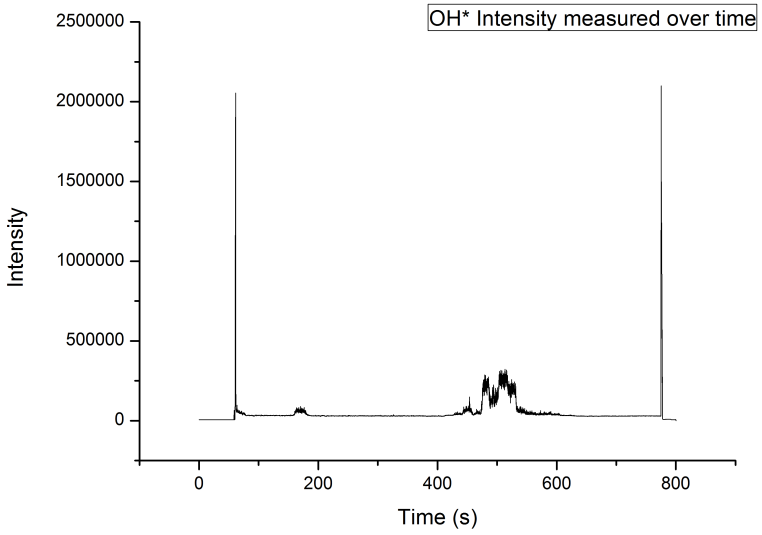

FIGURE 5.11: Vulcain 2.1: OH^* intensity over time

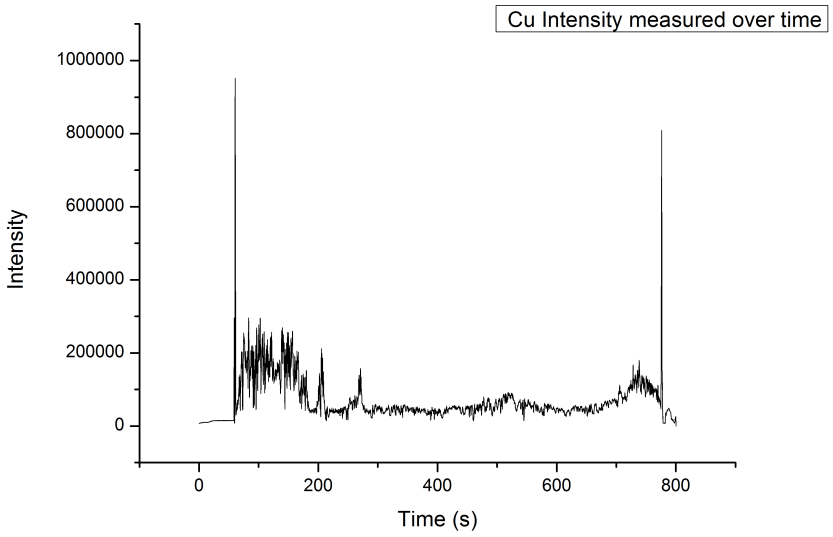

FIGURE 5.12: Vulcain 2.1: Cu intensity over time

afterwards, probably due to change in ROF. The interval considered for the Cu was from 670 nm up to 685 nm.

5.2 Discussion Of The Second Hotrun: Vulcain 2.1

The second hotrun test that took place at DLR Test Bench P5 concerning the Vulcain 2.1 engine required the same procedure and setup of the first hotrun. The test's principal events are listed in Table 4.3. Figures and a short description of what is probably happening in the plume will be presented below in subsection 5.2

Test Analysis

In Figure 5.13 the beginning of the combustion is shown. This happened at the time considered t_0. It is interesting the comparison between the above mentioned figure and Figure 5.2.

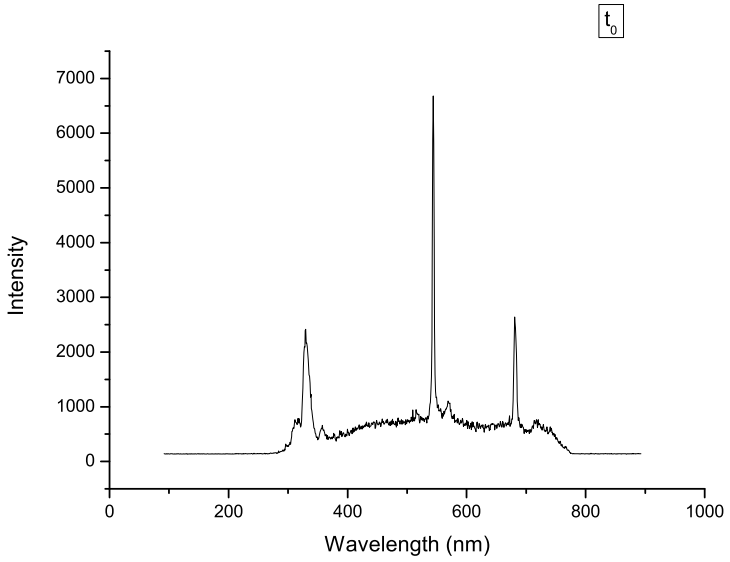

FIGURE 5.13: Second Hotrun of the Vulcain 2.1: Start of the combustion

As it is possible to see, the visible light regime is lower than the one registered during the first hotrun. The intensity is lower too, with strong peaks in the Cu wavelength. It is remarkable to note how the main elements detected are the OH^*, the Cu in its various ionization states.

After few moments, the combustion stabilizes and the plot captured by the spectrograph is quite similar to the one presented in Figure 5.14

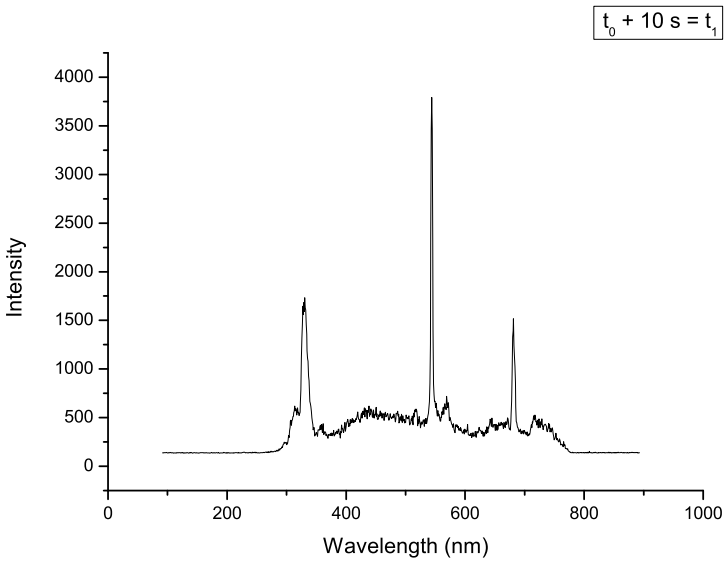

FIGURE 5.14: Second Hotrun of the Vulcain 2.1: Combustion Stability at t_1

It is remarkable to note how the intensity is way lower than the one presented in Figure 5.3 relatively to the first test. The low intensity of the visible light regime allows to identify quickly the elements playing a key role during this particular interval of time of t_1.

In Figure 5.15 is shown the transition between t_1 and t_3 of the combustion. The particularity of this short transition of time t_2 is of a overall decrease of the intensity of all elements. The OH^* has the lead here, implying a possible ROF change is happening for the duration of 1 s.

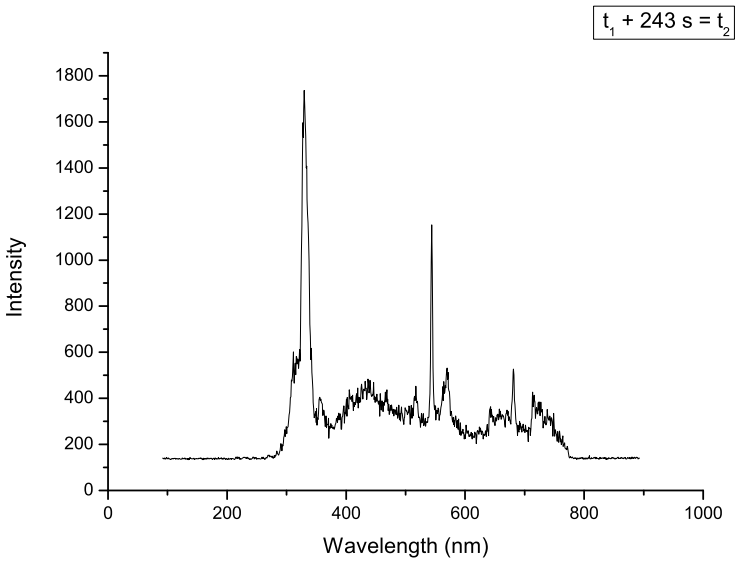

FIGURE 5.15: Second Hotrun of the Vulcain 2.1: Combustion Stability Decrease in Intensity at t_2

Following the brusque decrease of t_2 the intensity of all elements started to rise once again up to the values measured during t_1 as Figure 5.16 suggests.

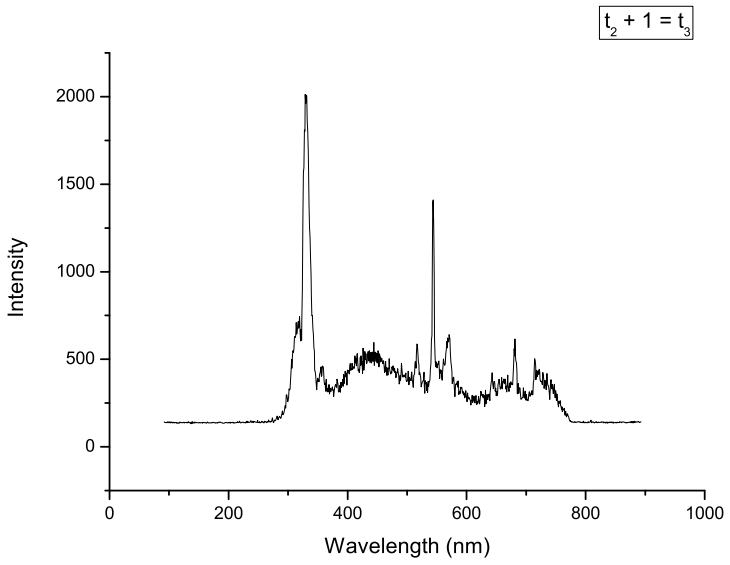

FIGURE 5.16: Second Hotrun of the Vulcain 2.1: Combustion Stability at t_3

The performance measured in Figure 5.16 went on with a similar pattern for some time, until the intensity dropped down once again for all the elements, implying another possible change in ROF as Figure 5.17 shows. It is important to denote that the intensity for 670 nm is very low now. Further on, during the t_4 interval of 18 s, the intensity for the whole spectra went almost to 0.

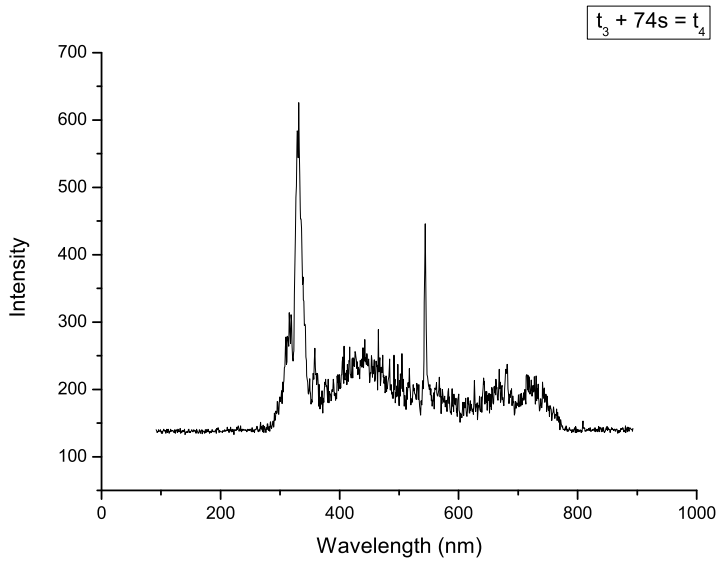

FIGURE 5.17: Second Hotrun of the Vulcain 2.1: Sudden drop in Intensity at t_4

352 s into the combustion process the pattern found during the 6 s at t_5 shows a spectra very variable. In order to explain the previous sentence it is better to visualize the process. In Figure 5.18 It is possible to see how the combustion is going for a couple of seconds. As it is possible to note, the pattern is not stable and it is quite

variable in intensity and emissions. It is also worth mentioning that the Z axis, representing time, is only of 1 s, showing how unstable this particular interval of time is.

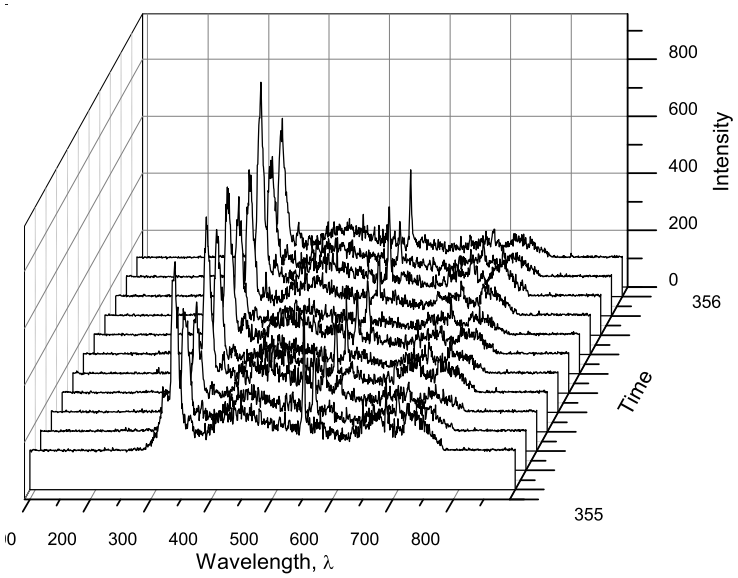

FIGURE 5.18: Second Hotrun of the Vulcain 2.1: Particular Set of Frames during t_5

Upon reaching t_6, all the elements intensities are quite low, except for some instantaneous peaks at OH^*, as shown in Figure 5.19.

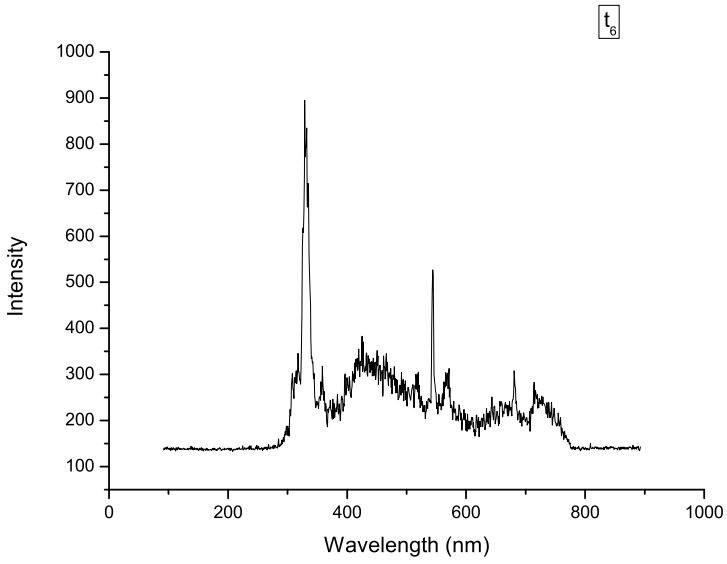

FIGURE 5.19: Second Hotrun of the Vulcain 2.1: Low Intensity at t_6

After 365 s of ignition, at t_7, a rise in the intensities of OH^*, Cu and what is thought to be Cu II/III is noted. t_7's intensity is exponential. During the first seconds, intensity is very low and it increases second after second until t_8 is reached after 21 s. Once again, the intensity is not constant, symptom of an unstable stage of combustion in this particular load point. The time considered in Figure 5.20 is

of 1 s. In such small amount of time, the intensity of OH^* and Cu varies a lot. It is remarkable to state that even the most likely to be Cu II/III is present in small quantities.

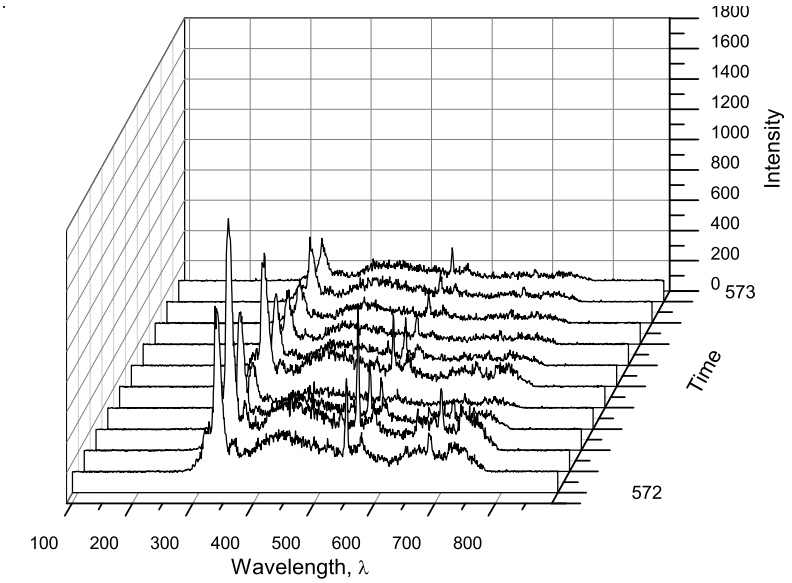

FIGURE 5.20: Second Hotrun of the Vulcain 2.1: Pre-Combustion at t_7

The combustion that follows is the one presented in Figure 5.21. It represents a long interval encountered at t_8 which lasted for almost 10 s. It shows high peaks in OH^* and Cu together with an high presence for the element at 670 nm. The combustion is not stable in this interval, since the intensity of the elements changes unexpectedly.

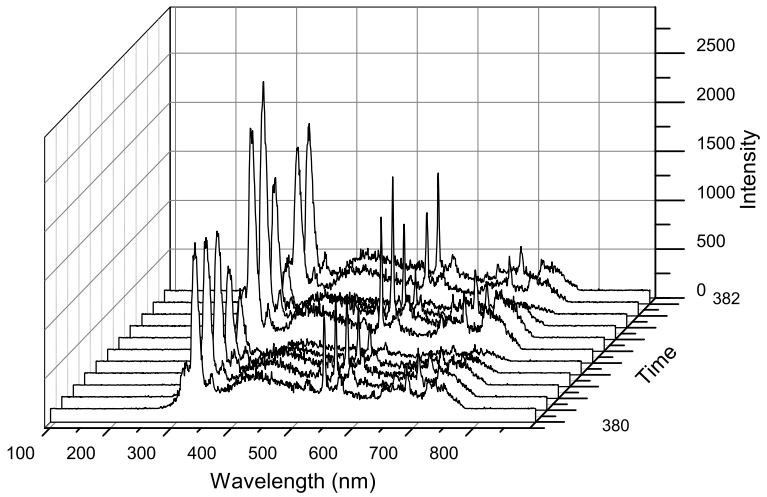

FIGURE 5.21: Second Hotrun of the Vulcain 2.1: Unstable Combustion at t_8

After 10 s, t_9 checkpoint is reached and the a more stable combustion is achieved for approximately 30 s. Figure 5.22 shows the values reached in this stage. As it is possible to see, intensity of OH^* reaches peaks of almost 3000 while the Cu is almost at 2600. What is suspected to be Cu II/III is still low, but in the spectra it is easily noticed at 670 nm.

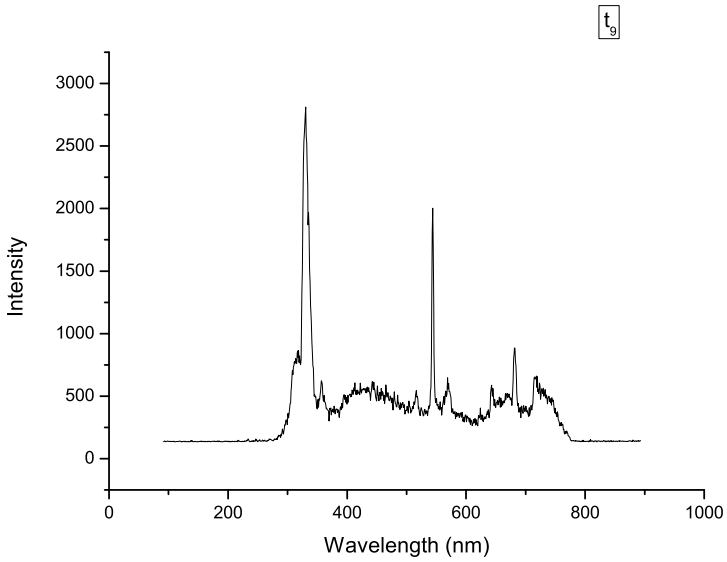

FIGURE 5.22: Second Hotrun of the Vulcain 2.1: Stable Combustion at t_9

After the combustion of t_9 a sudden decrease of approximately 15 s happened on the whole intensity spectra during t_{10} until reaching t_{11}. The reason why this happened could be a sudden change of ROF for the last stage of the combustion or the start of the end of combustion processes. The combustion seems stable anyway, but lower in intensity. Figure 5.23 shows the decrease during a time of 2 s. As it is possible to see, the intensity is chaotic with sudden peaks.

Upon reaching t_{11}, an increase in intensity for Cu, OH^* and the other element is registered for the whole 30 s until t_{12} checkpoint is reached. This could have been another combusted test which was earlier announced by the combustion instabilities or by the previous ROF change found during t_{10}. Figure 5.24 shows the average spectra recorded.

During the 4 s transition from t_{12} to t_{13} the combustion is unstable as Figure 5.25 shows for a smaller interval of 2 s. It is easy to see the sudden change in intensity from one frame to the other.

The last time frame examined, t_{13}, represents a constant combustion interval of 90 s that represented the last stable combustion happened in this test before the shut down. The average intensity for OH^* is of 2200, while the Cu is very high at 4000. The element that is thought to be Fe II instead is around 1300 for the whole duration of this time step. Figure 5.26 represents what previously said. t_{14} is the time interval where the ignition is shut down due to the end of the test, and for this reason it is renamed t_{fin}.

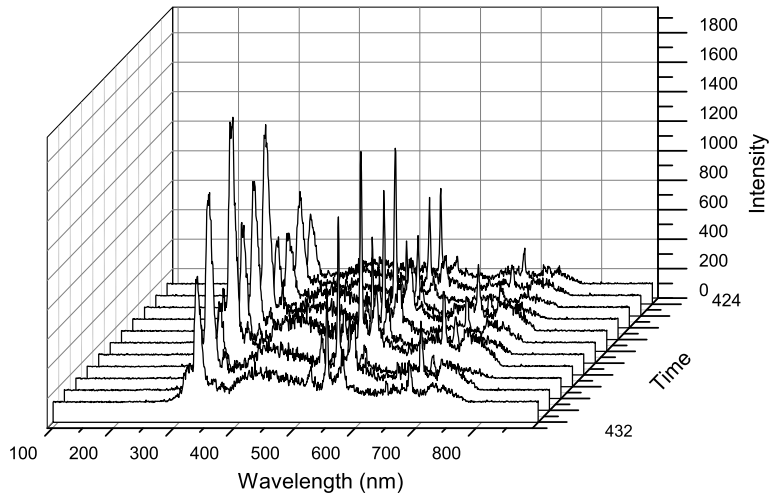

FIGURE 5.23: Second Hotrun of the Vulcain 2.1: Change in ROF or End Of Combustion processes at t_{10}

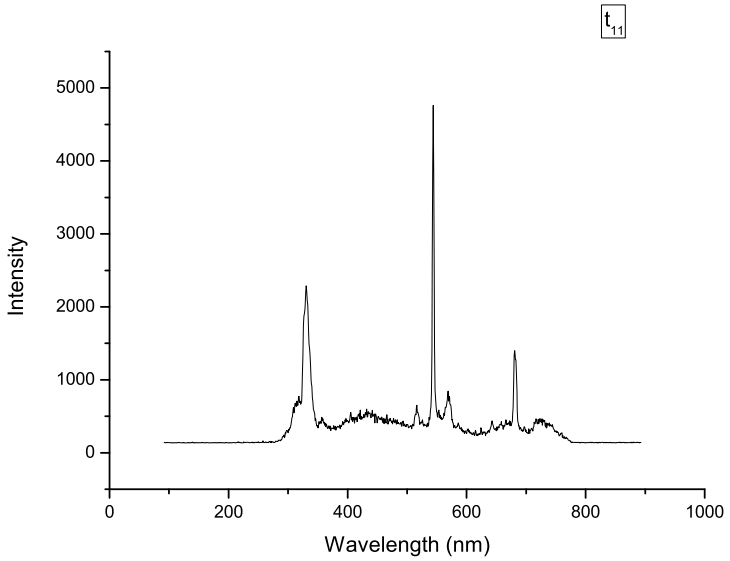

FIGURE 5.24: Second Hotrun of the Vulcain 2.1: Stable combustion during t_{11}

5.3 Lumen Project: Discussion of the Hotruns

5.3.1 Assumptions

This section includes the theoretical and practical assumptions considered during the hotruns relative to the Lumen Project engine. It has been given for granted that the spectrograph was correctly calibrated before the tests by the dedicated technicians. The tolerance of the instrument has been considered of 1 nm. When looking for a element emission, if on the theoretical value nothing is marked but in a reasonable closeness there is a spike, that has been assumed to be the desired element.

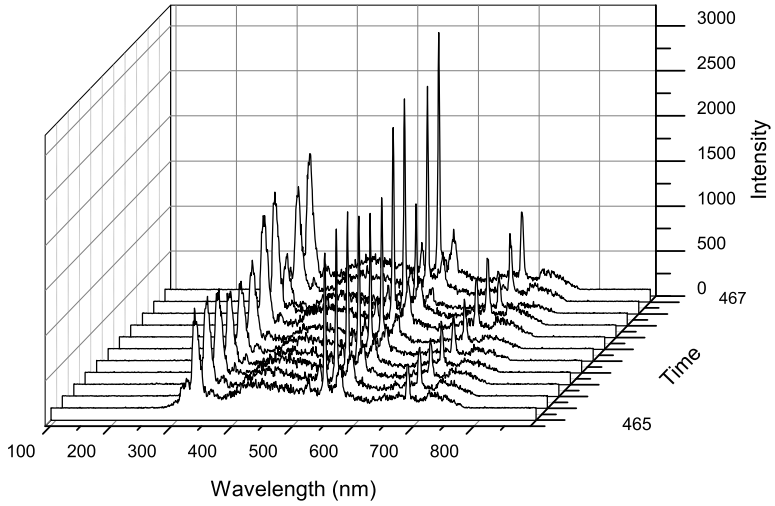

FIGURE 5.25: Second Hotrun of the Vulcain 2.1: Unstable combustion during t_{12}

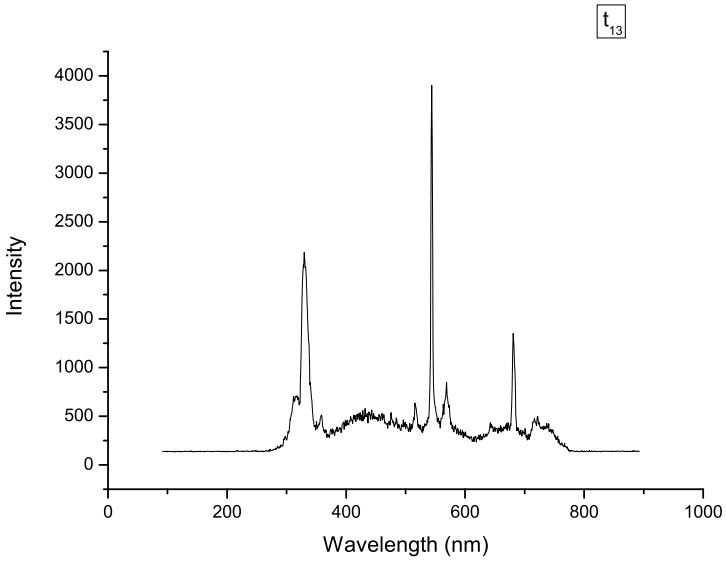

FIGURE 5.26: Second Hotrun of the Vulcain 2.1: Last Stable Combustion before Shut-Down during t_{13}

As an example, H_β on paper is at 486.165 nm but on the spectra there is a peak at 486.05 nm, that is considered H_β. [50]

It has furthermore been assumed that the scattered plasma light detected by the spectrograph related to the third and fourth hotrun did not suffer any intensity or energy loss.

5.3.2 Hotrun 1 and 2 : 29/4/2019

The presence of the baseline given by the Bound-Free and Free-Free transitions is problematic for the accuracy of the results. Filtering them with MATLAB gave the

results presented in Figure 5.27, this is a better way of visualizing it since every possible misunderstanding derived from the previously mentioned transitions has been erased and only the Bound-Bound transitions are present (which are the only ones worth mentioning when an LTE process is interested).

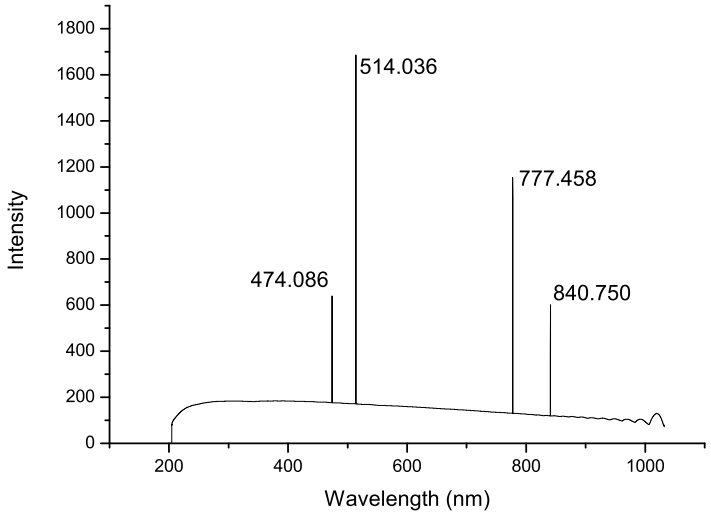

FIGURE 5.27: LUMEN Project Hotruns: First detection of Plasma 1/1 the 29/4/2019

As it is possible to see, the peaks are only located on 474.086 nm, 514.036 nm, 777.458 nm and 840.750 nm. Using the NIST website and knowing the propellants, it has been found that the first peak at 474.086 nm is OII , the second ionization stage of Oxygen, while the second one at 514.036 nm is a mixture of OII and CII. The third peak line at 777.458 nm is OI and the last one at 840.750 nm is the third ionization stage of Carbon, $CIII$. Even trying, with this particular frame it will not be possible to determine the LTE presence with Boltzmann Plot since there are not three separate ionization stages of a single element.

5.3.3 Hotrun 3 and 4 : 13/5/2019

The scattered plasma-emission was recorded since the spot where the plasma was generated was not in the line of sight of the optical probe. The probe was anyway able to detect some scattered light, but the intensity values of it can not be entrusted to directly calculate the plasma temperature and LTE. Once again, the ideal spectra that must be found will have at least three peaks. The plot in Figure 5.28 represents one of the two potential candidates with three peaks found during the third hotrun.

Using the NIST website encyclopedia on atomic emissions, it has been determined that the first peak at 525.398 nm has a very low chance of being CII or $CIII$, since their general intensity and transition probability at that wavelength are neglectable. It could be any other material composing the combustion chamber or the injection plate. The next peak at 564.885 nm has a very high chance of being CII having taken a look at the transition probability (A_{nm}) and since the intensity average recorded is almost equal. The last peak at 675.361 nm is mostly certainly CI for the same reasons stated for the previous peak. In conclusion, even in this case, it is not possible to determine the existence of an LTE.

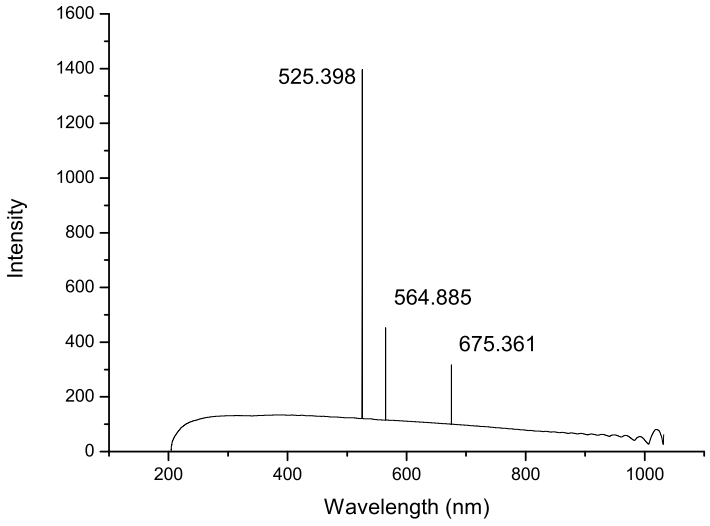

FIGURE 5.28: LUMEN Project Hotruns: Detection of Plasma - Third Hotrun 1/2 the 13/5/2019)

The plot presented in Figure 5.29 represents the plasma spectra of a particular frame happened after the one in Figure 5.28. It is the last one interesting for the LTE measurements during the third hotrun. The three intensity lines which are interesting are located at 396.213 nm, 548.345 nm and 555.313 nm. According to the Analysis performed with the NIST website, the user experience and the spectra observed, the first peak at 396.213 nm is most likely a mixture of CuI and OII while the peak at 548.345 nm is $CuII$ and the last one on the right at 555.313 nm is representative of the first ionization stage of Carbon, CI.

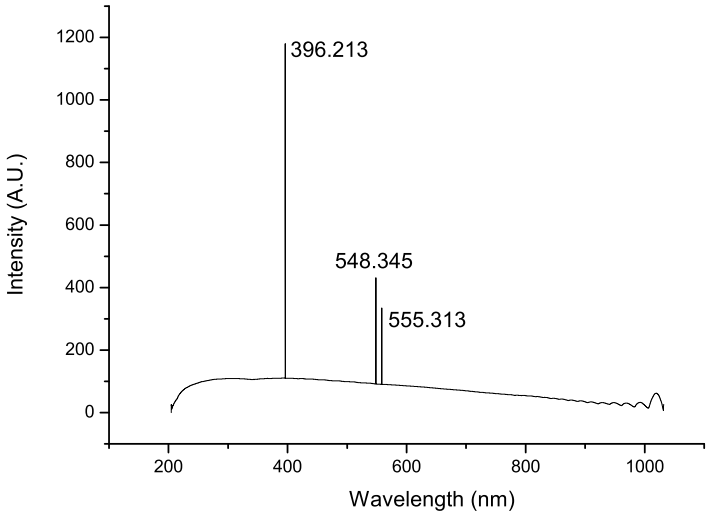

FIGURE 5.29: LUMEN Project Hotruns: Detection of Plasma - Third Hotrun 2/2 on the 13/5/2019

A lot of elements have been detected and many frames were full of plasma lines.

For this reason, and for the sake of clarity and to keep this thesis as short and clear as possible, only the frames where three different ionization stages of the same element have been found are presented below.

One of the best spectra that has been found is presented in Figure 5.30. It is remarkable because, even if at a first glance it could seem chaotic, it is the only frame where it has been estimated the existence of all the first three lines of Hydrogen of the Balmer Series. Using MATLAB, it was possible to zoom in a particular section

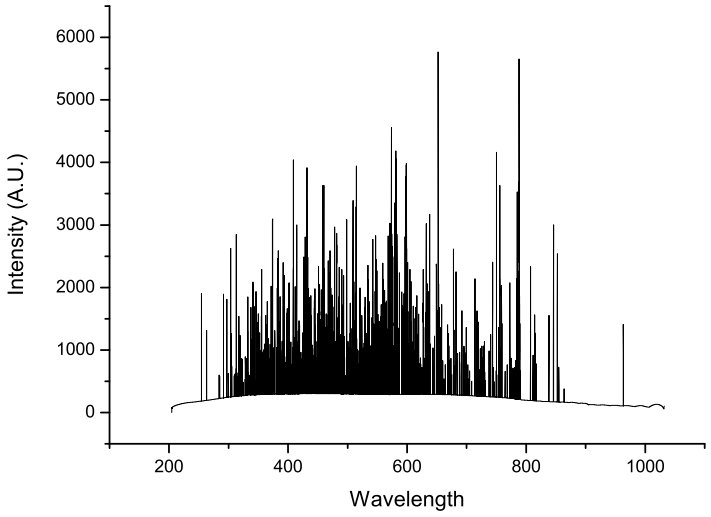

FIGURE 5.30: LUMEN Project Hotruns: Detection of Three Lines for Hydrogen - Fourth Hotrun 1/1 on the 13/5/2019

of the spectra in order to study it in more detail. Doing so, the Figures 5.31, 5.32 and 5.33 show, in correlation with Table 2.1, the existence of the above mentioned ionized states.

Since this particular frame is a good candidate for the Boltzmann Plot and LTE determination, some extra calculations are necessary.

First of all it is mandatory to perform a peak analysis. As it is possible to see from Figures 5.31, 5.32 and 5.33 the peaks may be the result of the sum of lower wavelengths peaks. Once this has been done, the measured wavelength must be filtered accordingly with the quantum efficiency curve cited in section 2.2.7. Furthermore, now that the intensities have been smoothed and filtered, the ratio between H_α/H_β, H_β/H_γ must be compared with the ratio of the same elements with the intensity values taken from NIST website. If these values are close, there is a really high chance of having encountered Hydrogen lines.

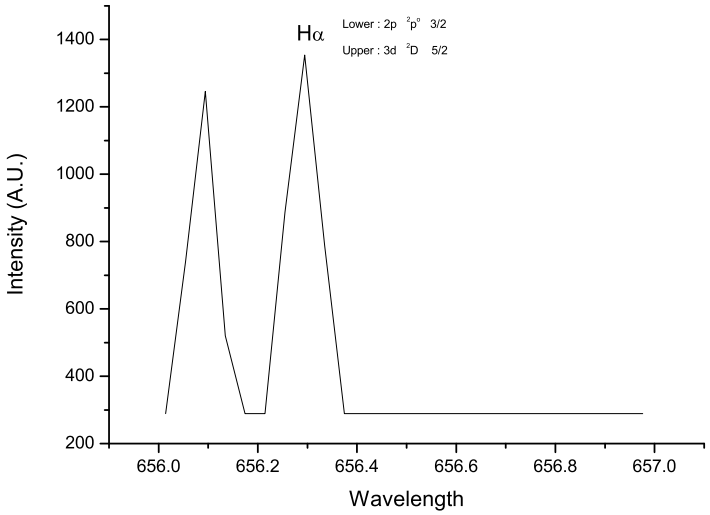

FIGURE 5.31: LUMEN Project Hotruns: H_α - Fourth Hotrun 1/1 on the 13/5/2019

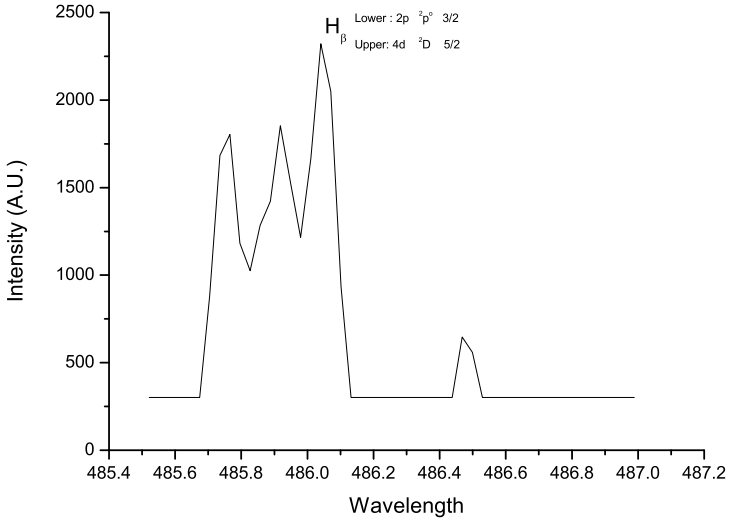

FIGURE 5.32: LUMEN Project Hotruns: H_β - Fourth Hotrun 1/1 on the 13/5/2019

With the filtered intensity values, the Boltzmann Plot can be drawn and the linearity can be proven. In Figure 5.34 is shown the real value of the intensity for the H_α taking into account the quantum efficiency curve presented in Figure 2.5, considering that the one used is the W-AGT 03, which is approximately 10%.

In Figure 5.35 instead, first an approximation of the real value of the intensity of H_β is presented. Considering a quantum efficiency of 15% for the wavelength range between 485.5 nm and 487 nm the new intensity is bigger than the one measured before. However, H_β is the last peak of three, this could mean that its intensity is the sum of other intensities. In order to be more precise, a peak analysis is performed with the aid of ORIGIN 8.1 and the result is shown in Figure 5.36. In order to present

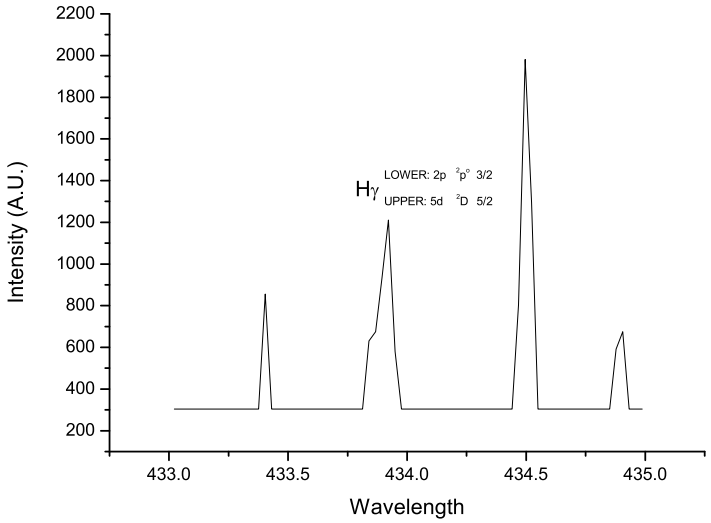

FIGURE 5.33: LUMEN Project Hotruns: H_γ - Fourth Hotrun 1/1 on the 13/5/2019

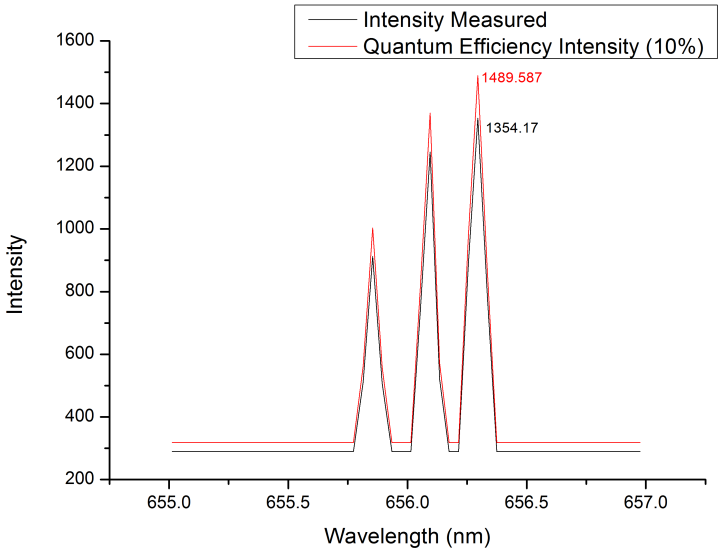

FIGURE 5.34: LUMEN Project Hotruns: H_α with Quantum Efficiency - Fourth Hotrun 1/1 on the 13/5/2019

the most precise result, a wide number of sub-curves have been created. It is possible to denote the small curve that is representative of H_β in black at 486.165 nm. The new intensity of this curve is the actual one and it is equal to 1077.77.

In Figure 5.37 is presented the H_γ frame with the quantum efficiency increase of the 15%.

H_γ may suffer the same increase of intensity as H_β. For this reason, a less complex analysis of the peaks is done, given the presence of only a smaller peak. Figure 5.38 shows the result of the above cited peak analysis and the new intensity value for H_γ is 652

A first comparison of the ratio between the measured intensities between the

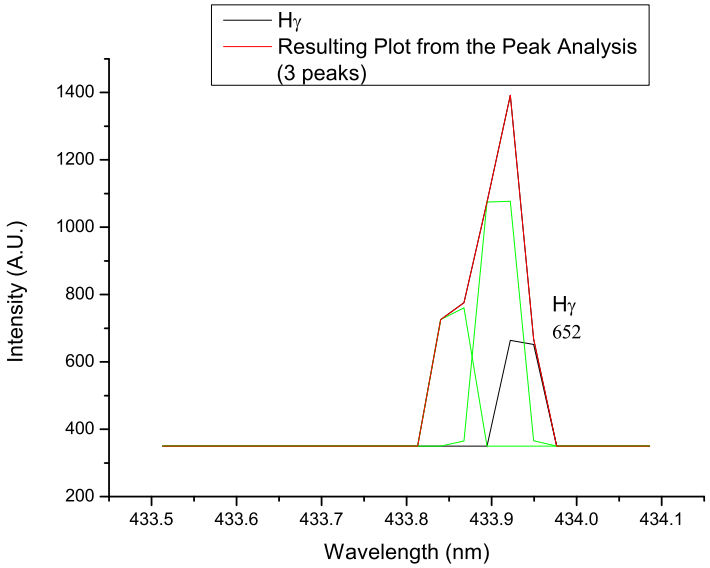

FIGURE 5.35: LUMEN Project Hotruns: H_β with Quantum Efficiency - Fourth Hotrun 1/1 on the 13/5/2019

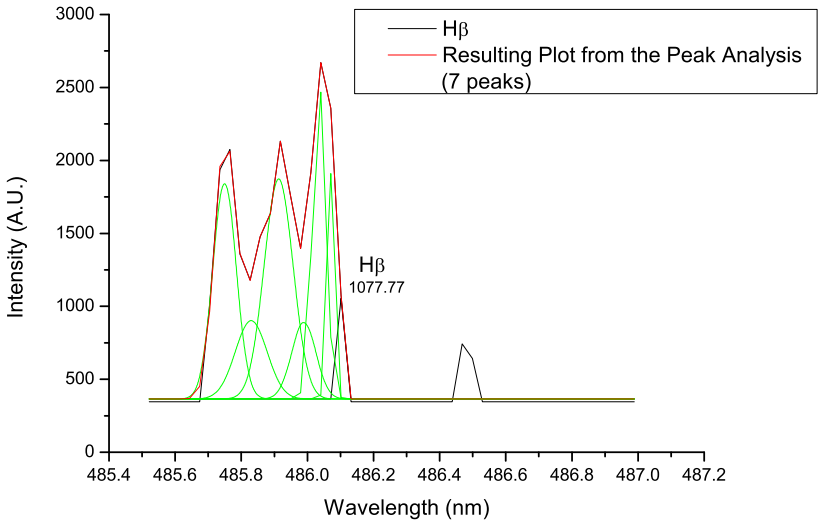

FIGURE 5.36: LUMEN Project Hotruns: H_β with Quantum Efficiency and Peak Analysis - Fourth Hotrun 1/1 on the 13/5/2019

three ionization stages of hydrogen and the NIST website data Boltzmann Plot can be done. If the ratios match, the LTE quality will be high and the LTE measured via Boltzmann Plot will be accurate. Eq. 5.1, 5.2, 5.3 and eq. 5.4 show the result of the two ratio for H_α, H_β and H_γ.

$$\frac{H_\alpha(NIST)}{H_\beta(NIST)} = \frac{500000}{180000} = 2.77777 \tag{5.1}$$

$$\frac{H_\alpha(meas)}{H_\beta(meas)} = \frac{1489.567}{1077.77} = 1.38208 \tag{5.2}$$

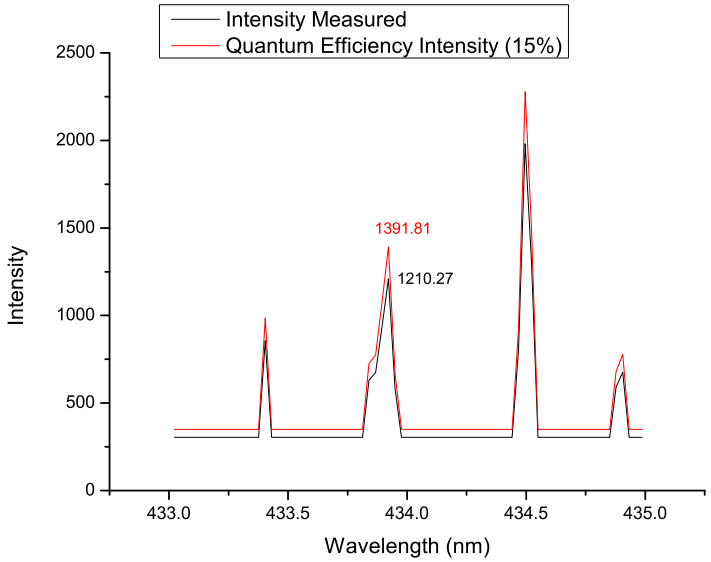

FIGURE 5.37: LUMEN Project Hotruns: H_γ with Quantum Efficiency - Fourth Hotrun 1/1 on the 13/5/2019

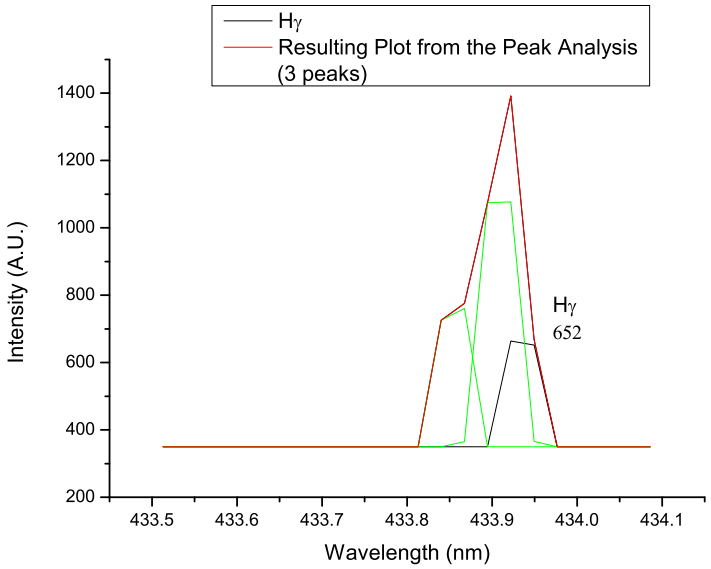

FIGURE 5.38: LUMEN Project Hotruns: H_γ with Quantum Efficiency and Peak Analysis - Fourth Hotrun 1/1 on the 13/5/2019

$$\frac{H_\beta(NIST)}{H_\gamma(NIST)} = \frac{180000}{90000} = 2 \tag{5.3}$$

$$\frac{H_\beta(meas)}{H_\gamma(meas)} = \frac{827.677}{652} = 1.26840 \tag{5.4}$$

As it is possible to see, the ratios are not similar for the H_α/H_β but are closer for H_β/H_γ. This is an indication of the quality of the LTE. Most likely, the Boltzmann plot linearity and the temperature calculated with it will have a certain inaccuracy.

The best way to proceed now will be with the Boltzmann Plot in order to visualize the slope.

The Equation used is the one presented in Eq. 2.7. On the Y axis the left part of the equation is plotted ($ln\frac{(I_{nm}\lambda_{nm})}{(A_{nm}g_n}$)) in Arbitrary Units (A.U.), while on the X axis will be the upper energy E_n measured in eV. Figure 5.39 shows the results of the Boltz-

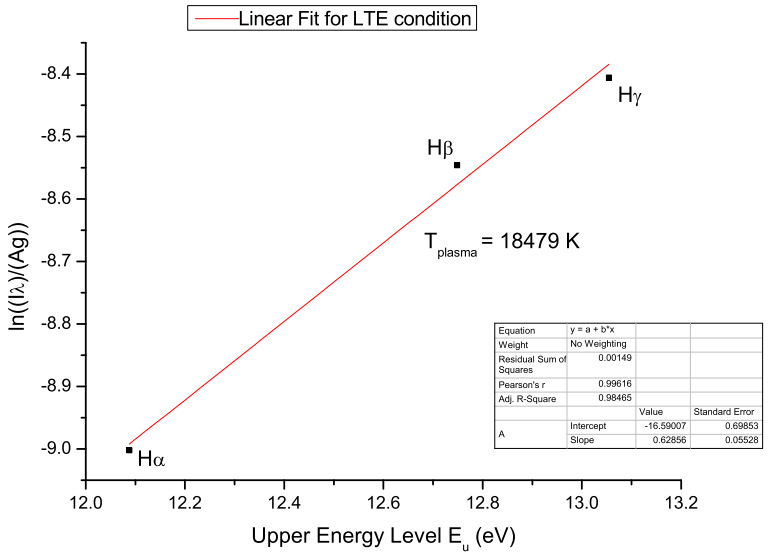

FIGURE 5.39: LUMEN Project Hotruns: Hydrogen Boltzmann Plot Linearity and Temperature of the Plasma - Fourth Hotrun 1/1 on the 13/5/2019

mann Plot for the Hydrogen ionization stages taken int account. As it is possible to note, the slope inclination is the opposite of the one presented in Figure 2.10. This is a strange effect that needs to be investigated. One reason might be that the last assumption regarding intensity and energy losses made in Section 5.3.1 might not be valid. The temperature calculated via Eq. 2.18 gave a result of 18 479 K. The points relative to the various ionization stages are really close to the line, meaning that the temperature value can be considered almost exact.

LTE quality is now determined by the closeness of the points, since they are close enough, the LTE is precise. It might be that the other elements present in the combustion chamber (O and C) may give better results. For the sake of clarity and for keeping this chapter as simple as possible, only the final considerations and final results are presented.

Starting with Carbon, an analysis has been conducted following the same path that has been taken for Hydrogen. This means that first the user has checked for the presence of peaks on the wavelengths presented Figures 2.8. Once this has been done, the wavelength and intensities have been isolated and plotted taking into account the quantum efficiency curve and the possible presence of sub-curves. Furthermore, from these plots, the peaks have been extracted and via Eq 2.7, the points of the Boltzmann Plot have been computed and fitted with a line. The Figures above mentioned are presented in the Appendix while the Boltzmann Plot related to Carbon is shown in Figure 5.40. As it is possible to see, the inclination of the slope is following the theoretical one presented in Figure 2.11. The temperature measured with Eq 2.18 gave a final result of 165 780 K which is a reasonable result for a Carbon plasma, as stated in [16], even if Carbon itself, as measured during this frame, is far

from thermodynamic equilibrium as the distance from the points and the line suggests. It is remarkable to note how $C\ III$ is not present, this is because the intensity for the given wavelengths of the third ionization stage of Carbon was too poor to be detected.

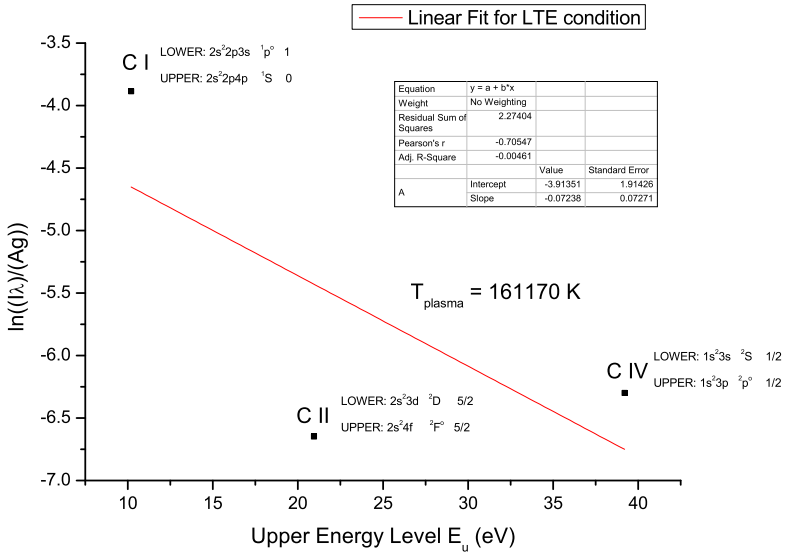

FIGURE 5.40: LUMEN Project Hotruns: Carbon Boltzmann Plot Linearity and Temperature of the Plasma - Fourth Hotrun 1/1 on the 13/5/2019

Oxygen fit with the Boltzmann Plot followed the same procedure of the elements described before. It is remarkable to note that the linearity has been confirmed using $O\ II$, $O\ IV$ and $O\ V$. The reason why the other ionization stages have been skipped is because the intensity relative to the given wavelengths of these ionization stages were not powerful enough to be considered. The resulting Boltzmann Plot is presented in Figure 5.41. All the plots concerning the single peaks of the various ionization stages recorded are presented in the Appendix A.2.2. The temperature calculated with Eq. 2.18 gave a resulting plasma temperature of 464 180 K.

As it is possible to notice, Oxygen plasma seems to be really close to LTE conditions, for this reason the reliability of this temperature is quite high.

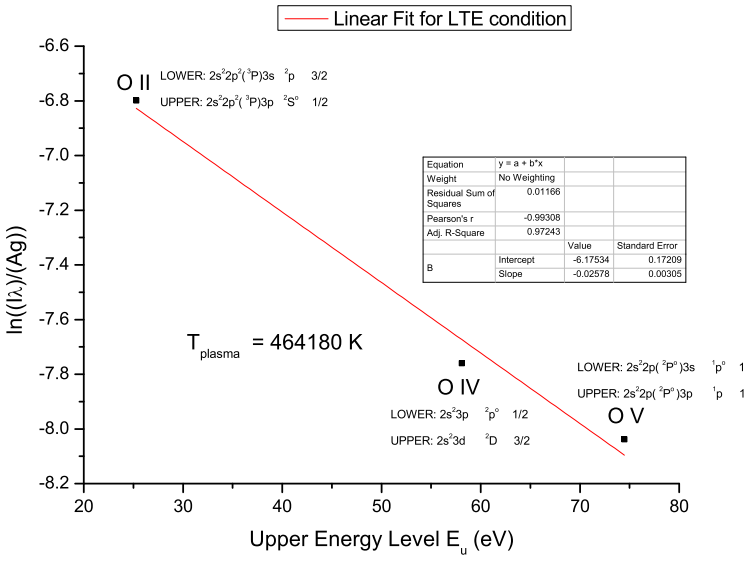

FIGURE 5.41: LUMEN Project Hotruns: Oxygen Boltzmann Plot Linearity and Temperature of the Plasma - Fourth Hotrun 1/1 on the 13/5/2019

Chapter 6

Conclusions

6.1 Vulcain 2.1: Conclusions

This section includes the conclusions relative to the Vulcain 2.1 hotruns that have been analyzed and described in this thesis.

The experimental procedure, the basics for understanding the working principle of the engine and the tools used to capture the plume chemical composition have been described.

From a scientific point of view, the results deriving from the analysis of the data are complete. The chemical composition, the variation of the OH^* during the tests and the Blue Radiation have been analyzed, listed and completely understood. The research conducted on the plume has been precise, simple and sequential, always moving from a timestep to the next one methodologically.

The analysis of the plume used a mixture of logical thinking, software aid and literature in order to deliver the most precise results and plots.

It is remarkable to denote how the plots relative to the flame emissions are different in the two hotruns. The OH^* intensity is varying due to the changes performed in the ROF, allowing an high flexibility to the engine in terms of chances of changing parameters during the hotruns. The Cu level, which is cooling film material, is recorded as predicted by ArianeGroup.

The tests have been recorded and listed accordingly to what expected by engineers and technicians and the work executed has been useful for the analysis of the performances of the engine.

6.2 Lumen Project: Conclusions

This section includes all the conclusions relative to the Lumen Project part of this thesis. The tools used, the methodology and the setup of the experiments have been widely explained and analyzed. The assumptions taken have been clearly stated in Section 5.3.1 and the results relative to the analysis of the data obtained have been listed and described in Section 5.3.

As it could be clear by now to the reader, the plasma analysis has been conducted with the aid of various software and the aid of many papers and books, all listed in the Bibliography.

The experiments were conducted correctly but some technical issues did not allow the perfect detection of LIBS. The second two hotruns had a problem with the alignment of the probe dedicated to the plasma detection that led to the recording of plasma generated scattered light. With the data obtained it was possible anyway to perform the first technical analysis of LIBS and Boltzmann Plot for the determination of the temperature of the plasma and an estimation of the LTE condition. The

results obtained are satisfactory for the Oxygen and the Carbon plasma but further research is needed for the Hydrogen plot as presented in Figure 5.39. It could be with a positive slope for many reasons, one of those could be the time at which the hydrogen emissions lines hit the glass fiber, which could have occurred later than the other elements and for this reason the intensity could have been compromised. Another possible reason for this result could be that the assumption of considering a peak close to the exact wavelength of an ionization stage of hydrogen, as stated in the Balmer Series [28], to effectively be hydrogen was not correct. Since the results are satisfactory for the Carbon and Oxygen plasma, it could also be that Hydrogen plasma was not detected in the combustion chamber. The temperature obtained for Oxygen based plasma is of 464 180 K, while the one for the Carbon is of 161 170 K and for what is assumed to be Hydrogen is of 18 749 K. The LTE condition, which is obtained when the data points fit perfectly with the linear fitting, has been almost achieved for Oxygen and Hydrogen, while for Carbon they are quite far from it. In perfect LTE conditions all the plasma must be at the same temperature but, considering that the data obtained are relative to scattered light, the reliability of the temperature results presented in this thesis are not accurate. Due to the actual setup for the Lumen Project, it was not possible to change the delay time in these hotruns. For the upcoming test campaigns it is planned to increase the quality of the LTE measured. This will be achieved testing multiple delay times series in the future hotruns in order to achieve the best result for the LTE measurements. This is the reason why in the hotruns discussed in this thesis the LTE condition has not been fully satisfied. In Figure 6.1 a graphic explanation of what has just been stated is presented. As it is possible to note, the LTE condition could be optimal in another interval of the descending curve representing the life span of the plasma generated by the impulse of the laser and, for this reason, further research is needed.

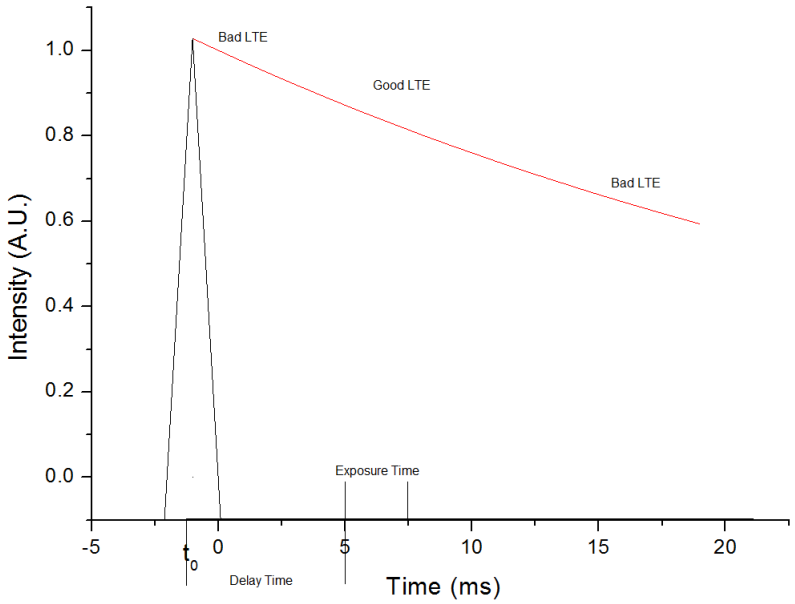

FIGURE 6.1: Laser Pulse

The experience gained in this present test campaign will be used to obtain further results that will help in determining an even more precise LTE condition.

Appendix A

Appendix

A.1 Matlab Codes

A.1.1 Absolute Values over time of various molecules during the Vulcain 2.1 Hotruns

```
% Author : Carlo Girardello

% Description : This file first extrapolate the data from an
    .asc
% file, then it puts them in a matrix. Afterwards, it is
    opened in thw
% workspace and plotted for a single row over 8000 frames.



clc
clear all
close all


frequency= 10;% Hz
time_frame= 0.1; %s



data = fopen('second.asc', 'r'); % Open the selected file in
    Matlab
second = textread('second.asc'); % Rename it
fclose(data);
frames=length(second(2,1:end));

wantedwavelength = 543;
wavelengthlist = second(:,1);
[value index] = min(abs(wavelengthlist-wantedwavelength));


% OH* Maximum Values
Rows_OH = second(189:287,:); % Rows with OH wavelength (from
    300 nm to 340 nm)
Max_value_OH = max(Rows_OH(:,:));
```

```
time=(1:1:5794)/frequency;
%length(Max_value_OH)

% Copper Maximum Values
Rows_Copper = second(547:597,:);
Max_value_Copper = max(Rows_Copper(:,:));


% Fe II Maximum Values
Rows_Fe = second(731:750,:);
Max_value_Fe = max(Rows_Fe(:,:));

figure
hold on
plot(time,second(260,:),'r')
plot(time,Max_value_OH(:,:), 'b')
plot(time,second(567,:),'g')
plot(time,Max_value_Copper(:,:),'k')
plot(time,second(731,:))
plot(time,Max_value_Fe(:,:), 'y')


%single(index,2:8000));
title('Plot of the Intensity of the Major Elements over the
    entire Hotrun')
xlabel('Time')
ylabel('Intensity')
legend('OH* at \lambda=330nm','OH* Maximum values for the
    range 300nm<\lambda<340nm', 'Copper at \lambda=543 nm' , '
    Copper Maximum values for the range 523nm<\lambda<563nm',
    'unknown element at \lambda= 670','Unknown Element Maximum
     Values for the range 660nm<\lambda<680nm')

hold off

% Integers

% Now we try to calculate the integer of the function on a
    definite range,
% as an example, we want to calculate the OH* value of the
    integral on a
% fixed interval throughout all the aquisition period.

% OH* Value of the iontegral


dt = 1/frequency;
timelist = dt:0.1:579.3; %seconds
timelist = timelist(2:end);

intensity_list_OH = [];
```

```
76
77 % OH*
78
79 for timestep = timelist
80     %timestep = 1:8002; %seconds
81     time_index = round(timestep*frequency); %index of time=
           timestep
82
83     %frequency range at which you integrate (wavelength)
84     minwavelength = 300;
85     maxwavelength = 340;
86
87
88
89     wavelengths = second(:,1);
90     [val begin_index] = min(abs(wavelengths-minwavelength));
91     [val end_index] = min(abs(wavelengths-maxwavelength));
92
93     intensity_sum_OH = 0;
94
95      for index = begin_index:end_index
96
97          intensity_val_OH = second(index,time_index);
98          intensity_sum_OH = intensity_sum_OH+intensity_val_OH
               *(second(index+1,1)-second(index,1));
99
100     end
101
102
103    integrated_intensity_OH = intensity_sum_OH;
104    intensity_list_OH = [intensity_list_OH
           integrated_intensity_OH];
105 end
106
107 figure
108 title('OH* Relationship Between Interger and Absolute Value
       Over Time')
109 yyaxis left
110 plot(timelist,intensity_list_OH)
111 ylabel('OH* Integrated intensity')
112 yyaxis right
113 plot(time,Max_value_OH(:,:))
114 ylabel('OH Absolute Value intensity')
115 xlabel('Time')
116
117
118 % Copper
119 intensity_list_Cu = [];
120 for timestep = timelist
121     %timestep = 1:8002; %seconds
```

```
122     time_index = round(timestep*frequency); %index of time=
            timestep
123
124     %frequency range at which you integrate (wavelength)
125     minwavelength = 527;
126     maxwavelength = 557;
127
128
129
130     wavelengths = second(:,1);
131     [val begin_index] = min(abs(wavelengths-minwavelength));
132     [val end_index] = min(abs(wavelengths-maxwavelength));
133
134     intensity_sum_Cu = 0;
135
136      for index = begin_index:end_index
137
138         intensity_val_Cu = second(index,time_index);
139         intensity_sum_Cu = intensity_sum_Cu+intensity_val_Cu
                *(second(index+1,1)-second(index,1));
140
141      end
142
143
144     integrated_intensity_Cu = intensity_sum_Cu;
145     intensity_list_Cu = [intensity_list_Cu
            integrated_intensity_Cu];
146 end
147
148 figure
149 title('Cu Relationship Between Integer and Absolute Value
        Over Time')
150 yyaxis left
151 plot(timelist,intensity_list_Cu)
152 ylabel('Cu Integrated intensity')
153 yyaxis right
154 plot(time,Max_value_Copper(:,:))
155 ylabel('Cu Absolute Value intensity')
156 xlabel('Time')
157
158
159
160 % Unknown Element
161 intensity_list_Fe = [];
162 for timestep = timelist
163     %timestep = 1:8002; %seconds
164     time_index = round(timestep*frequency); %index of time=
            timestep
165
166     %frequency range at which you integrate (wavelength)
167     minwavelength = 660;
```

```
168     maxwavelength = 680;
169
170
171
172     wavelengths = second(:,1);
173     [val begin_index] = min(abs(wavelengths-minwavelength));
174     [val end_index] = min(abs(wavelengths-maxwavelength));
175
176     intensity_sum_Fe = 0;
177
178      for index = begin_index:end_index
179
180         intensity_val_Fe = second(index,time_index);
181         intensity_sum_Fe = intensity_sum_Fe+intensity_val_Fe
               *(second(index+1,1)-second(index,1));
182
183      end
184
185
186     integrated_intensity_Fe = intensity_sum_Fe;
187     intensity_list_Fe = [intensity_list_Fe
           integrated_intensity_Fe];
188 end
189
190 figure
191 title('Unknown Element Relationship Between Integer and
       Absolute Value Over Time')
192 yyaxis left
193 plot(timelist,intensity_list_Fe)
194 ylabel('Unknown Element Integrated intensity')
195 yyaxis right
196 plot(time,Max_value_Fe(:,:))
197 ylabel('Unknown Element Absolute Value intensity')
198 xlabel('Time')
199 time_origin = time';
200 intensity_Fe_origin = intensity_list_Fe';
```

A.1.2 Function to Smooth Baseline for Plasma Emissions

```
1  clear all
2  close all
3  clc
4
5
6  % Scope: To average the baseline of a LIPS  in order to have
       a smooth line
7  % as a background
8  % Author: Carlo Girardello
9  % Date: 16/5/2019
10
11 % Step 1 : Import Data
```

```
12 single_frame = uiimport('sep0044.asc');
13
14 %Step 2: Average the Spectra below a certain intensity (200)
15
16 xx = single_frame.sep0044(:,2); % Intensity Column
17 yy = smooth(xx,40); % Smoothing the intensity column
18 zz = xx-yy; % Original Plot - Smooth
19
20 % Set every Element in  the zz frame to be 0 below a certain
       intensity
21 indexlist = zz<200;
22 zz(indexlist) = 0; % Only the peaks
23
24 result = zz+yy; % The smoothened + the peaks
25
26 figure
27 subplot(4,1,1)
28 plot(single_frame.sep0044(:,1), xx)
29 title('Original')
30 ylim([-200,1700])
31 subplot(4,1,2)
32 plot(single_frame.sep0044(:,1), yy)
33 title('Smoothened')
34 ylim([-200,1700])
35 subplot(4,1,3)
36 plot(single_frame.sep0044(:,1), zz)
37 title('Just the Peaks')
38 ylim([-200,1700])
39 subplot(4,1,4)
40 plot(single_frame.sep0044(:,1), result)
41 title('Smoothened + Peaks')
42 ylim([-200,1700])
43
44 % Step 3: The noise derived from the chip has been removed.
       Now it is time
45 % to remove the wave form of the Echelle spectrograph. The
       procedure will
46 % be the same of the previous one but with a severe
       smoothening.
47 % WARNING: It is relative to the the already smoothened
       function, not the
48 % original.
49
50
51 yy2 = smooth(yy,20000); % Very strong smoothening
52 zz2 = xx-yy2; % Subtract to the original plot the smoothened
       one, in order to obtain the peaks
53
54
55 indexlist2 = zz2<200;
56 zz2(indexlist2) = 0;
```

```
result2 = yy2+zz2;

figure
plot(single_frame.sep0044(:,1), result2)
title('Smoothened + Peaks')
ylim([0,1700])


% Step 4 : Exponentially fit the values of the already
    smoothened function
% in order to have a 0 interference by the chip or the
    mechelle
% spectrograph.
% In this way we will obtain only the peaks with no risk for
    the quality of
% the results.
indexlist3=zz2<1;
zz3(indexlist3)=0;
zz3=zz3';


result3=yy2+zz3;


figure
plot(single_frame.sep0044(:,1), result3)
title('Smoothened + Peaks')
ylim([-10,1700])
```

A.1.3 Reduce Wavelength only to an Interesting Range

```
% Author: Carlo Girardello 24/5/19


% Goal: To filter chaotic spectra only on the interested
    wavelength.
% Example: A spectra is full of plasma lines and I am
    interested only in
% Hydrogen lines.



clear all
close all
clc


% Step 1. Import the Spectra

single_frame = uiimport('sep0108.asc');
```

```
19
20 % Step 2. Smooth the curve
21
22 xx = single_frame.sep0108(:,2); % Intensity Column
23 yy = smooth(xx,10); % Smoothing the intensity column
24 zz = xx-yy; % Original Plot - Smooth
25
26 % Set every Element in  the zz frame to be 0 below a certain
     intensity
27 indexlist = zz<200;
28 zz(indexlist) = 0; % Only the peaks
29
30 result = zz+yy;
31
32
33 % Step 3: Repeat to cut off the Spectrograph noise
34 yy2 = smooth(yy,20000); % Very strong smoothening
35 zz2 = xx-yy2; % Subtract to the original plot the smoothened
     one, in order to obtain the peaks
36
37
38 indexlist2 = zz2<200;
39 zz2(indexlist2) = 0;
40 result2 = yy2+zz2;
41
42
43 % Final Result: Spectra Only with Peaks
44
45 figure
46 plot(single_frame.sep0108(:,1), result2)
47 title('Smoothened + Peaks')
48 ylim([0,5500])
49
50
51 % Step 4 : Filter the peaks
52
53 % Bigger First
54 pos=(single_frame.sep0108(:,1)<657).*(single_frame.sep0108
     (:,1)>656);
55 reduced_wv = single_frame.sep0108(:,1).*pos;
56 inten = result2.*pos;
57 reduced_wv(reduced_wv==0)=[];
58 inten(inten==0)=[];
59 figure
60 plot(reduced_wv, inten)
61 title('Reduced Wavelength')
62 %ylim([0,5500])
63
64
65
```

```
% Step 5: Introduce Quantum Efficiency Curve and smooth the intensity for a
% certain percentage, depending on the wavelength selected
quantum_int = inten + inten*9/100;
figure
plot(reduced_wv, quantum_int)
title('Real Wavelength')
```

A.1.4 Boltzmann Plot

```
% Author: Carlo Girardello
%
% Goal: To calculate the Boltzmann Plot linearity
% The user must compile the following code with the ionization states
% paramters and run it in order to obtain a Figure with the points of the
% Boltzmann Plot.
% Once this has been obtained, a Linear Fit must be performed and the slope
% inclination must be inserted in the last equation for calculating the
% plasma temperature

% Date: 20/6/19



clc
clear all
close all


% Ionization State 1 or alpha
I_alpha =  160000;
lambda_alpha = 0.00000050521 ; % [m]
Ag_alpha =1.3e-1 ;
E_alpha = 10.13;
yaxis_alpha = log((I_alpha*lambda_alpha)/(Ag_alpha));



% Ionization State 2 or beta
I_beta = 800;
lambda_beta = 0.0000004267; %[m]
Ag_beta = 1.34e+1;
E_beta = 20.950;
yaxis_beta = log((I_beta*lambda_beta)/(Ag_beta));

% Ionization State 3 or gamma
I_gamma =200;
```

```
lambda_gamma = 0.000000581198;
Ag_gamma =6.32e-1;
E_gamma = 39.681;
yaxis_gamma = log((I_gamma*lambda_gamma)/(Ag_gamma));

% The procedure can be repeted for every ionization state
    desired. The more
% are present, the more the Boltzmann Plot will be accurate.



% Group values into vectors for Origin 8.1 future export
y  = {yaxis_alpha, yaxis_beta, yaxis_gamma};
e = {E_alpha, E_beta, E_gamma};
e1 = transpose(e);
y1=transpose(y);

E=cell2mat(e1);
Y=cell2mat(y1);

% Boltzmann Plot
figure
hold on
plot(E,Y, 'x')


% Temperature Determination
 m = 0.232;
 k = 8.617333262145*10^(-5);
 T = 1/(m*k);
```

A.2 Extra Figures

A.2.1 Carbon Ionization Stages Figures

This Section of the Appendix contains all the Figures relative to the carbon emission lines recorded during the fourth hotrun of the Lumen Project on the 13th of May 2019. These emission lines were necessary to calculate the Boltzmann Plot and to verify the quality of the LTE. The identification values are presented in Figure 5.40.

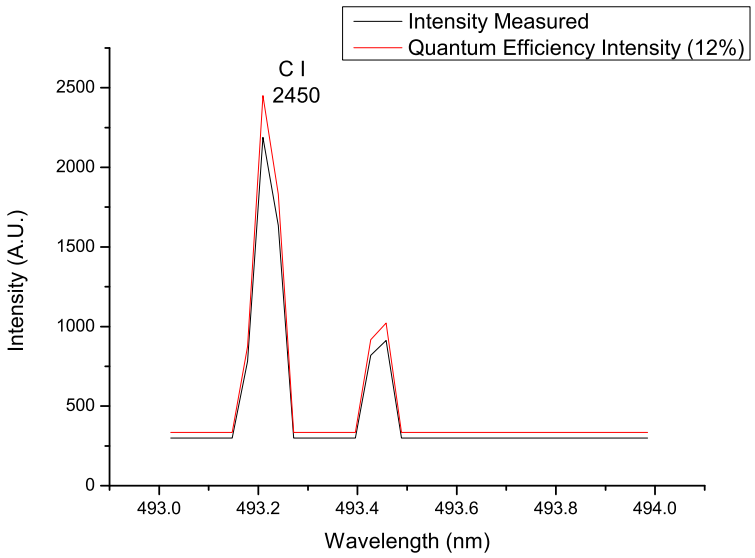

FIGURE A.1: LUMEN Project Hotruns: Carbon I with Quantum Efficiency - Fourth Hotrun 1/1 on the 13/5/2019

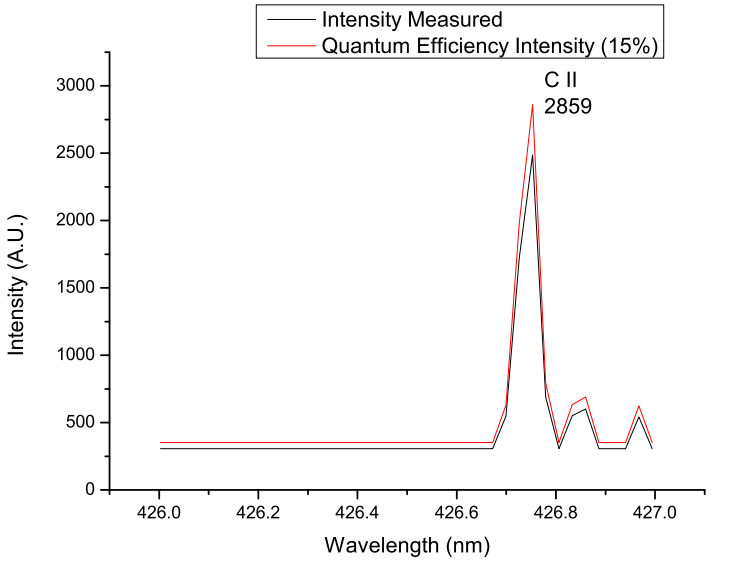

FIGURE A.2: LUMEN Project Hotruns: Carbon II with Quantum Efficiency - Fourth Hotrun 1/1 on the 13/5/2019

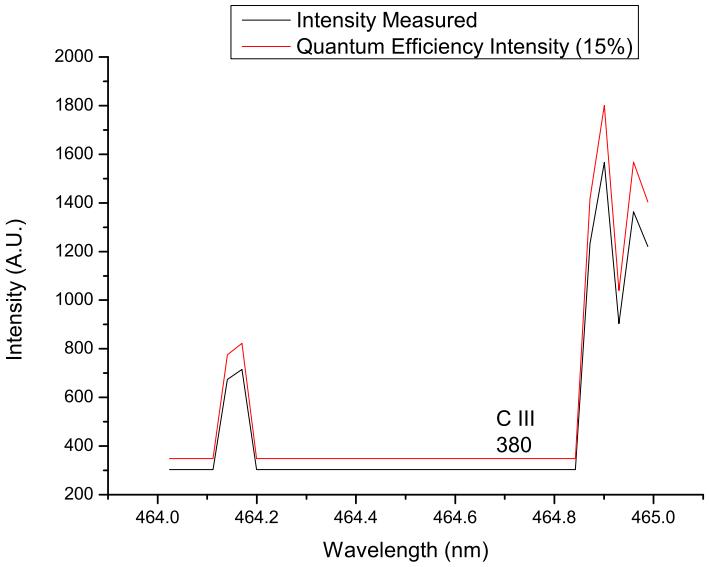

FIGURE A.3: LUMEN Project Hotruns: Carbon III with Quantum Efficiency - Fourth Hotrun 1/1 on the 13/5/2019

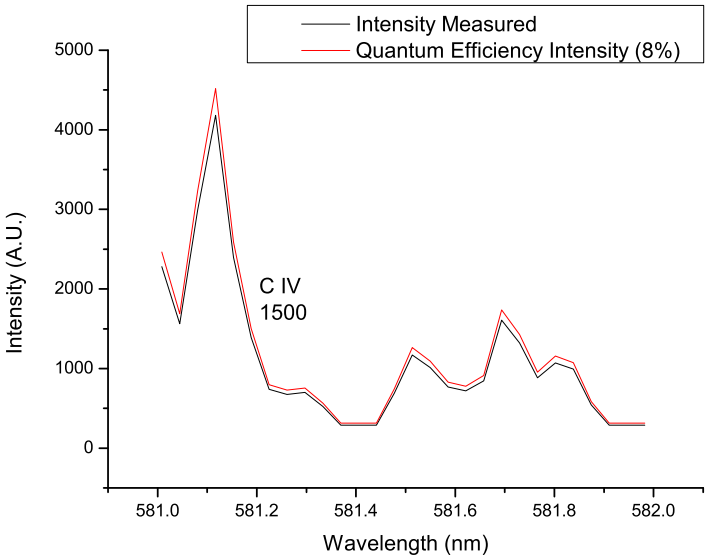

FIGURE A.4: LUMEN Project Hotruns: Carbon IV with Quantum Efficiency - Fourth Hotrun 1/1 on the 13/5/2019

A.2.2 Oxygen Ionization Stages Figures

This Section of the Appendix contains all the Figures relative to the oxygen emission lines recorded during the fourth hotrun of the Lumen Project on the 13th of May 2019. These emission lines were necessary to calculate the Boltzmann Plot and to verify the quality of the LTE. The identification values are presented in Figure 5.41.

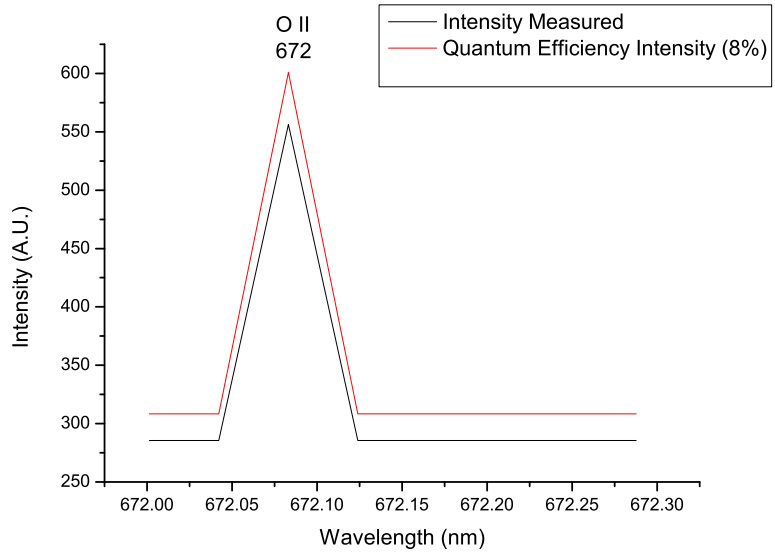

FIGURE A.5: LUMEN Project Hotruns: Oxygen II with Quantum Efficiency - Fourth Hotrun 1/1 on the 13/5/2019

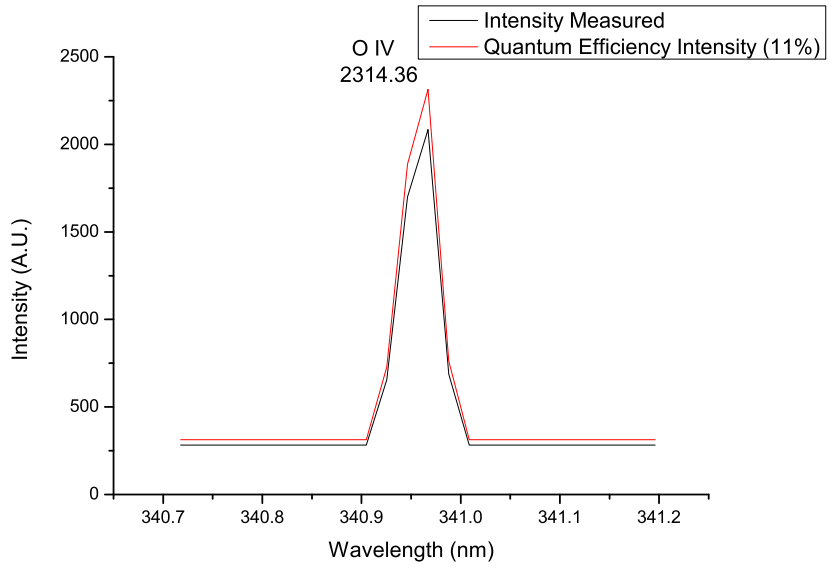

FIGURE A.6: LUMEN Project Hotruns: Oxygen IV with Quantum Efficiency - Fourth Hotrun 1/1 on the 13/5/2019

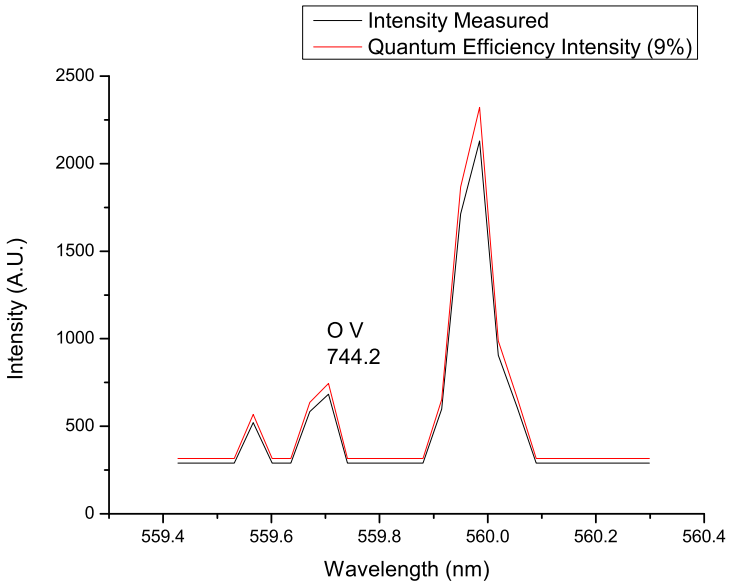

FIGURE A.7: LUMEN Project Hotruns: Oxygen V with Quantum Efficiency - Fourth Hotrun 1/1 on the 13/5/2019

Bibliography

[1] Technology Andor. *An Introduction to the ICCD Camera*. URL: https://andor.oxinst.com/learning/view/article/intensified-ccd-cameras.

[2] Technology Andor. *Mechelle 5000 User Manual*. 2011. URL: http://www.tokyoinst.co.jp/product_file/file/AD11_man01_ja.pdf.

[3] Technology Andor. *User Manual for the iStar sCMOS 18 F 03*. 2015. URL: https://andor.oxinst.com/assets/uploads/documents/andor-istar-scmos-specifications.pdf.

[4] Technology Andor. *User Manual for the Shamrock SR-163*. 2008. URL: http://www.tokyoinst.co.jp/product_file/file/AD09_man01_ja.pdf.

[5] Andor, Technology. *iStar DH720/DK720 Gen II Datasheet*. 2006.

[6] LOT Group Andor Technology. "*Diagnostics of silicon plasmas produced by visible nanosecond laser ablation*". In: *ICCD Detectors, Course Notes* (2003).

[7] Zhang S. & Wang X. & He M. & Jiang Y. & Zhang B. & Hang W. & Huang B. *Spectrochimica Acta Part B: Laser-Induced Plasma Temperature*. 2014. URL: https://www.sciencedirect.com/science/article/abs/pii/S0584854714000615.

[8] Olivier Barthélemy et al. "*Investigation of the state of local thermodynamic equilibrium of a laser-produced aluminum plasma*". In: *Applied spectroscopy* 59.4 (2005), pp. 529–536.

[9] Alejandro G Belluscio. "*SpaceX advances drive for Mars rocket via Raptor power*". In: *NASAspaceflight. com* (2014).

[10] S.G. Djorgovski & M. Bolte. *Spectrographs and Spectroscopy (UV/Visible/IR)*. 2012. URL: http://www.astro.caltech.edu/~george/ay122/Ay122a_Spectroscopy.pdf.

[11] Michael Börner, Chiara Manfletti, and Michael Oschwald. "*Laser re-ignition of a cryogenic multi-injector rocket engine*". In: *6th European Conference for Aeronautics and Space Sciences*. 2015.

[12] Michael Börner et al. "Experimental Study of a Laser-Ignited Liquid Cryogenic Rocket Engine". In: *Laser Ignition Conference*. Optical Society of America, 2015, Th2A.5. DOI: 10.1364/LIC.2015.Th2A.5. URL: http://www.osapublishing.org/abstract.cfm?URI=LIC-2015-Th2A.5.

[13] Luisa María Cabalín et al. "*Deep ablation and depth profiling by laser-induced breakdown spectroscopy (LIBS) employing multi-pulse laser excitation: application to galvanized steel*". In: *Applied spectroscopy* 65.7 (2011), pp. 797–805.

[14] Francis F Chen. *Introduction to plasma physics and controlled fusion*. Vol. 1. Springer, 1984.

[15] Emanuela D'Aversa and more. "*LOX/Methane Gap Assesment Report*". In: *International Agency Working Group* -.- (2016), pp. I–20.

[16] CD David Jr and H Weichel. "*Temperature of a Laser-Heated Carbon Plasma*". In: *Journal of Applied Physics* 40.9 (1969), pp. 3674–3679.

[17] DLR. *Institute of Space Propulsion Lampoldhausen: Status Report 2011-2017*. 2017. URL: https://www.dlr.de/ra/Portaldata/55/Resources/dokumente/2017/Institute_of_Space_Propulsion_-_Status_Report_2017.pdf.

[18] Craig Dr. Fisher et al. *Quantum Numbers*. 2017. URL: https://chem.libretexts.org/Bookshelves/Physical_and_Theoretical_Chemistry_Textbook_Maps/Supplemental_Modules_(Physical_and_Theoretical_Chemistry)/Quantum_Mechanics/10%3A_Multi-electron_Atoms/Quantum_Numbers.

[19] RP Photonics Encyclopedia. *Spectrometers*. URL: https://www.rp-photonics.com/spectrometers.html.

[20] European Space Agency ESA. *Ariane 6's Vulcain Engine Set For First Firing*. URL: https://www.esa.int/Our_Activities/Space_Transportation/Ariane_6_s_Vulcain_engine_set_for_first_firing.

[21] Grossmann F. *Atoms and Molecules in Strong Laser Fields*. 2008.

[22] Thomas Fiala. "*Radiation from high pressure hydrogen-oxygen flames and its use in assessing rocket combustion instability*". PhD thesis. Technische Universität München, 2015.

[23] Alexander Fridman and Lawrence A Kennedy. *Plasma physics and engineering*. CRC press, 2004.

[24] WC Gardiner Jr et al. "*Shock-Tube Study of OH (2 Σ—2 Π) Luminescence*". In: *The Physics of Fluids* 12.5 (1969), pp. I–120.

[25] Alferd Gaydon. *The spectroscopy of flames*. springer science & business media, 2012.

[26] David J Griffiths and Darrell F Schroeter. *Introduction to quantum mechanics*. Cambridge University Press, 2018.

[27] Kazuyuki Higashino et al. "*Fundamental study on coking characteristics of LNG Rocket Engines*". In: *44th AIAA/ASME/SAE/ASEE Joint Propulsion Conference & Exhibit*. 2008, p. 4753.

[28] Jan Homann. *Balmer Series*.

[29] Geoff Tyler Horiba Jobin-Yvon France. *Cerny Turner Design*. 2007. URL: http://www.thespectroscopynet.eu/?Spectrometers:Monochromator:Cerny_Turner_Design.

[30] Zuhaib Haider & Yusof Munajat & Raja Kamarulzaman Raja Ibrahim. *Laser-Induced Breakdown spectroscopy (LIBS) a promising technique, its limitations and a proposed method*. 2012. URL: https://www.researchgate.net/publication/286415874_Review_Laser-Induced_Breakdown_spectroscopy_LIBS_a_promising_technique_its_limitations_and_a_proposed_method.

[31] Thorlabs Inc. *FOFMS - In-Line Multimode Fiber Optic Filter Mount*. 2018. URL: https://www.thorlabs.com/thorproduct.cfm?partnumber=FOFMS.

[32] Oriel Instruments. *Typical Spectra of Calibration Lamps*. URL: https://www.newport.com/medias/sys_master/images/images/h55/hfd/8797293281310/Typical-Spectra-of-Spectral-Calib-Lamps.pdf.

[33] George A Jeffrey and George A Jeffrey. *An introduction to hydrogen bonding*. Vol. 32. Oxford university press New York, 1997.

[34] W Koschel. "*The European Test Bench P8 - 20 Years in Service for R&T on Liquid Propulsion*". In: Jan. 2015.

[35] A. Kramida et al. NIST Atomic Spectra Database (ver. 5.6.1), [Online]. Available: https://physics.nist.gov/asd [2019, July 9]. National Institute of Standards and Technology, Gaithersburg, MD. 2018.

[36] DLR Lampoldhausen. "*First ignition for Europe's most powerful rocket engine, the Vulcain 2.1* ". In: *DLR* (2018).

[37] Stützer R.& Börner M.& Oschwald M. *Optical Investigation of a Laser-Ignited Cryogenic Rocket Combustion*. 2015. URL: https://www.researchgate.net/profile/Robert_Stuetzer/publication/280090937_Optical_Investigation_of_a_Laser-Ignited_Cryogenic_Rocket_Combustion/links/55a7e08c08aea3d0867c13f0/Optical-Investigation-of-a-Laser-Ignited-Cryogenic-Rocket-Combustion.pdf.

[38] Hotinceanu Mihai, Borsos Zoltan, and Dinu Octavian. *Aspects of Thermodynamic Equilibrium In Plasma*. 2016. URL: http://bmif.unde.ro/docs/20101/pdf_final_11%20MHotinceanu.pdf.

[39] M Milan and JJ Laserna. "*Diagnostics of silicon plasmas produced by visible nanosecond laser ablation*". In: *Spectrochimica Acta Part B: Atomic Spectroscopy* 56.3 (2001), pp. 275–288.

[40] Nikhil More. *Optical Characterization of Laser Induced Helium Plasmas*. 2017.

[41] C. R. Nave. *Hydrogen Spectrum*. 2006. URL: http://hyperphysics.phy-astr.gsu.edu/hbase/hyde.html#c4.

[42] Dr. Rüdiger Paschotta. *Lasers*. 2008. URL: https://www.rp-photonics.com/lasers.html.

[43] DLR Space Propulsion. *Test Facilities*. URL: https://www.dlr.de/ra/en/desktopdefault.aspx/tabid-8483/14618_read-36493/.

[44] John S Rigden. *Hydrogen: the essential element*. 2003.

[45] Hitachi High-Technology Global & Willy Sanders. *What is Optical Emission Spectroscopy (OES)?* 2017. URL: https://hha.hitachi-hightech.com/en/blogs-events/blogs/2017/10/25/optical-emission-spectroscopy-(oes)/.

[46] Gerhard Kroupa & Gudrun Bruckner & Nico Rackemann & Sebastian Soller. *Laser Ignition For Aerospace Applications using the Rugged Miniaturized HiPoLas Nd-YAG Laser System*. 2017. URL: https://www.osapublishing.org/abstract.cfm?uri=LIC-2017-LThA4.1.

[47] Stützer R.& Hardi J.& Gröning S.&Webster S.& Oschwald M. & Fiala T. & Sattelmayer T. *Comparison Between Excited Hydroxyl Radical and Blue Radiation from Hydrogen Rocket Combustion*. 2017. URL: https://arc.aiaa.org/doi/10.2514/1.B36280.

[48] Hiroshi Tamura et al. "*LOX/methane staged combustion rocket combustor investigation*". In: *23rd Joint Propulsion Conference*. 1987, p. 1856.

[49] Thorlabs. *Special Considerations with Echelle Gratings*. 2018. URL: https://www.thorlabs.de/newgrouppage9.cfm?objectgroup_id=1124.

[50] J. R. W. Wiese J. Fuhr. *Accurate Atomic Transition Probabilities for Hydrogen, Helium and Lithium*. URL: https://zenodo.org/record/1232309#.XTbVbvL7SUk.

[51] Giorgio Zizak. "*Flame emission spectroscopy: fundamentals and applications*". In: (2000).

[52] ETH Zurich. *PCV - Spectroscopy of atoms and molecules*.